DENDRIMER-ENCAPSULATED METAL NANOPARTICLE THIN FILMS ON SOLID SURFACES: PREPARATION, CHARACTERIZATION, AND APPLICATIONS TO ELECTROCATALYSIS

A Dissertation

by

HEECHANG YE

Submitted to the Office of Graduate Studies of
Texas A&M University
in partial fulfillment of the requirements for the degree of

DOCTOR OF PHILOSOPHY

December 2006

Major Subject: Chemistry

DENDRIMER-ENCAPSULATED METAL NANOPARTICLE THIN FILMS ON SOLID SURFACES: PREPARATION, CHARACTERIZATION, AND APPLICATIONS TO ELECTROCATALYSIS

A Dissertation

by

HEECHANG YE

Submitted to the Office of Graduate Studies of
Texas A&M University
in partial fulfillment of the requirements for the degree of

DOCTOR OF PHILOSOPHY

Approved by:

Co-Chairs of Committee,	Richard M. Crooks
	D. Wayne Goodman
Committee Members,	Raymond E. Schaak
	Daniel F. Shantz
Head of Department,	Emile A. Schweikert

December 2006

Major Subject: Chemistry

ABSTRACT

Dendrimer-Encapsulated Metal Nanoparticle Thin Films on Solid Surfaces: Preparation, Characterization, and Applications to Electrocatalysis. (December 2006)

Heechang Ye, B.S., Yonsei University

Co-Chairs of Advisory Committee: Dr. Richard M. Crooks
Dr. D. Wayne Goodman

Dendrimer-encapsulated nanoparticles (DENs) were prepared, characterized, and immobilized on solid surfaces. The resulting films were applied as electrocatalysts for the oxygen reduction reaction (ORR).

First, the synthesis, physical and chemical properties, and stability of Pd DENs prepared within poly(amidoamine) (PAMAM) dendrimers were studied in aqueous solution. In this part of the study, the following new findings were reported: (1) the maximum Pd ion loading in the dendrimer was correlated to the number of interior amines available for complexation; (2) Pd DENs could be synthesized within amine-terminated Pd DENs by controlling the solution pH; (3) the oxidative stability of Pd DENs was significantly improved by removing solution-phase impurities; (4) exposure to hydrogen gas reversibly converts partially oxidized Pd DENs back to the zerovalent state.

Second, Pt and Pd DENs were prepared using amine-terminated PAMAM dendrimers, and then the free amine groups on the periphery were used to immobilize Pt and Pd DENs onto Au surfaces via an intermediate self-assembled monolayer. The

resulting DEN films were more robust and had higher coverages of DENs compared to the DEN films prepared via physisorption.

Third, Pt DENs were prepared and immobilized on glassy carbon electrodes using an electrochemical coupling method. The resulting films were electrochemically active for the ORR. These electrocatalytic monolayers were also robust, surviving up to 50 consecutive electrochemical scans for ORR and sonication in acid solution with no significant change in activity.

Finally, PtPd bimetallic nanoparticles containing an average of 180 atoms (~1.8 nm in diameter) and composed of seven different Pt:Pd ratios were prepared within sixth-generation, hydroxyl-terminated PAMAM dendrimers. Transmission electron microscopy and single-particle energy dispersive spectroscopy confirmed the sizes and compositions of the particles. These DENs were immobilized on glassy carbon electrodes, and their electrocatalytic properties were evaluated as a function of composition using cyclic voltammetry and rotating disk voltammetry. The results showed that the maximum rate for the ORR occurs at a Pt:Pd ratio of 5:1, which corresponds to a relative mass activity enhancement of 2.5 compared to otherwise identical monometallic Pt nanoparticles.

DEDICATION

To my beloved wife, Hyunjoo,

and my parents,

for their devotional support

ACKNOWLEDGMENTS

First of all, I would like to express my gratitude to my research adviser, Prof. Richard M. Crooks, for giving me a chance to join the Crooks group and to work on a very interesting research topic and for providing guidance, advice, and encouragement. Also, he has been my excellent standard model of a good scientist to follow. I would also like to thank Prof. D. Wayne Goodman, Prof. Raymond E. Schaak, and Prof. Daniel F. Shantz for serving as my committee members.

Second, I would like to thank my research colleagues in the Crooks group, Dr. Rob Scott, Dr. Sang-Keun Oh, Dr. Li Sun, Dr. Yong-Gu Kim, Dr. Marc Knecht, Dr. Julio Alvarez, and Dr. Gregory Perez, for their valuable discussions, comments and technical assistance on my research. I would also like to thank all the other Crooks group members who have worked with me in the office and lab for the past five and a half years.

Finally, I would like to thank my wife, Hyunjoo, who has been my biggest supporter. She was always my source of power to overcome the difficulties and frustration during my study.

Financial support of my work from the U. S. Department of Energy, the National Science Foundation, and the Robert A. Welch Foundation is also greatly acknowledged.

TABLE OF CONTENTS

LIST OF FIGURES

FIGURE Page

FIGURE Page

FIGURE Page

LIST OF TABLES

CHAPTER I

INTRODUCTION

1.1 Motivation and Objectives

Nano sized materials have unique physical and chemical properties compared to bulk materials. Therefore, they are of great interest in the fields of catalysis, electronics, sensors, and biotechnology.

Here we are interested in application of metal nanoparticles to catalysis reactions, especially the electrochemical oxygen reduction reaction (ORR). Recently, we reported a new approach for synthesizing nanoparticles using dendrimers as templates.[1,2] The synthesis is carried out in two steps. First, metal ions are extracted into dendrimers and coordinate in fixed stoichiometries with interior functional groups in solution phase. Second, the metal-ion/dendrimer composites are reduced to yield dendrimer-encapsulated nanoparticles (DENs). DENs[1,2] have a number of interesting properties, including: (1) they are catalytically active; (2) particle sizes are small (< 3 nm) and highly monodisperse; (3) particle size and composition can be easily controlled; and (4) surface groups of the dendrimers can be used for attaching the DENs to surfaces.

The ORR is an important reaction, because it is the greatest source of inefficiency in fuel cells.[3-5] Therefore, the development of efficient catalysts and electrodes has been a focus in this field. It is well known that Pt is the most effective catalyst for oxygen reduction. However, the optimization of Pt catalysts to increase

---

This dissertation follows the style of *Journal of the American Chemical Society*.

catalytic activity by reducing particle size and adding other metals is essential because of the high cost and limited supply of Pt.

Several objectives were addressed in this project. First, the synthesis, physical and chemical properties, and stability of DENs were studied (Chapter III). Second, DENs were immobilized on electrode surfaces with proper stability (Chapter IV and V). Third, the electrocatalytic properties of the resulting DEN films were studied (Chapter V and VI).

1.2 Dendrimer-Encapsulated Nanoparticles (DENs)

Dendrimers. Dendrimers are three-dimensional, tree-like macromolecules composed of repetitive branch units. The physical and chemical properties of dendrimers depend on the chemical structure of core, repetitive branch units, terminal functional groups, and size which can be changed by the generation of dendrimers. The dendrimers used in this research are poly(amidoamine) (PAMAM) dendrimers, which are commercially available from Dendritech, Inc. (Midland, MI). The structure of second-generation, amine-terminated PAMAM is shown in Figure 1.1 (G2-NH_2, G2 denotes generation 2). The PAMAM dendrimer has ethylenediamine core, an amidoamine repetitive branching structure, and terminal primary amine groups. The primary amine terminal groups can be converted into hydroxyl groups (G2-OH) to provide different physical and chemical properties. PAMAM dendrimers are hydrophilic, and so they are completely soluble in water and methanol. They are insoluble in most nonpolar organic solvents. However, it is possible to make them soluble in organic solvents by converting

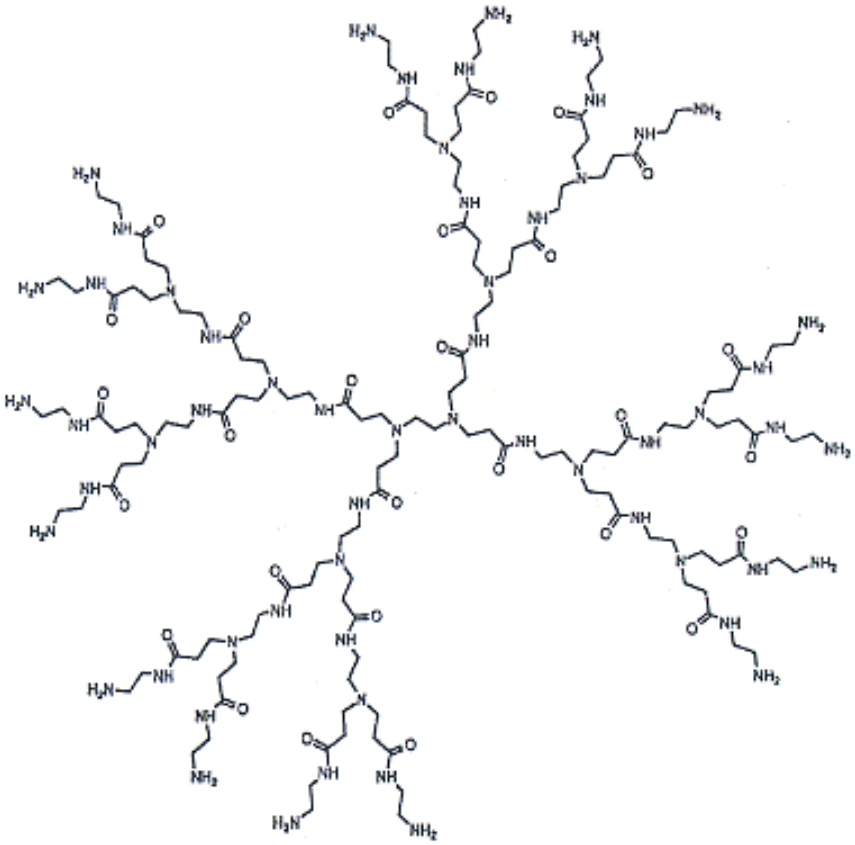

Figure 1.1. Structure of a second-generation, amine-terminated PAMAM dendrimer.

Table 1.1. Physical properties of PAMAM dendrimers (G0 – G10).

Generation	Number of surface group	Number of tertiary amines	Molecular weight[a]	Diameter (nm)[b]
0	4	2	517	1.5
1	8	6	1,430	2.2
2	16	14	3,256	2.9
3	32	30	6,909	3.6
4	64	62	14,215	4.5
5	128	126	28,826	5.4
6	256	254	58,048	6.7
7	512	510	116,493	8.1
8	1024	1022	233,383	9.7
9	2048	2046	467,162	11.4
10	4096	4094	934,720	13.5

[a] Molecular weight is based on defect free, idea-structure, amine-terminated dendrimers.

[b] Diameters were determined by size-exclusion chromatography.

the surface groups. Table 1.1 summarizes some physical properties of amine-terminated PAMAM dendrimers as a function of their generations (G0 to G10).

Synthesis of DENs. One of the promising applications of dendrimers is to use PAMAM dendrimers as hosts for synthesizing nanoparticles.[2] The synthesis process is very simple and consists of two steps (Figure 1.2). First, a dendrimer solution is mixed with metal ion solutions having a desired stoichiometric ratio. This allows metal ions to coordinate with interior functional groups of the dendrimers. Second, the metal-ion/dendrimer composites are reduced using excess BH_4^- to yield zerovalent nanoparticles encapsulated within the dendrimers. This strategy makes it possible to synthesize both monometallic nanoparticles (Cu, Pd, Pt, Au) and bimetallic nanoparticles (PtPd, PdAu, and AuAg).[2,6] It is also possible to control the structure of bimetallic DENs using slightly different synthetic procedures (Figure 1.3).

DENs have several unique properties. This include: (1) the encapsulated nanoparticles are small (<3 nm) and in some cases nearly monodisperse; (2) the particle size can be controlled by selecting different dendrimer generations and metal ion to dendrimer ratios; (3) the encapsulated nanoparticles are partially confined by steric effects, and therefore at least part of the surface is available for catalytic reactions; (4) dendrimer branches and surface groups can be used as selective gates to control access of small molecules to the encapsulated nanoparticle; (5) the solubility of DENs can be tuned by modifying the peripheral groups of the dendrimer.[2,7] Taken together, these five points suggest that DENs are interesting materials and useful for applications in homogeneous and heterogeneous catalysts as we will discuss in the next section.

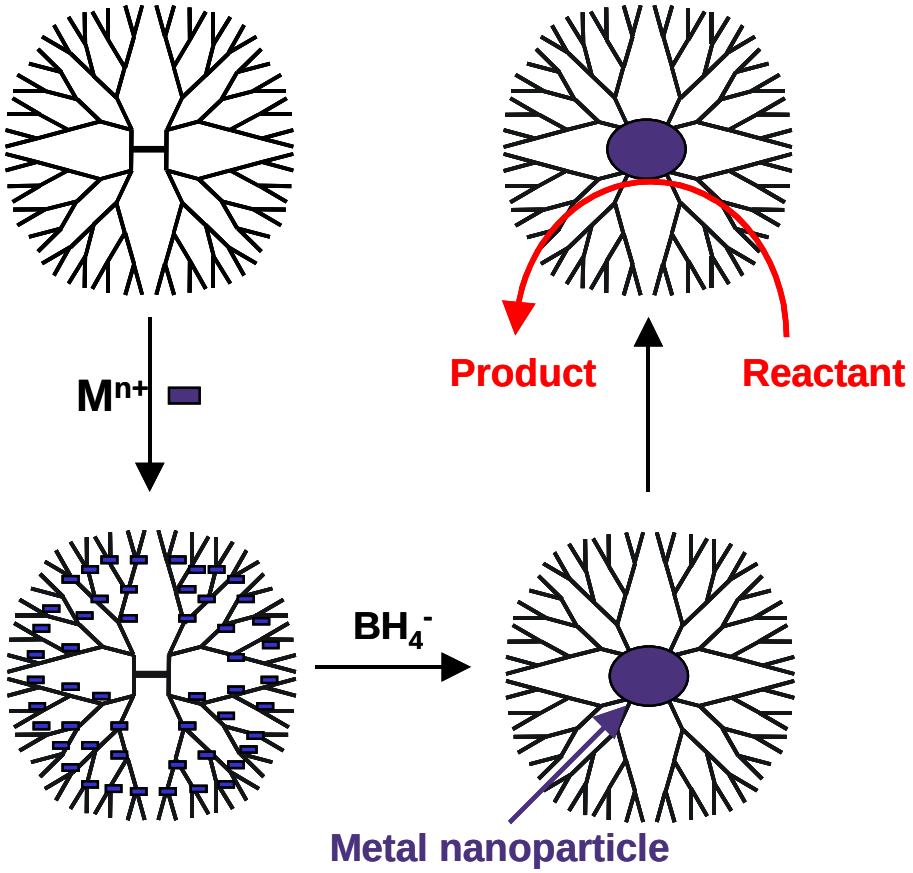

Figure 1.2. General synthetic procedure of dendrimer-encapsulated nanoparticles.

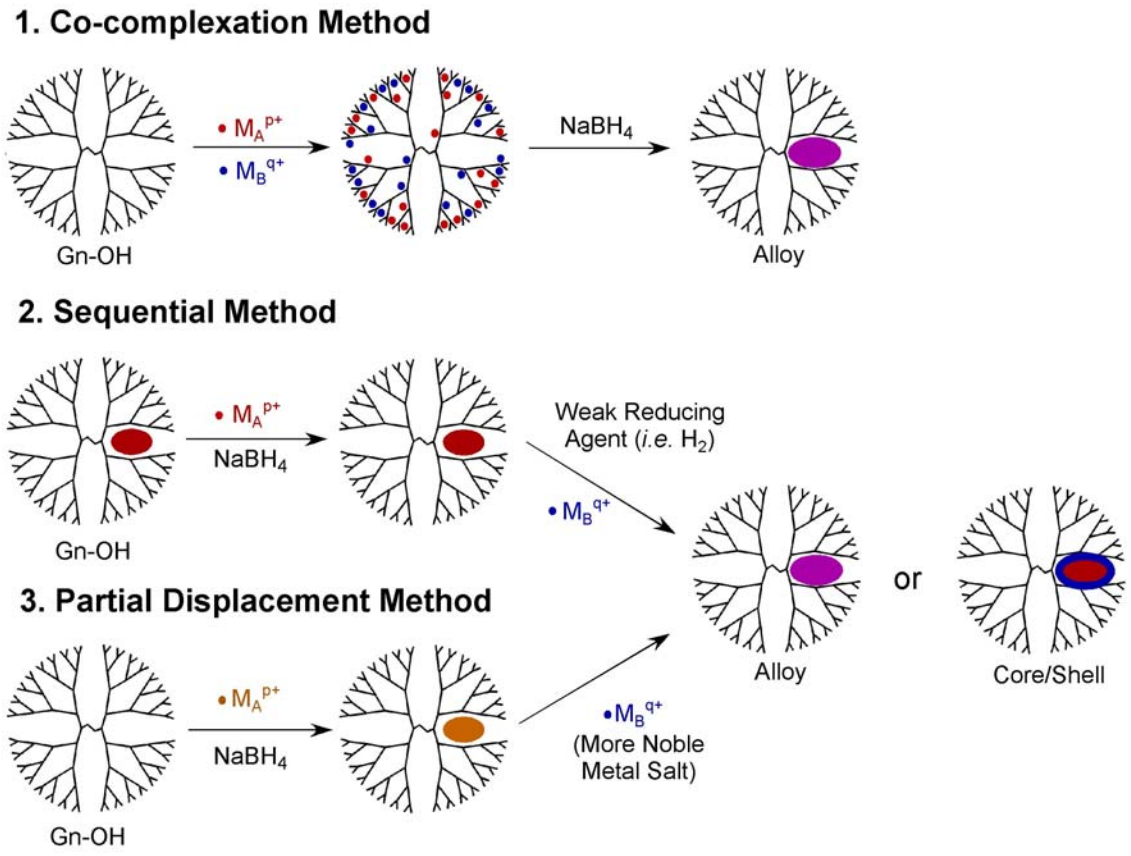

Figure 1.3. Schematic representation of three synthetic methods of bimetallic DENs. (Adapted from ref. 2)

Applications of DENs to Catalysis. The most interesting application of DENs is to utilize them as catalysts. Accordingly, there has been a considerable amount of effort expended in this direction. Monometallic and bimetallic DENs have previously been studied as homogeneous catalysts if they are dissolved in solution and heterogeneous catalysts if they are immobilized on supports.[2,8]

Homogeneous catalysts, Pd DENs have been used in hydrogenation reactions of both linear and branched alkenes in aqueous and methanol solutions. Catalysis has also been used as a tool to study the properties of DENs. These include a study of size-selective hydrogenation as a function of dendrimer generation,[9] a molecular ruler study to investigate the average distance between the surface of Pd DENs and the periphery of its dendrimer host,[8] and a study of the effect of Pd DEN size on hydrogenation.[10] Bimetallic DENs have also been prepared and tested as catalysts for hydrogenation reactions. For example, PdPt alloy[11] and PdAu alloy and core/shell bimetallic DENs[12] having various metal-to-metal ratios were investigated and the alloy particles showed some enhancement in catalytic activity for hydrogenation. In addition, DENs have been used as homogeneous carbon coupling catalysts for the Heck reaction,[13-15] Suzuki reaction,[16] and Stille reaction.[17] In this case, various solvents have been used such as water, organic solvents, biphasic fluorous solvents, and even supercritical CO_2.

DENs have been also immobilized on supports and used as heterogeneous catalysts. In some cases, dendrimers were removed by thermal treatments and the remaining free metal catalysts on supports were active for olefin hydrogenation and CO oxidation reactions.[18-21] However, removal of the dendrimers usually resulted in

increased particle size and size distribution. DENs have also been used as electrocatalysts, which is the main focus of this research. Previously, monolayers of Pt DENs immobilized on Au electrode showed electrocatalytic activity for the oxygen reduction reaction.[7] However, they were not very stable so it was not possible to perform a more detailed electrochemical study using these DEN films.

1.3 Oxygen Reduction Reaction in Fuel Cells

Fuel cells are environmentally clean electrochemical devices, in which chemical energy is converted into electrical energy. In most fuel cells, there are two electrodes which are separated by an electrolyte. Figure 1.4 shows the structure of a H_2/O_2 fuel cell, and its reactions based on the proton exchange membrane fuel cell (PEMFC).[3] Hydrogen gas is oxidized at the anode to produce protons and electrons. The electrons move to the cathode through an external circuit, while the protons move to the cathode through the electrolyte membrane, which should have a low gas permeability. Typical electrolytes include H_2SO_4 and H_3PO_4, and acidic polymer membranes such as Nafion are typically used in commercial fuel cells. At the cathode, oxygen gas is reduced, typically via a Pt catalyst, producing H_2O. The anodic and cathodic half-reactions and their standard electrode potential are shown as:

$2\ H_2 \rightarrow 4H^+ + 4e^-$ $\quad E^0 = 0$ V $\quad$ Anode

$O_2 + 4H^+ + 4e^- \rightarrow 2H_2O$ $\quad E^0 = 1.23$ V $\quad$ Cathode

The overall (cell) reaction is $O_2 + 2H_2 \rightarrow 2H_2O$ $\quad E^0_{cell} = 1.23$ V

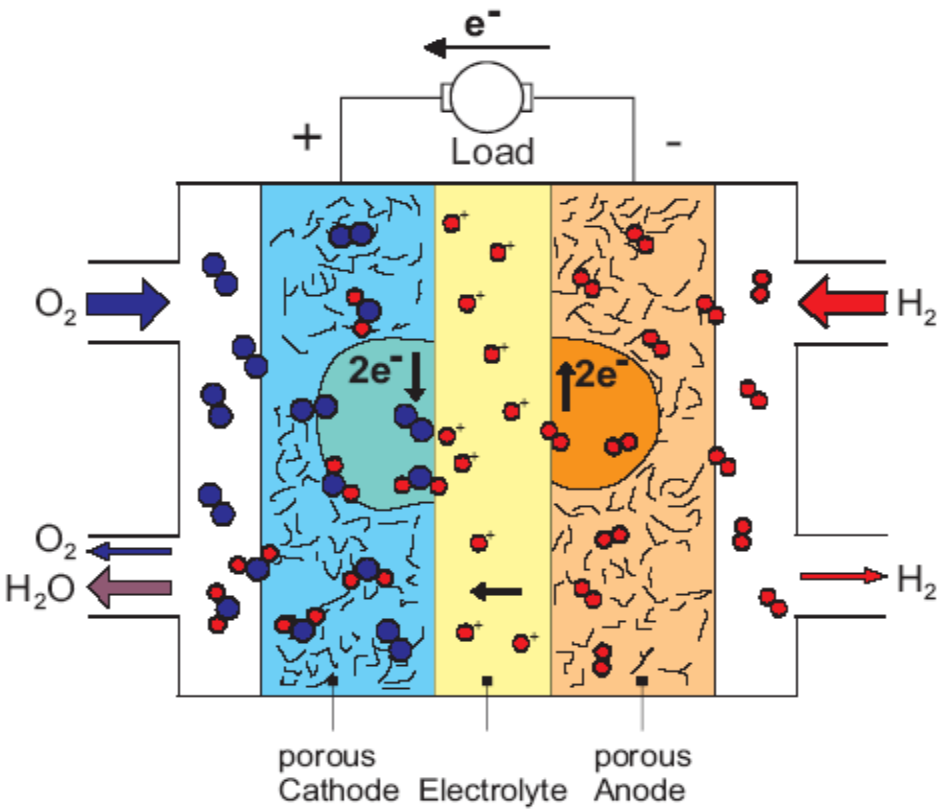

Figure 1.4. Schematic drawing of a H_2/O_2 fuel cell (Adapted from ref. 3)

The E^0_{cell} value (1.23 V) is a theoretical value and cannot be achieved in reality because of the cathode and anode overpotentials (Figure 1.5). Compared with the overpotential of the anode, the overpotential of the cathode is high due to the strong kinetic inhibition of the oxygen reduction reaction (ORR). This leads to cell voltage losses of at least 300 to 400 mV in typical PEMFC operating conditions. The low rate (or exchange current density) for ORR at the cathode is a limiting factor in the efficiency of fuel cells. In addition, oxygen reduction can also occur through an intermediate $2e^-$ H_2O_2 route, which can limit the efficiency of the cell and can be deleterious to the stability of the polymer electrolyte membrane.[3] Therefore, the most effective catalysts to enhance the efficiency of fuel cells should accelerate the kinetics of the ORR at the cathode and minimize the production of H_2O_2. It is well known that Pt is the most effective catalyst for the oxygen reduction. However, the cost of Pt is very high and its supply is limited. Therefore, improvement of ORR catalysts to increase catalytic activity is a very important subject that has been addressed by adding other metals to the Pt catalysts and by reducing particle sizes to achieve high surface area.

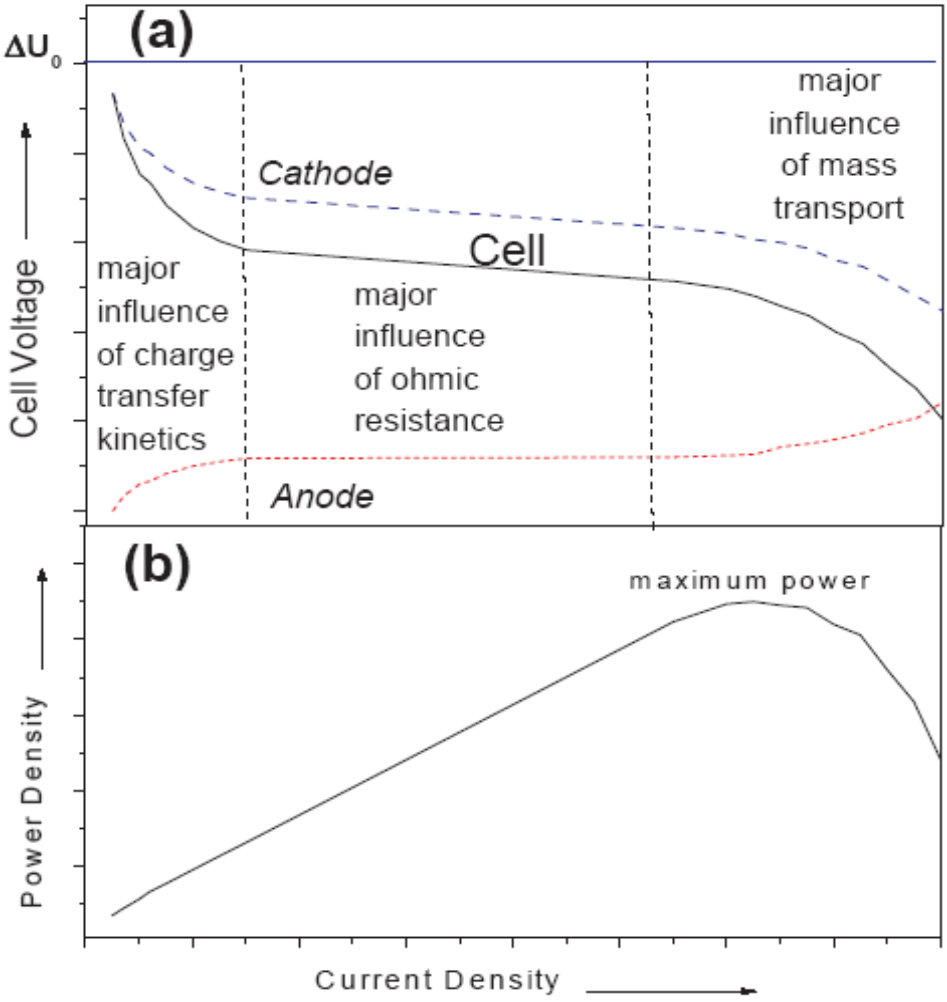

Figure 1.5. Schematic of (a) the fuel cell voltage vs. current density and (b) the power density vs. current density. The cathode and anode overpotentials are shown in (a). (Adapted from ref. 3)

1.4 Bimetallic Catalysts for ORR

The first way to increase the catalytic activity of the ORR and to reduce the cost of the catalysts is to introduce a second or third (cheaper) metal to the Pt catalyst. Some preliminary studies have involved the use of bulk alloy electrodes[22,23] or thin alloy films prepared by sputtering [24,25] to try to quantify the enhancement of catalytic activity for the ORR. However, for the studies of bimetallic nano-catalysts for the ORR, carbon-supported bimetallic catalysts (some of them are commercially available from E-TEK) have been generally used.[26-32] Usually, carbon-supported Pt alloy catalysts are prepared by the impregnation of the second metal on Pt/C and then heating to >700 °C under an inert gas or hydrogen atmosphere. Another way to prepare carbon-supported Pt alloy catalysts is the use of organometallic compounds (e.g. metal carbonyl complex) as precursors. Pt-Sn,[33] Pt-Cr[34] and Pt-Ni[35] alloy catalysts prepared by this method showed small particle size (~3 nm) and narrower size distribution (1.1 – 1.4 nm) than those prepared by the usual method and exhibited very good performance for the catalytic activity studies of the ORR. However, one of the difficulties in studying the alloy effect using supported catalysts is that the activity of supported catalysts can show a wide range of values, because the activity of alloy catalysts depends not only on their composition, but also on their structure, shape, size, and method of preparation.

Various Pt-alloy catalysts such as Pt-Co, Pt-Ni, Pt-Fe, Pt-Sn, and Pt-Cr have been studied so far and most of researchers reported a catalytic activity enhancement for the ORR using these alloy catalysts. For example, Watanabe and coworkers[25] found maximum enhancement factors of 10-20 for Pt alloys with Ni, Co, and Fe, prepared by

sputtering in comparison to pure Pt, while most other researchers[29-31] generally reported ORR activity enhancement by factors of 1.5 to 3 for Pt alloy catalysts. There have been several attempts to explain the enhanced catalytic activity of alloy catalysts by factors such as structure and electronic effects. Jalan and Taylor[36] investigated various Pt-based alloy catalysts for the ORR and observed the enhancement of catalytic activity. They suggested that this enhanced catalytic activity of alloy catalysts is due to the shorter nearest-neighbor distance between Pt atoms. Min *et al*.[30] reported ORR activity enhancement with carbon-supported Pt-Co, Pt-Cr, and Pt-Ni catalysts is due to the reduced Pt-Pt neighboring distance which is favorable for the adsorption of O_2. Electronic factors related to d-band vacancies are also reported as the reason of enhanced catalytic activity of Pt alloys for the ORR. Mukerjee *et al*.[29] correlated the enhancement of catalytic activity not only with favorable Pt-Pt interatomic distance (geometric factor) but also with an increase in the Pt d-band vacancy (electronic factor) based on in situ EXAFS and XANES investigation of Pt-Cr, Pt-Mn, Pt-Fe, Pt-Co, and Pt-Ni catalysts. They also report that the electronic factor of alloy catalysts induces lower coverage of oxygenated species, which are inhibitors for ORR, from electrolytes on Pt atoms. Similarly, Markovic and coworkers proposed that the change in ORR activity was due to an inhibition in the formation of surface Pt-oxygenated species bonds, due to the ease of oxidation of nearby Co or Ni atoms.[4] Watanabe and coworkers postulated that the increase in activity of the Pt atoms on the alloy electrode surface was due to increased vacancy in the Pt 5d orbitals.[25] This electronic effect would lead to increased strengths of Pt-oxygen interactions, which would weaken the O-O bonds and result in fast bond

scission and new bond formation, as shown in Figure 1.6.[25] Proof of this conjecture was shown by sputtering Pt onto alloy catalysts. Upon increase of the pure Pt layer beyond 4 nm the ORR activity approaches that of pure Pt. Some recent theoretical studies provide insight into the origin of activity enhancements in bimetallic ORR catalysts.[37-42] Finally, there have also been a number of recent studies to eliminate Pt from ORR catalysts, and some of materials have shown ORR activities corresponding to that of Pt.[43-45]

On the other hand, there have been several reports which did not observe enhancement of catalytic activity on Pt alloys. Glass *et al*. reported that Pt-Cr alloy catalysts for the ORR are not as active as pure Pt catalysts in phosphoric acid due to the bulk nature of the electrodes used in their study.[22] Beard and Ross also reported that the activity of the Pt-Co alloy is lower than that of the pure Pt and that stability is not as good as that of pure Pt.[28]

1.4 Particle Size Effect of ORR Catalysts

To enhance the kinetics of the ORR and to reduce the amount of Pt-catalyst needed, introduction of nano-sized Pt particles as ORR catalysts was essential because as the particle size gets smaller, the surface-to-volume ratio increases, which should lead to higher catalytic efficiency for the same amount of Pt. Interestingly, it has been found that smaller Pt nanoparticles do not always give better catalytic efficiency with the same mass of Pt for ORR. There are two kinds of catalytic activities that have been used in the literatures. The first one is called ‘mass activity’ and is defined as catalytic activity

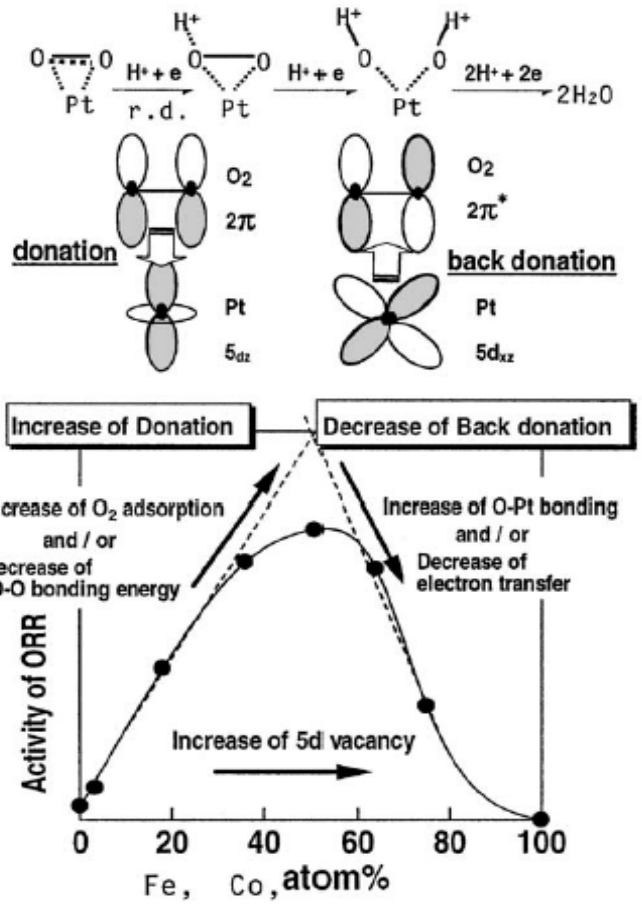

Figure 1.6. Schematic representation of enhancement of ORR by electronic effects. (Adapted from ref. 25)

normalized by the mass of Pt catalysts. There is another way to represent catalytic activity, which is the 'specific activity' defined as catalytic activity normalized by the surface area of Pt catalysts. Ideally, if the particle-size effect does not exist, the mass activity should go up with a decrease of Pt catalyst size and the specific activity should be the same for all range of Pt catalyst sizes. However, several reports have shown particle-size effects of Pt catalysts for the ORR, which means that specific activity decreases with decreased particle sizes, especially in nanometer-size range. It is not well understood what causes these particle-size effects.

Kinoshita proposed correlation of geometric consideration with the particle size effect.[46] Small Pt particles are generally assumed to be cubo-octahedral structures consisting of Pt atoms arranged on (100) and (111) crystal faces bounded by edge and corner atoms. The concentration of different site (crystal faces, edges, corners) changes a lot as the particle size decrease from 15 nm to 1 nm. Figure 1.7[46] shows the relationship between particle size and the different surface sites for particles having a cubo-octahedral structure. In this figure, the distribution of surface atoms is normalized by the total number of atoms in the particle (MAD) and by the surface of the particle (SAD). Interestingly, the maxima in MAD (100) and (111) crystal faces are observed at a particle size of ~3.5 nm and ~2 nm, respectively. On the other hand, SAD (100) and (111) decrease with a decrease in particle size. Therefore, they suggested that the maximum in mass activity, which has been observed at ~3.5 nm in several studies,[47,48] is attributed to the maximum in the surface fraction of Pt atoms on the (100) and (111) crystal faces, which are probably the active sites for the ORR.

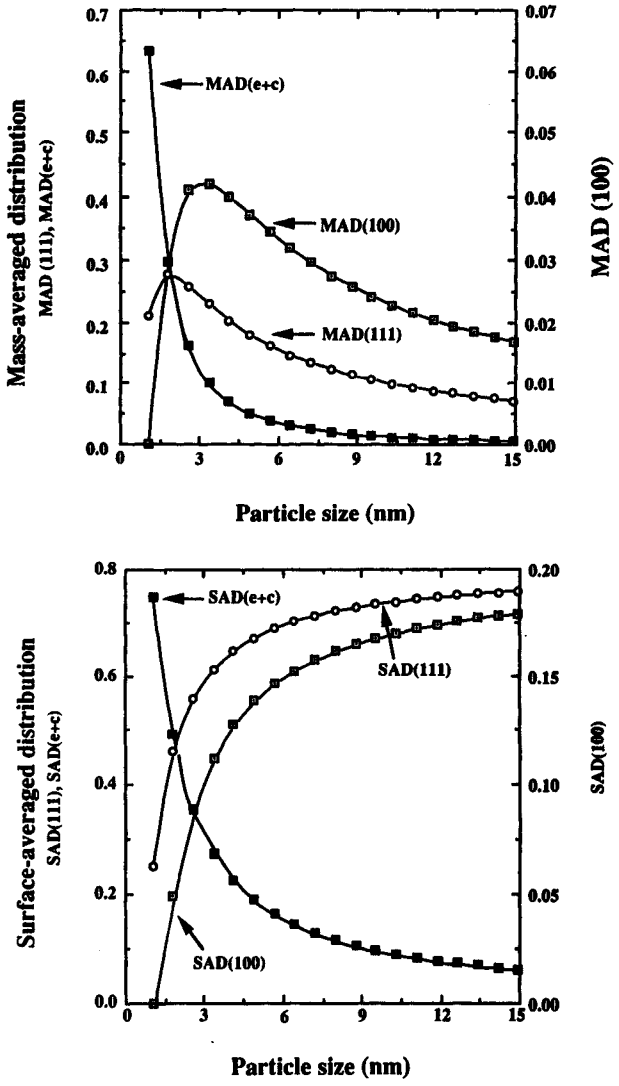

Figure 1.7. Mass-averaged distribution and surface-averaged distribution of atoms on the (111) and (100) crystal faces and on the edge and corner sites of a cubo-octahedral. (Adapted from ref. 46)

There is another way to explain the origin of particle size effect. In this case, the origin of particle size effects in the ORR is attributed to stronger adsorption of oxygenated species on smaller Pt particles. Chung et al.[26] showed that the dependence of peak potential for oxide reduction (adsorption strength of OH) on the particle size is identical to the specific activity results of various particle sizes. A more negative potential, which means stronger adsorption of OH, is observed with smaller particles and this adsorbed OH acts as an inhibitor of the ORR. Takasu *et al.*[49] also reported that particle-size effects correlated to an increase in adsorption strength of oxygenated species with a decrease in Pt particle size. This was derived from XPS measurements of core-level binding energy of electrochemically prepared Pt particles on a glassy carbon electrode. These results were also supported by Mukerjee and coworkers using in situ X-ray absorption spectroscopy (XAS).[27] They examined several carbon-supported Pt electrocatalysts with particle sizes in the range of 2.5 nm to 9 nm with XAS. The results show that as the particle size is reduced below 5 nm, the strength of adsorption of H, OH and CO is increased. They concluded that the reduced specific activity for ORR in small particles is due to the strong adsorption of OH. Most recently, Mayrhofer *et al*. reported particle size effect using carbon-supported Pt nanoparticles with mean diameters of 1-1.5 nm, 2-3 nm, 5 nm, and 30 nm.[50] In this work, the potential of total zero charge obtained from measurements of the CO displacement charge shifts approximately 35 mV negative by decreasing the particle size from 30 nm to 1 nm, which means that the adsorption of oxygenated species becomes stronger with small particles and the surface coverage of oxygenated species increases with decreasing particle size at the same potential. The

high coverage of oxygenated species in small particles leads to a decrease in specific activity for ORR because oxygenated species block the active sites required for the adsorption of O_2 or the splitting of O-O bond. However, in the case of CO bulk oxidation, small particles show better specific activity because adsorbed oxygenated species act as promoters of CO bulk oxidation.

Some researchers have suggested completely different explanations for the particle-size effect.[51-53] Watanabe and coworkers reported that particle-size effect is not really dependent on the size of Pt particle size, but rather on the interparticle distance in the support. That is, sufficiently separated nanoparticles (> 20 nm separation) show no particle-size dependence of specific activity for the ORR.[52,53]

There is one more interesting report about particle-size effect for the ORR. This report showed that Pt-Fe alloy catalysts do not exhibit a particle-size effect, while pure Pt catalysts have normal particle-size effect.[26]

CHAPTER II

EXPERIMENTAL

2.1 Synthesis of DENs

The poly(amidoamine) (PAMAM) dendrimers used in this study were purchased from Dendritech, Inc. (Midland, MI). DENs are prepared in two steps. First, metal salts and dendrimers are mixed and stirred in solution with fixed stoichiometries. In this process, metal ions are extracted into dendrimers and coordinate with interior functional groups. Second, the metal-ion/dendrimer composites are reduced with $NaBH_4$ to yield encapsulated nanoparticles. More detailed procedures to prepare DENs are described in the experimental section in each chapter.

2.2 Rotating Disk Voltammetry

Rotating disk voltammetry is a used hydrodynamic voltammetry technique in which the mass transport is controlled by the rotation rate of the electrode. Figure 2.1 shows a scheme of rotating disk voltammetry setup, a bottom view of a rotating disk electrode (RDE) and a rotating ring-disk electrode (RRDE), and a typical rotation disk voltammogram. By using this technique, it is possible to obtain detailed and quantitative kinetic information about electrochemical reactions. To obtain kinetic information from rotating disk voltammograms (RDVs), Koutecky-Levich equation (Eq. 2.1) and the corresponding plot of $1/j$ vs. $1/\omega^{1/2}$ are used.

$$\frac{1}{j} = \frac{1}{j_K} + \frac{1}{0.20nFD_O^{2/3}\omega^{1/2}\nu^{-1/6}C_O} = \frac{1}{j_K} + \frac{1}{B\omega^{1/2}} \quad (2.1)$$

j : Measured current density (mA/cm^2)

j_K : Kinetic current density (mA/cm^2)

F : Faraday constant (96485 C/mol)

D_O : Diffusion coefficient of O_2 (cm^2/s)

ω : Electrode rotation rate (rpm)

ν : Kinematic viscosity (cm^2/s)

C_O : Concentration of O_2 (mol/cm^3)

A Tafel plot (potential vs. kinetic current density) is used to display the kinetic data and to compare them as a function of potential and catalyst structure. More detailed information and practical applications of the RDE re provided in the Results and Discussion part of Chapter VI.

The rotating ring-disk electrode has a ring electrode around the disk electrode (Figure 2.2b), which makes it possible to measure the product distribution of electrochemical reactions. For example, the oxygen reduction reaction has two possible products (H_2O and H_2O_2) depending on the reaction pathway. The H_2O_2 can be selectively oxidized at the ring electrode by applying the proper potential. Figure 2.1c shows a typical RDV and the corresponding ring current. Comparison of the magnitudes of disk and ring currents provides information about product distributions. This is

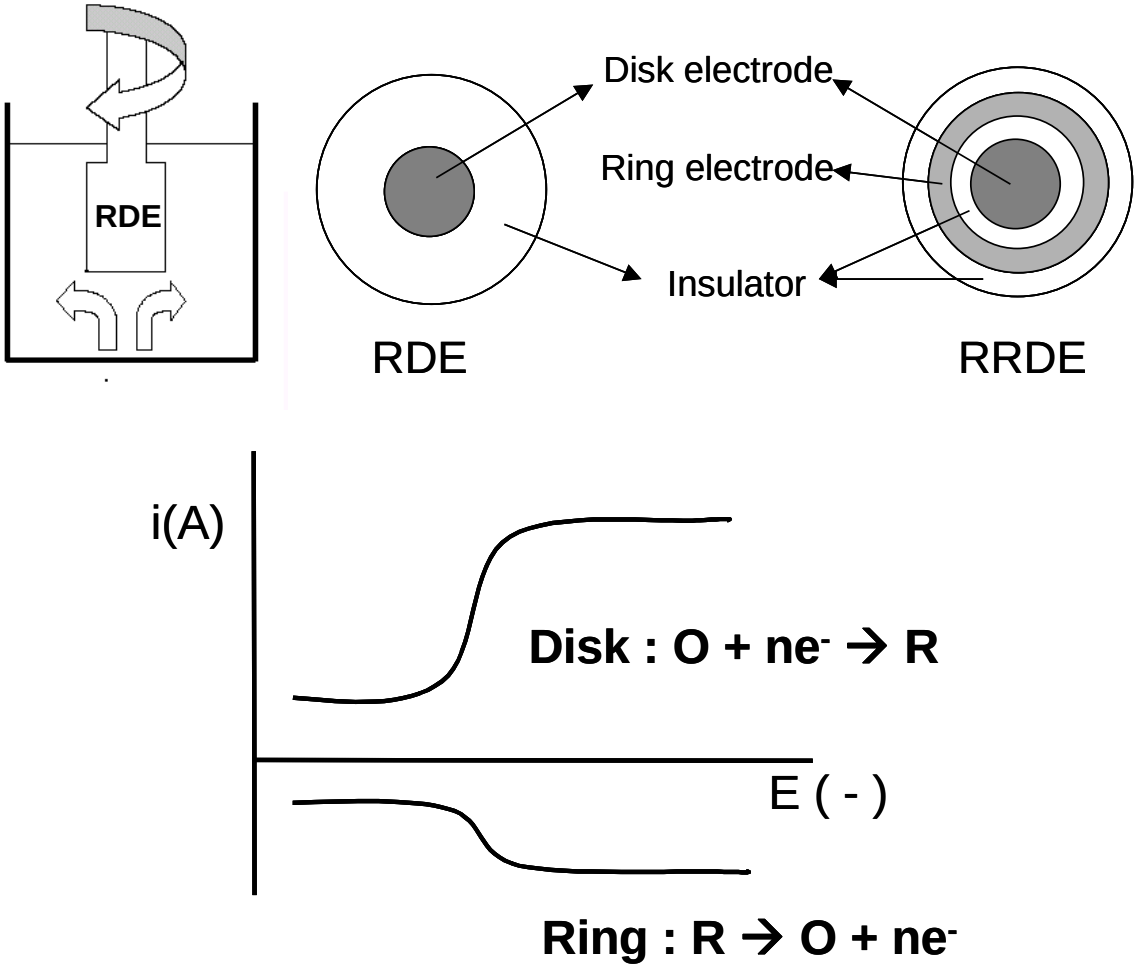

Figure 2.1. (a) Schematic of a rotating electrode voltammetry setup. (b) Bottom view of rotating disk electrode (RDE) and rotating ring-disk electrode (RRDE). (c) A typical rotating-ring disk voltammogram.

important because H_2O_2 can lower the efficiency of fuel cells and decrease the stability of the polymer electrolyte membranes.

2.3 Additional Techniques

Transmission Electron Microscopy and Energy Dispersive Spectroscopy. Transmission electron microscopy (TEM) is an advanced microscopic technique that provides very high spatial resolution (up to 0.1 nm). It has been used to investigate biological samples such as DNA and viruses, and nano-sized materials. As for a normal optical microscope, a beam is passed through lenses to generate a magnified image of a sample. However, electromagnetic lenses are used instead of glass lenses, so the adjustment of lenses and magnification can be done easily by changing the lens current. Highly energetic electron beams are used under high vacuum instead of visible or ultra-violet light, which enables one to obtain a high resolution compared to a usual optical microscope. In this research, the TEM technique is mainly used to examine shape, size, and size distribution of DENs. The TEM images have been obtained using JEOL-2010 TEM and JEOL-2010F TEM. The cross section of JEOL-2010F TEM column is shown in Figure 2.2.

TEM does not provide elemental information about samples. Therefore, a TEM is generally equipped with an elemental analysis technique. The most common and powerful technique used for this is energy dispersive spectroscopy (EDS). In EDS, when an electron beam hits a sample, characteristic X-rays are generated depending on the present elements. These x-rays are analyzed by an EDS detector (here, an Oxford INCA

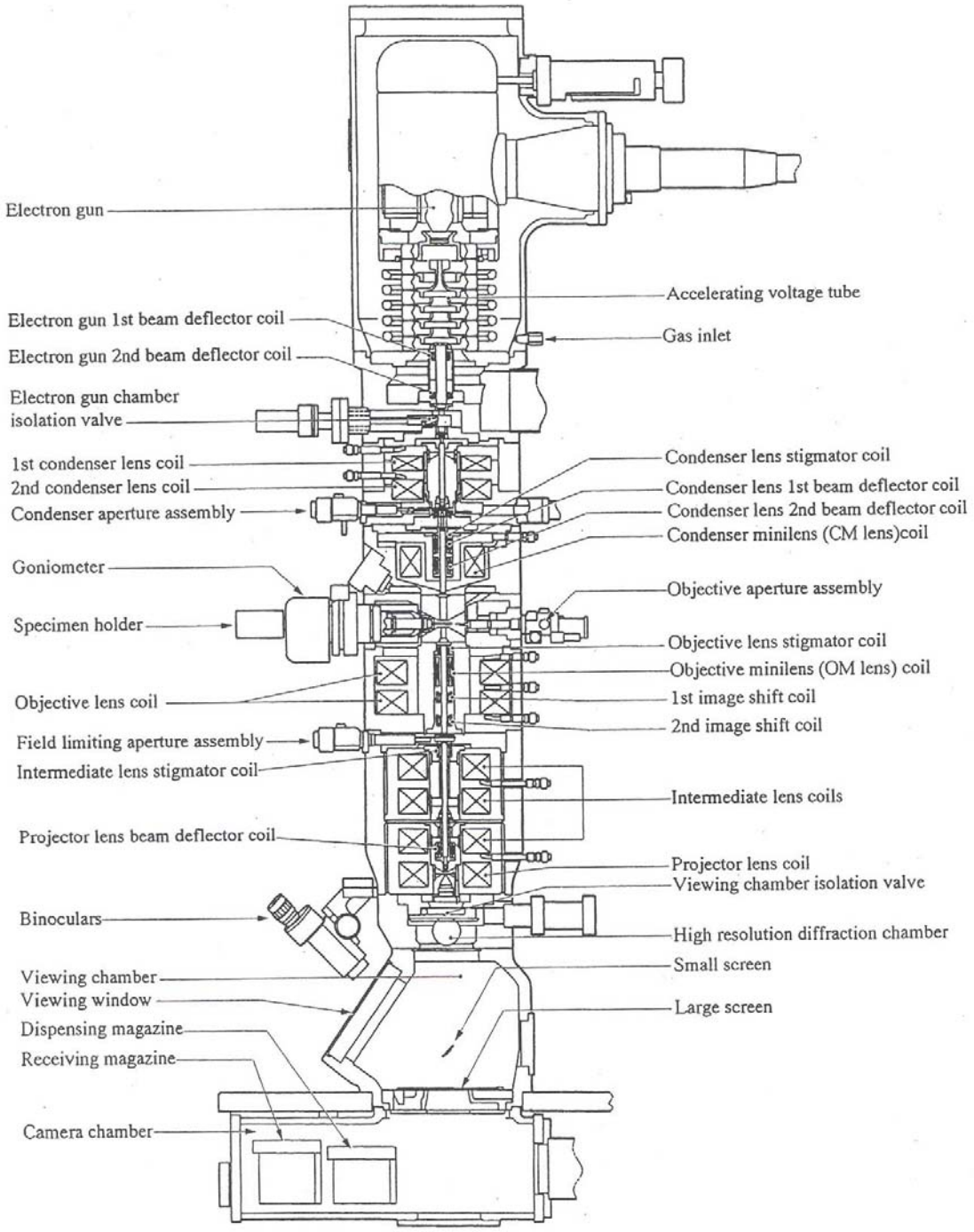

Figure 2.2. Cross section of TEM column. (Taken from ref. 54)

EDS) and the results contain not only qualitative elemental information but also quantitative elemental information. More importantly, this method can be applied to particles as small as 1 nm, which makes it possible to quantitatively analyze a single DEN particle. In the work reported here, EDS is used to analyze the composition of bimetallic DENs.

X-ray Photoelectron Spectroscopy. X-ray photoelectron spectroscopy (XPS) is an electron spectroscopic method used to analyze composition of solid surfaces. XPS provides not only elemental information of samples but also information about the structure and oxidation state of the compounds. Figure 2.3 is a schematic illustration of the basic operative process in XPS. An X-ray beam having known energy (hν) irradiates a sample and photoelectrons, which have different kinetic energies (KE) depending on the binding energy (BE) of the electrons, are emitted. The energy of emitted electrons can be represented as

$$KE = h\nu - BE - w$$

where w is the work function of the spectrometer. The BE of an emitted electron is characteristic of the atom and orbital from which the electron is emitted. In this our research, XPS is used to quantitatively analyze the elemental composition and oxidation state of atoms in DENs after they are immobilized on electrode surfaces. The spectra were acquired using an Axis His 165 Ultra (Kratos, Manchester, UK) with a Mg K_α X-ray source.

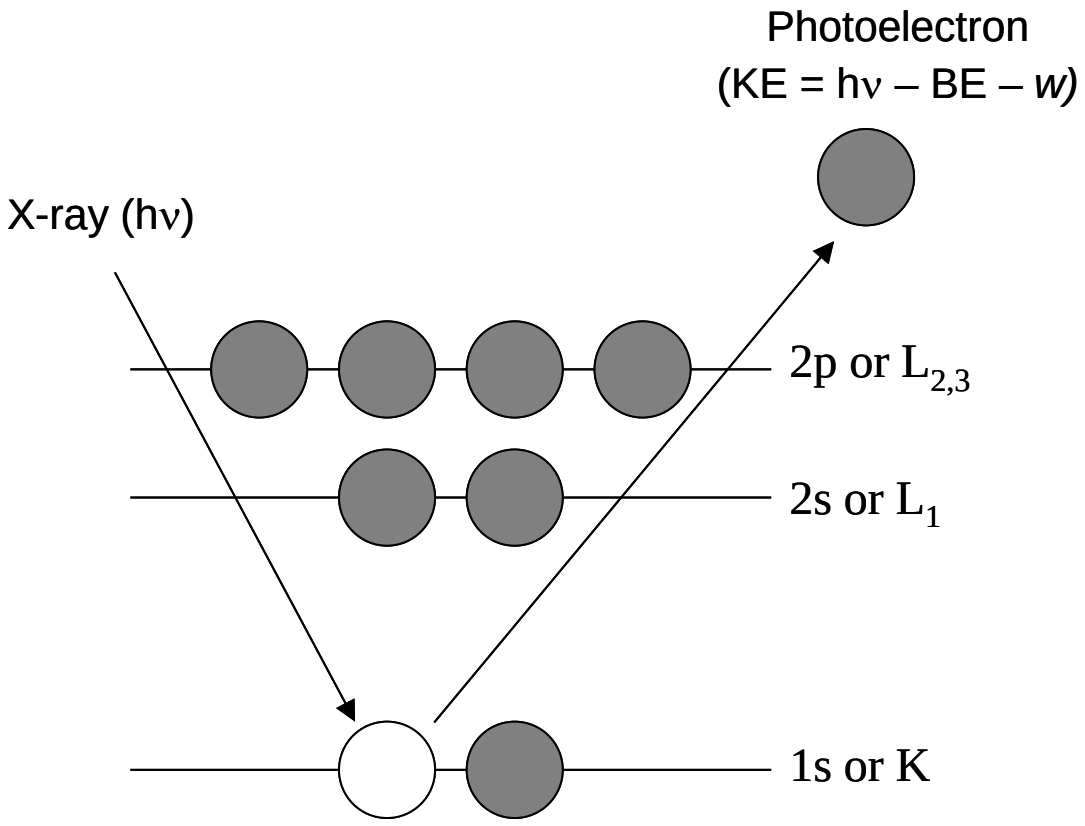

Figure 2.3. Schematic illustration of generating a photoelectron in XPS.

CHAPTER III

SYNTHESIS, CHARACTERIZATION, AND STABILITY OF DENDRIMER-ENCAPSULATED PALLADIUM NANOPARTICLES*

3.1 Synopsis

Here, we report on the synthesis, physical and chemical properties, and stability of Pd nanoparticles encapsulated within poly(amidoamine) (PAMAM) dendrimers. Specifically, amine- and hydroxyl-terminated PAMAM dendrimers ranging in generation from 4 to 8 were studied. Under appropriate conditions, addition of K_2PdCl_4 results in covalent attachment of the $PdCl_3^-$ hydrolysis product of this complex to tertiary amines within the dendrimers. Reduction with $NaBH_4$ results in conversion of dendrimer-encapsulated $PdCl_3^-$ to nearly size monodisperse, encapsulated, zerovalent Pd nanoparticles. Details regarding the Pd species present in solution and within the dendrimer prior to reduction are reported, as is the maximum Pd^{2+} loading of the dendrimers. Dendrimer-encapsulated Pd nanoparticles undergo oxidation in air, but this process is slowed significantly when coordinating ions are removed from solution. In the absence of O_2, dendrimer-encapsulated Pd nanoparticles are stable indefinitely. The oxidation product is not PdO, but rather Pd ions coordinated to the dendrimer interior. Dendrimer generation does not affect the rate of Pd oxidation. The dendrimer itself undergoes irreversible oxidation in the presence of O_2. Finally, the oxidation of

* Reprinted with permission from Scott, R. W. J.; Ye, H.; Henriquez, Ronald R.; Crooks, R. M. *Chem. Mater.* **2003**, *15*, 3873-3878: copyright 2003 American Chemical Society.

dendrimer-encapsulated Pd nanoparticles is reversible. Specifically, H_2 gas can be used to re-reduce partially oxidized Pd nanoparticles without changing their average size.

3.2 Introduction

Here, we report on the synthesis, physical and chemical properties, and stability of Pd nanoparticles encapsulated within poly(amidoamine) (PAMAM) dendrimers.[1,55] This study is motivated by recent applications of Pd dendrimer-encapsulated nanoparticles (DENs) to catalysis,[1,9,13-16,56-59] and the corresponding need to better understand the fundamental properties of this emerging class of materials. The following four new findings have implications relating to the use of these materials for that purpose. First, the maximum Pd ion loading in the dendrimer is correlated, in a 1:1 stoichiometric ratio, to the number of interior amines available for complexation. Second, Pd DENs can be synthesized within amine-terminated Pd DENs by controlling solution pH. Third, the oxidative stability of Pd DENs is significantly improved by removal of solution-phase impurities. Fourth, exposure to hydrogen reversibly converts partially oxidized Pd DENs back to the zerovalent state, which is significant in the context of catalyst recycling.

DENs are prepared using a template approach in which metal ions are sequestered within the dendrimer and then reduced (Figure 3.1).[1,55,60] As a consequence of this synthetic approach, the encapsulated metal particles do not agglomerate and can be nearly monodisperse in size. Metals such as Pd, are of special interest because even when encapsulated within dendrimers a substantial fraction of their surface is unpassivated and

therefore catalytically active. Specifically, Pd DENs have been shown to be active for hydrogenation[9,14,56-59] and carbon-coupling[13-16] reactions. Finally, the dendrimer itself can be used to discriminate between substrates, which provides a means for imparting selectivity to intrinsically nonselective Pd catalysts,[9,56,59] and the periphery can be tailored to control solubility of the catalyst.[13,14,57,58] Since our original report,[60] other types of metallic,[7,61,62] bimetallic,[11,63] and semiconductor[64] DENs have been reported by our group and others.

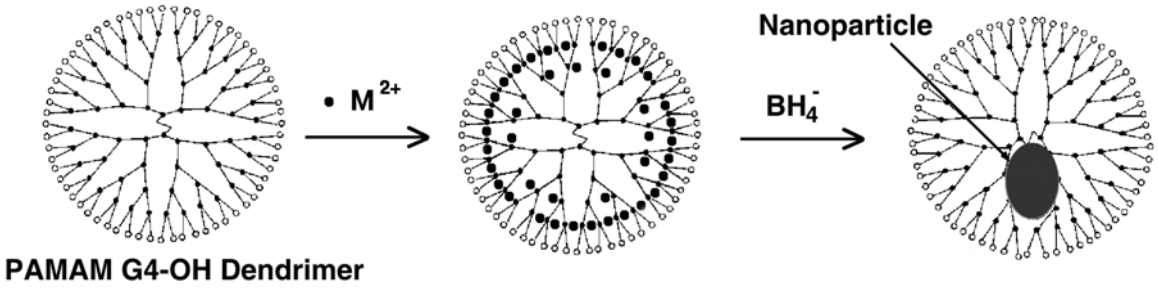

Figure 3.1. Schematic illustration of preparation of DENs.

The results of this study show that the maximum loading of K_2PdCl_4 into both hydroxyl- and amine-terminated dendrimers correlates with the number of available interior amine binding sites. UV-vis absorption spectroscopy and X-ray photoelectron spectroscopy (XPS) indicate that Pd DENs, prepared by chemical reduction, are prone to air oxidation. Purification of DENs by dialysis improves their stability, however, and the oxidation by air is reversible upon exposure to hydrogen gas. A key objective of this report is to provide a detailed synthetic procedure for preparing Pd DENs using either

hydroxyl- or amine-terminated PAMAM dendrimers and describe the optimal conditions under which they can be stored and used.

3.3 Experimental Section

Materials. Hydroxyl-terminated fourth-, sixth-, and eighth-generation (G4-OH, G6-OH, and G8-OH, respectively) and amine-terminated fourth-generation (G4-NH_2) PAMAM dendrimers having ethylenediamine cores were obtained as 10-25% methanol solutions (Dendritech Inc., Midland, MI). Prior to use the methanol was removed under vacuum at room temperature. K_2PdCl_4 (Strem Chemicals Inc.) and $NaBH_4$ (Aldrich Chemical Co., Milwaukee, WI) were used without further purification. 18 MΩ·cm Milli-Q deionized water (Millipore, Bedford, MA) was used to prepare aqueous solutions. Cellulose dialysis sacks having a molecular weight cutoff of 12,000 were purchased from Sigma Diagnostics Inc.

In a typical preparation of G4-OH dendrimers containing nominally 40-atom nanoparticles (G4-OH(Pd_{40})), 125 μL of a 0.5 mM aqueous solution of G4-OH dendrimer was dissolved in 9.8 mL of deionized water, followed by slow addition of 25 μL of an aqueous 0.1 M K_2PdCl_4 solution with stirring. After stirring for 1 h, 50 μL of a freshly prepared, aqueous 1.0 M $NaBH_4$ solution was added. G6-OH(Pd_{40}) and G8-OH(Pd_{40}) DENs were prepared via the same route by substituting G6-OH and G8-OH solutions for the G4-OH dendrimer solution. G4-NH_2(Pd_{40}) DENs were prepared by a similar route except that the pH of the G4-NH_2 solution was adjusted to 3 by addition of

HCl prior to addition of K_2PdCl_4. After addition of $NaBH_4$ (which results in a significant pH increase), HCl was added to the solution to maintain a pH of ~8.

Characterization. Absorption spectra were recorded on a Hewlett-Packard HP 8453 UV-vis spectrometer. The optical path length was 1.0 cm, and deionized water or aqueous dendrimer solutions were used as references. XPS data were acquired using an Axis HSi 165 Ultra Kratos instrument (Manchester, UK). XPS data acquisition employed an Al anode set at 15 mA and 15 kV. The carbon peak at 285.0 eV was used as an internal reference. High-resolution transmission electron micrographs (HRTEM) were obtained with a JEOL-2010 microscope having a point-to-point resolution of 0.19 nm. Samples were prepared by placing a drop of solution on a holey-carbon-coated Cu TEM grid and allowing the solvent to evaporate in air.

3.4 Results and Discussion

Figure 3.2a shows UV-vis spectra of dilute aqueous solutions of K_2PdCl_4 in deionized water. The aqueous Pd salt has two strong ligand-to-metal charge-transfer bands at 207 nm ($\varepsilon = 9000\ M^{-1}\ cm^{-1}$) and 235 nm ($\varepsilon = 4400\ M^{-1}cm^{-1}$). These two bands correspond to literature values for the hydrolysis product $PdCl_3(H_2O)^-$.[65] Upon addition of the G4-OH dendrimer, a single UV-vis band is observed at $\lambda_{max} = 224$ nm ($\varepsilon = 16{,}500\ M^{-1}cm^{-1}$, Figure 3.2b) at Pd:G4-OH ratios of less than 80. This peak corresponds to a ligand-to-metal charge-transfer (LMCT) band associated with complexation of the complex Pd anion to interior tertiary amines of the G4-OH dendrimer.[56] Complexation likely occurs via displacement of water from $PdCl_3(H_2O)^-$, followed by covalent reaction

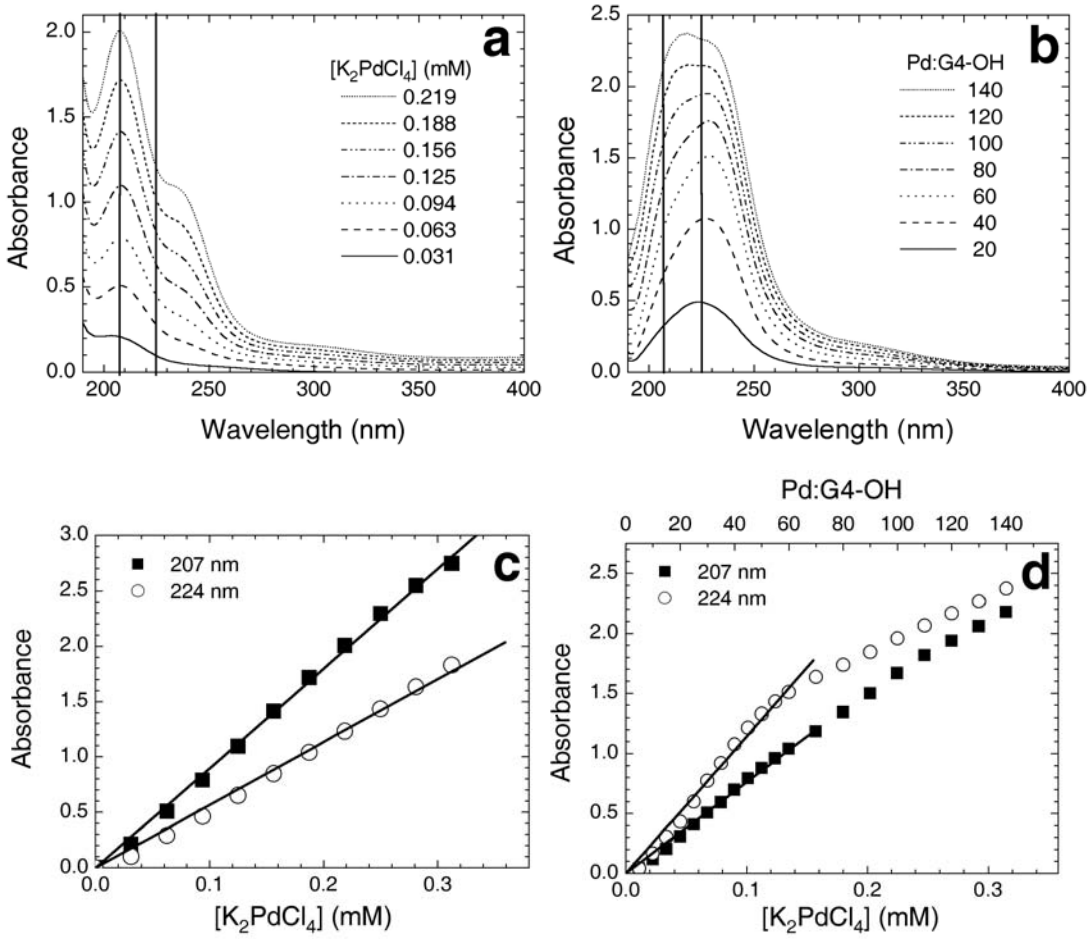

Figure 3.2. UV-vis absorbance spectra of (a) aqueous K_2PdCl_4 solutions and (b) G4-OH/K_2PdCl_4 solutions containing different Pd:G4-OH ratios. The concentration of G4-OH was 3.125 μM in both cases. Each spectrum was obtained 5 min after addition of K_2PdCl_4. (c) and (d) are Beer-Lambert plots obtained at 207 and 224 nm from the plots of (a) and (b), respectively.

with the interior tertiary amines of the dendrimer. This contention is supported by XPS data indicating a 1:3 Pd:Cl ratio after dialysis of G4-OH$(Pd^{2+})_{40}$ solutions prepared using K_2PdCl_4. Moreover, Ooe et al. have recently shown evidence of a strong interaction between Pd^{2+} and interior amines of PAMAM dendrimers using ^{14}N NMR.[59] Absorbance spectra of G4-OH$(Pd^{2+})_{40}$ solutions obtained before and after dialysis in water for several days were identical. This means that $PdCl_3^-$ is strongly bound to the G4-OH dendrimer; that is, that the amount of free $PdCl_3(H_2O)^-$ in solution is negligible. At Pd:G4-OH ratios greater than 80, a shoulder is apparent at ~215 nm and the peak at 224 nm broadens significantly. This is a consequence of the superposition of peaks corresponding to both dendrimer-encapsulated $PdCl_3^-$ (224 nm) and free $PdCl_3(H_2O)^-$ in solution (207 and 235 nm) at Pd ion concentrations exceeding that which can be accommodated by the dendrimer.

Figure 3.2c and d show Beer-Lambert plots at 207 and 224 nm derived from the absorbance spectra shown in Figure 3.2a and b, respectively. For aqueous K_2PdCl_4 solutions the plot is linear throughout the concentration range studied (Figure 3.2c), but plots obtained at the same wavelengths for solutions containing both G4-OH and K_2PdCl_4 are linear only up to Pd:G4-OH ratios of ~55 ± 5 (Figure 3.2d). These results suggest a maximum loading of ~55 ± 5 Pd ions per dendrimer.

The data in Figure 3.2c and d were used to obtain the titration data shown in Figure 3.3a. These plots of the concentration of dendrimer-encapsulated and free Pd ions as a function of the Pd:G4-OH ratio, were calculated using the Beer-Lambert Law for a multi-component system (Eqs. 3.1 and 3.2).

$$A(207\ nm) = \sum \varepsilon_1(207\ nm)c_1 l + \sum \varepsilon_2(207\ nm)c_2 l \qquad (3.1)$$

$$A(224\ nm) = \sum \varepsilon_1(224\ nm)c_1 l + \sum \varepsilon_2(224\ nm)c_2 l \qquad (3.2)$$

Here, c1 and c2 are the concentrations of $PdCl_3^-(H_2O)$ and intradendrimer, amine-coordinated $PdCl_3^-$, respectively. These results show that there is a maximum loading of 60 ± 5 Pd ions within the G4-OH dendrimers. Because there are 62 interior tertiary amines in G4-OH dendrimer, this result implies that each Pd ion is strongly coordinated with a single tertiary amine.

The behavior of G4-NH_2 dendrimers in the presence of K_2PdCl_4 solutions is different from that of the G4-OH dendrimers. Specifically, addition of K_2PdCl_4 to a solution of G4-NH_2 in deionized water results in immediate agglomeration and the formation of a white precipitate, presumably due to crosslinking of the dendrimers by Pd ions.[57,66] Such agglomeration is not observed for Gn-OH dendrimers, which emphasizes the poor affinity of Pd ions for hydroxyl groups. Agglomeration is avoided at pH < 5, however, because the peripheral primary amines of the dendrimers are completely protonated and thus unable to crosslink via Pd ions.[57,67,68] Figure 3.3b shows the results of a spectrophotometric titration of G4-NH_2 with K_2PdCl_4 carried out at pH 3. Consistent with the results for G4-OH, a maximum of 60 ± 5 Pd ions coordinate to each G4-NH_2 dendrimer under these conditions. That is, the peripheral primary amines remain protonated at low pH, even in the presence of Pd ions, whereas the interior tertiary amines are available for reaction. However, we find that much longer times (5-

10 min) are required for complete reaction between $PdCl_3(H_2O)^-$ and G4-NH_2 compared to G4-OH (< 1 min). A recent report from our group indicates that in the absence of metal ions over 95% of the interior amines in G4-NH_2 dendrimers are protonated at pH 3.[68] This suggests that the rate of the covalent reaction between $PdCl_3(H_2O)^-$ and the tertiary amines is slowed by the presence of competing protons. Titration of a G4-NH_2 solution with K_2PdCl_4 at pH 1.5 revealed no interaction between the dendrimer and the Pd ions even after 24 h.

Figure 3.4a shows absorbance spectra of G4-OH$(Pd^{2+})_{40}$ prior to reduction and after reduction with different mole ratios of $NaBH_4$. If the solutions used to obtain these spectra are kept under N_2, then they do not aggregate for at least 180 days. Three aspects of these spectra merit comment: first, as the amount of $NaBH_4$ used for the reduction increases, the well-defined LMCT peak of G4-OH$(Pd^{2+})_{40}$ present at 224 nm decreases; second, there is an increase in the featureless absorbance that monotonically increases towards higher energy; and third an isosbestic point is present at 258 nm. The first observation indicates that Pd^{2+} is consumed during reduction, and the second observation is a consequence of the continuous absorption arising from interband transitions of the newly formed intradendrimer Pd colloids.[56,69-71] The isosbestic point indicates that the Pd^{2+} present prior to reduction is exclusively converted to a single species, which we identify as zerovalent Pd. A large excess of $NaBH_4$ is required for complete Pd ion reduction, because parasitic proton reduction, which is significant under the conditions used for these experiments (initial pH = 4), competes for reducing equivalents.

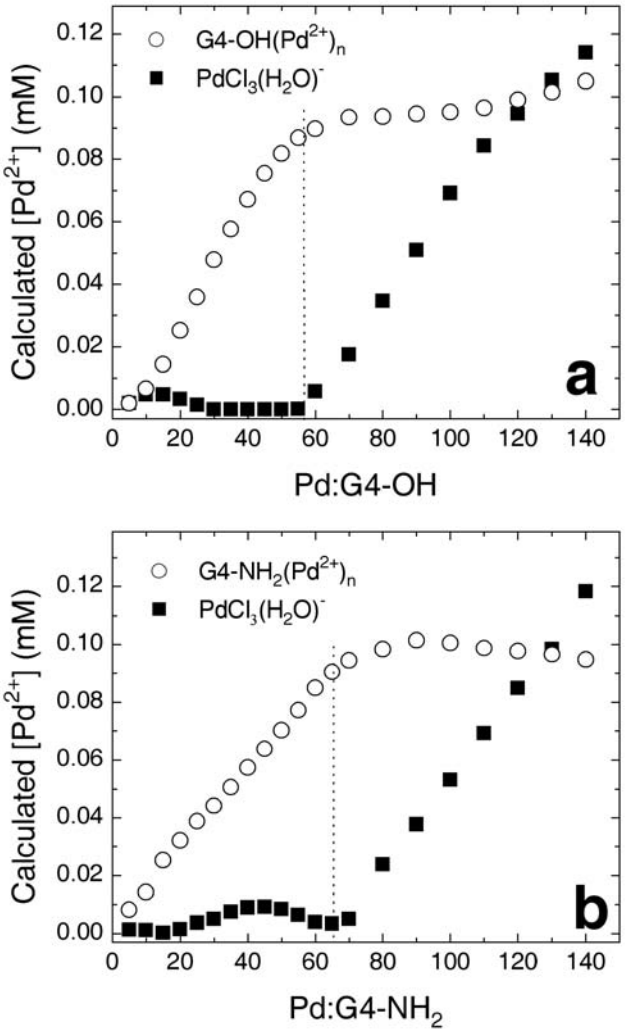

Figure 3.3. Plots of the concentration of free $PdCl_3(H_2O)^-$ and dendrimer-encapsulated Pd^{2+} as a function of the total Pd:dendrimer mole ratio. In (a) the dendrimer is G4-OH and in (b) it is G4-NH_2. The concentrations were calculated using Eqs. 3.1 and 3.2 and values obtained from the Beer-Lambert plots (shown for the G4-OH$(Pd^{2+})_n$ titration in Figure 3.2; data for G4-$NH_2(Pd^{2+})_n$ not shown).

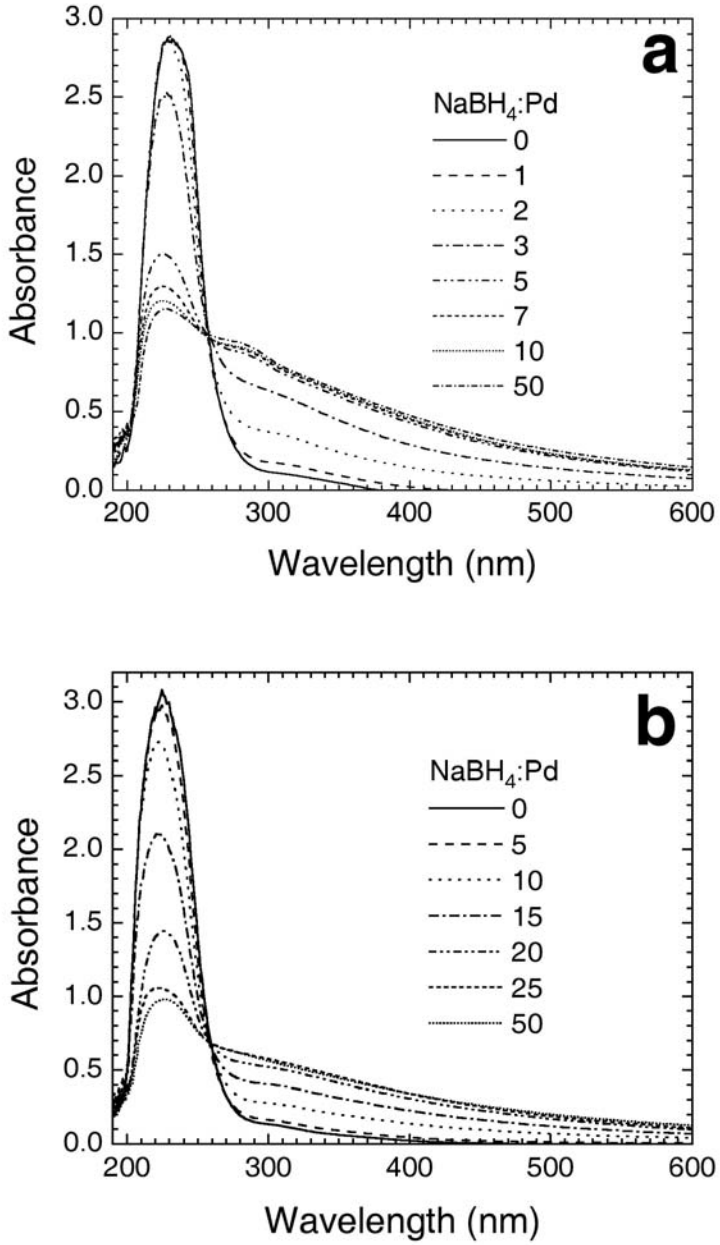

Figure 3.4. UV-vis absorbance spectra of aqueous solutions initially containing (a) G4-OH$(Pd^{2+})_{40}$ (initial pH = 4) and (b) G4-$NH_2(Pd^{2+})_{40}$ (initial pH = 3) as a function of the mole ratio of BH_4^- reducing equivalents per Pd^{2+}. The spectra were obtained in air 5 min after addition of $NaBH_4$.

Figure 3.4b shows absorbance spectra analogous to that in Figure 3.4a, except that G4-NH_2 was used to encapsulate the Pd nanoparticles. The initial pH in these experiments was reduced to 3 with HCl to avoid precipitation of the dendrimer (*vide supra*). After reduction, the absorbance spectra of the G4-$NH_2(Pd_{40})$ solutions have the same general features previously described for G4-$OH(Pd_{40})$ (Figure 3.4a). However, a greater excess of $NaBH_4$ is required to fully reduce G4-$NH_2(Pd^{2+})_{40}$ solutions because of the lower initial pH and correspondingly larger loss of reducing equivalents to proton reduction. The G4-$NH_2(Pd_{40})$ DENs precipitated after a few hours if the solution pH increased above 8 (due to proton reduction by BH_4^-). This was avoided by adding HCl to lower the pH; solutions of G4-$NH_2(Pd)_{40}$ did not aggregate for up to 30 days if the solution pH was kept below 8. Precipitation at pH > 8 is probably a consequence of dendrimer crosslinking of peripheral amines by Pd^{2+} that arise from air oxidation of Pd DENs (*vide infra*).

Transmission electron microscopy (TEM) of Pd DENs synthesized in hydroxyl- and amine-terminated dendrimers revealed near-monodisperse Pd nanoparticles having a mean diameter of 1.4 ± 0.4 nm for G4-$OH(Pd_{40})$ and 1.7 ± 0.5 nm for G4-$NH_2(Pd_{40})$ (Figure 3.5).[1,9,56]

Pd DENs are stable towards oxidation for at least 30 days when kept under N_2, but begin to oxidize within minutes upon exposure to air.[72,73] Figure 3.6a shows how the absorbance spectrum of an aqueous pH 8 solution of G4-$OH(Pd_{40})$ changes as a function of time when the solution is stirred in a vial open to the laboratory atmosphere. Under these conditions, the peak at 224 nm, which arises from the presence of G4-$OH(Pd^{2+})_n$,

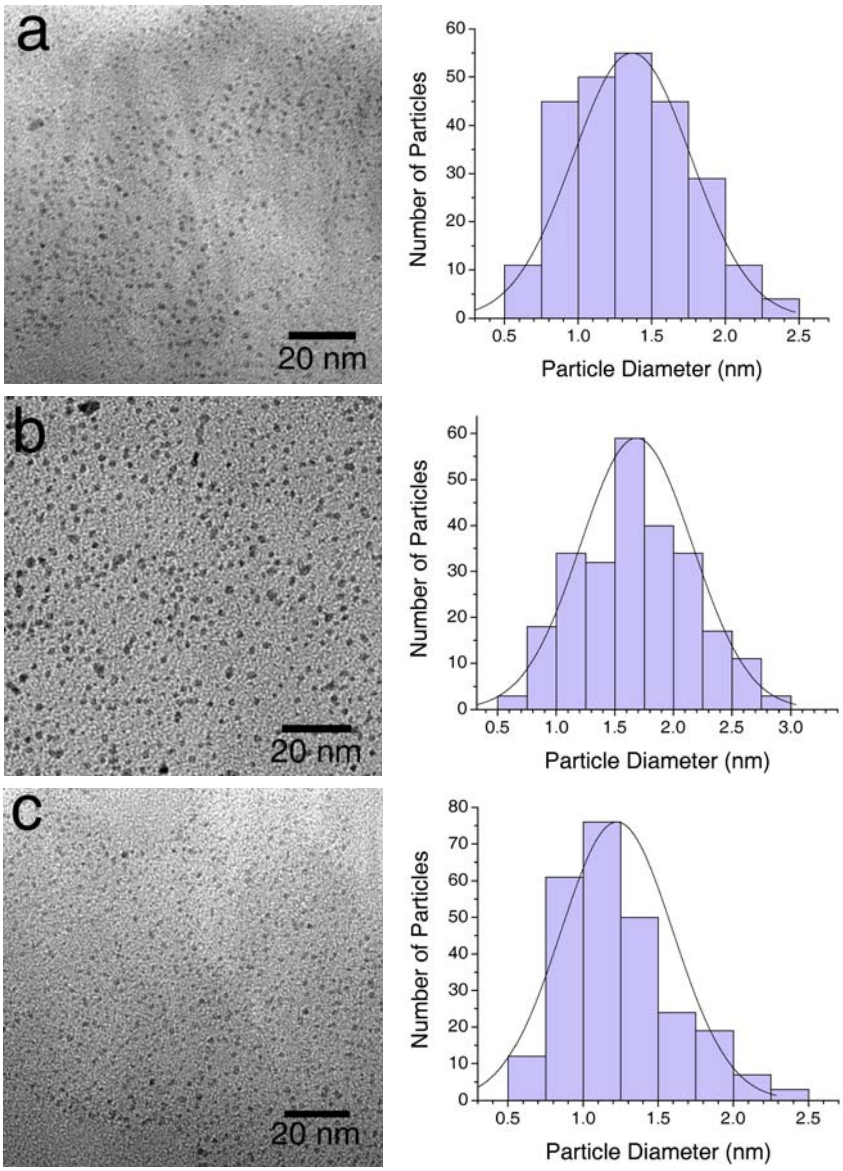

Figure 3.5. HRTEMs and size distribution plots for (a) G4-OH(Pd_{40}), (b) G4-NH_2(Pd_{40}) and (c) G4-OH(Pd_{40}) DENs after two 10 min O_2/ 10 min H_2 cycles.

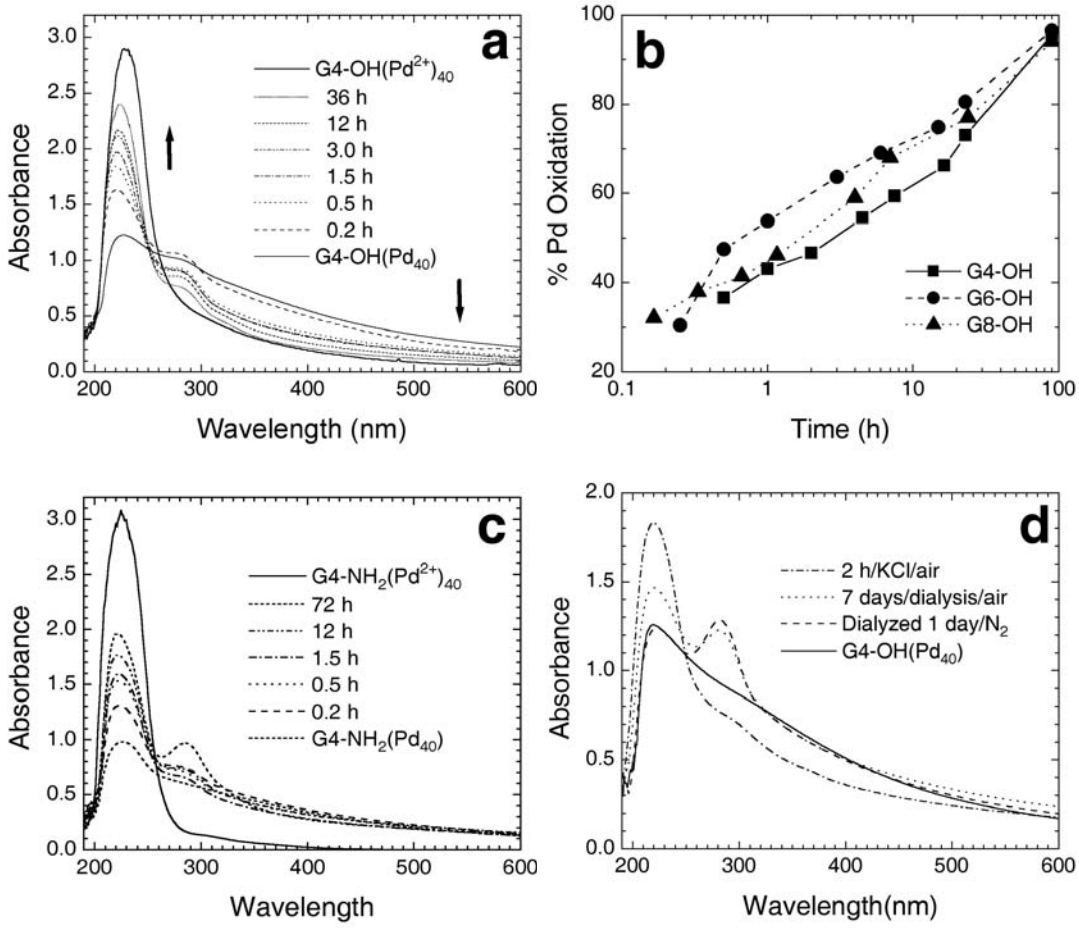

Figure 3.6. (a) UV-vis absorbance spectrum of G4-OH(Pd_{40}) as a function of the time the solution was exposed to air after initial reduction. For comparison, a spectrum of G4-OH(Pd^{2+})$_{40}$ is also shown. The pH of the solution was adjusted to 8 after reduction. (b) Plots of % Pd oxidation vs. time as a function of the dendrimer generation. The data were calculated using Eq. 3.3. (c) Same as (a), except for G4-NH_2(Pd_{40}). (d) UV-vis absorbance spectra of a G4-OH(Pd_{40}) solution before and after dialysis under N_2. Spectra are also shown for the dialyzed G4-OH(Pd_{40}) solution after exposure to air for 7 days, and then 2 h after addition of KCl (KCl:Pd ratio = 4:1).

increases and there is a corresponding decrease in the featureless absorption at higher wavelengths. The reappearance of the peak at 224 nm also suggests that any Pd^{2+} ions formed upon oxidation remain sequestered within the dendrimer via reaction with the interior amines. The isosbestic point present at ~250 nm confirms that zerovalent Pd is converted exclusively to a single species, which we identify as dendrimer-encapsulated Pd ions, upon oxidation. Notice, however, that a small, new peak appears at 285 nm; we believe this feature is due to an irreversible partial oxidation of the G4-OH dendrimers. This point will be discussed in more detail later.

Figure 3.6b presents a comparison of the oxidation rates of G4-OH(Pd_{40}), G6-OH(Pd_{40}), and G8-OH(Pd_{40}) DENs. The percentage of oxidized Pd was calculated as using Eq. 3.

$$\%\ \ Pd\ \ Oxidation = \frac{A_{224} - A_{224}(Gn-OH(Pd_{40}))}{A_{224}(Gn-OH(Pd^{2+})_{40}) - A_{224}(Gn-OH(Pd_{40}))} x100 \qquad (3.3)$$

Here n = 4, 6, or 8, A_{224} is the total absorbance of the solution at 224 nm, and A_{224}(Gn-OH(Pd^{2+})$_{40}$) and A_{224}(Gn-OH(Pd_{40})) are the absorbance of Gn-OH(Pd^{2+})$_{40}$ and Gn-OH(Pd_{40}) solutions at 224 nm, respectively. The results show that the oxidation rate is essentially independent of dendrimer generation. In all cases the Pd nanoparticles are more than 95% oxidized after 3 days. If the solution pH is adjusted to 5, G4-OH(Pd_{40}) DENs are more than 95% oxidized after only 1 h.

Figure 3.6c shows how the absorbance spectrum of an aqueous pH 8 solution containing G4-NH_2(Pd_{40}) DENs changes as a function of time when it is exposed to air. In this case the oxidation rate is slower than for G4-OH(Pd_{40}); after 3 days the Pd nanoparticles are only ~50% oxidized. This may be a consequence of peripheral amine groups stabilizing the encapsulated Pd nanoparticles by coordinating with surface Pd atoms.[74]

The oxidative stability of both the G4-OH(Pd_{40}) and G4-NH_2(Pd_{40}) DENs can be dramatically improved by dialyzing the original solution with 10 L of water for 24 h. Figure 3.6d compares absorbance spectra of G4-OH(Pd_{40}) before and after dialysis, and after exposure to air for 7 days. The solid line is the spectrum of G4-OH(Pd_{40}) prior to dialysis.[69-71] After dialysis for 1 day under N_2, a band appeared at 285 nm, which, as will be discussed in detail shortly, is probably due to oxidation of the dendrimer. The rest of the spectrum is essentially unchanged, however. When the same solution was then exposed to air, the oxidation of G4-OH(Pd_{40}) was much slower. Specifically, only ~10% of the Pd oxidized after a period of 7 days (contrast with the data shown in Figure 3.6a, in which 10% of the Pd oxidized within 0.2 h in the absence of dialysis). To determine if this stability is due to the removal of salts from the solution during dialysis, a stoichiometric amount of KCl (KCl:Pd ratio = 4:1) was added to the dialyzed G4-OH(Pd_{40}) solution. This resulted in an immediate increase in the oxidation rate of G4-OH(Pd_{40}): ~30% of the Pd oxidized within 2 h of adding KCl. This suggests that oxidation results in formation of the original G4-OH$(Pd^{2+})_n$ composite, and that this process is facilitated by the presence of coordinating anions.

XPS results confirm that the oxidation of the Pd nanoparticles occurs primarily via reformation of the G4-OH(Pd^{2+})$_{40}$ composite, and not by the formation of an oxide of Pd. Figure 3.7 shows XPS spectra of solutions containing G4-OH(Pd^{2+})$_{40}$, G4-OH(Pd_{40}), and G4-OH(Pd_{40}) after being exposed to air for 24 h. Before reduction, the Pd $3d_{5/2}$ peak is present at 338.2 eV, but it shifts to 336.1 eV after reduction. After oxidation in air for 24 h, peaks corresponding to both Pd^{2+} (338.2 eV) and zerovalent Pd (336.0 eV) are present. Significantly, no corresponding change in the oxygen 1s signal is observed, suggesting that the oxidation product of the Pd particles in aqueous solution is primarily a coordinated palladium salt and not an oxide of Pd.

To better understand air-induced oxidation of Pd DENs, G4-OH(Pd_{40}) solutions were treated with O_2 and H_2 gas. Figure 3.8 shows how the absorbance spectrum of G4-OH(Pd_{40}) changes upon sequential exposure of the solution to O_2 and H_2 gases. Upon exposure to O_2, the peak at 224 nm resulting from the presence of G4-OH(Pd^{2+})$_n$ increases and there is a corresponding decrease in the absorbance at higher wavelengths, along with the onset of a new peak at 285 nm. Upon treatment with H_2 gas the peak at 224 nm decreases and the intensity of the featureless absorption at high wavelength increases; however, there is no change in the intensity of the peak at 285 nm. This behavior persists over several oxidation/reduction cycles: O_2 treatment results in oxidation of the Pd DENs and an increase in the band at 285 nm, while H_2 treatment results in re-reduction of the Pd ions without changing the intensity of the band at 285 nm. It is interesting to note that freshly prepared solutions of G4-OH(Pd^{2+})$_{40}$ cannot be

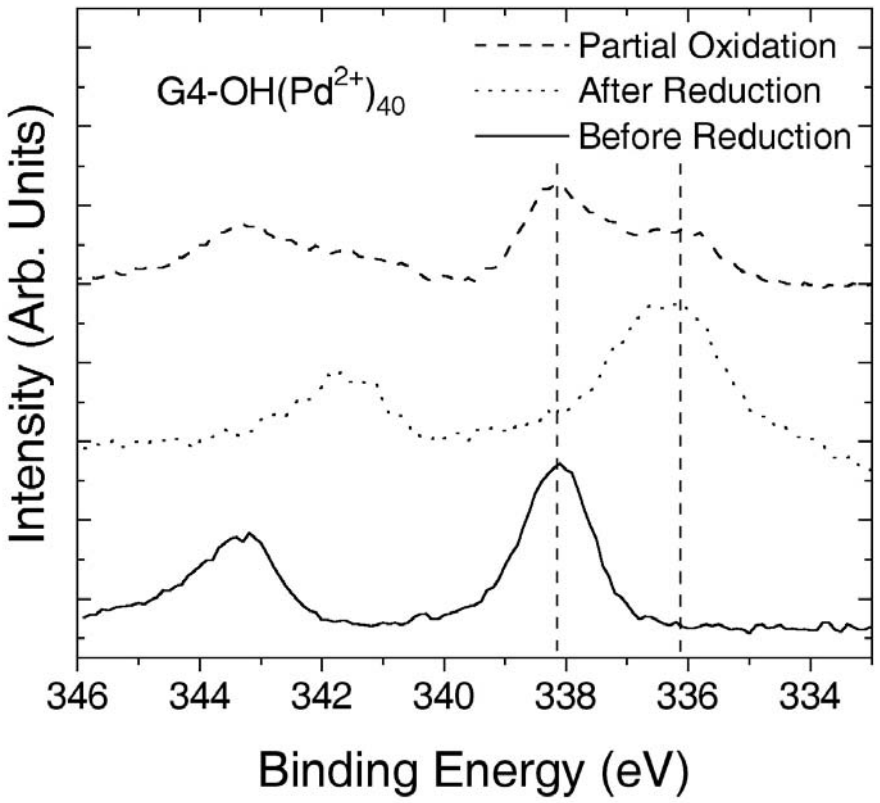

Figure 3.7. High-resolution XPS spectra of G4-OH$(Pd^{2+})_{40}$ before and after reduction with 20 equiv of $NaBH_4$ (solution pH adjusted to 8 with HCl after reduction), and after partial oxidation by exposure to air for 2 days. The Pd $3d_{5/2}$ and $3d_{3/2}$ peaks are shown.

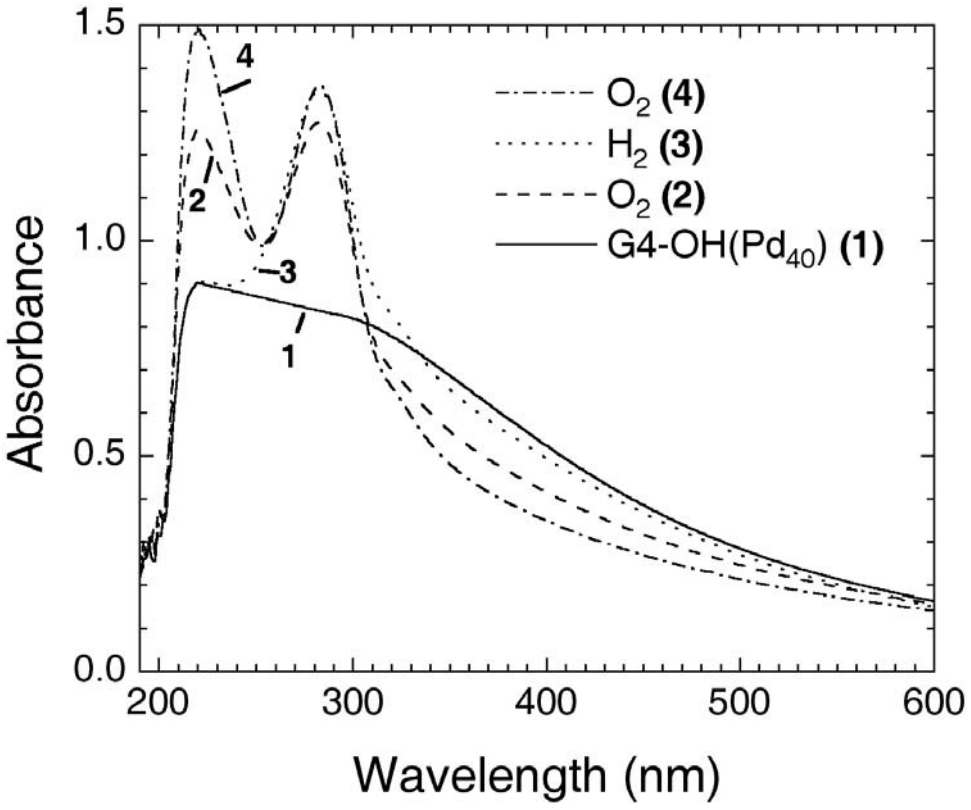

Figure 3.8. UV-vis absorbance spectra of a G4-OH(Pd_{40}) solution after sequential exposure to O_2, H_2, and O_2. The exposures were carried out for 10 min each. The initial reduction was performed using 20 equiv of $NaBH_4$ and the final solution pH was adjusted to 8 with HCl.

reduced by addition of H_2, thus the presence of zerovalent Pd seeds is apparently necessary to drive the H_2-induced reduction.

HRTEM images of a G4-OH(Pd_{40}) DENs before and after two O_2/H_2 cycles were similar, with an average particle size after two O_2/H_2 cycles of 1.2 ± 0.4 nm (Figure 3.5). Thus the Pd DENs can be reconstituted after oxidation with no growth in the average nanoparticle size. This finding is consistent with our earlier contention that oxidation does not result in loss of Pd salts from the dendrimer interior. We suspect that the peak at 285 nm, which forms upon O_2 exposure, arises from oxidation of the dendrimer. Interestingly, this peak does not appear in the absence of the encapsulated Pd nanoparticles, suggesting that the oxidation reaction is catalyzed by zerovalent Pd. Esumi and coworkers previously showed that a similar dendrimer oxidation peak at 285 nm forms during the *in situ* reduction of $HAuCl_4$ salts by UV irradiation in the presence of G4-NH_2 dendrimers.[61] We have also found a band at 285 nm that appears when G4-OH dendrimers spontaneously reduce $HAuCl_4$ salts in the absence of an intentionally added reducing agent.[75]

The finding that partially oxidized Pd DENs can be fully reduced by H_2 gas is important, because these materials have found use as hydrogenation and carbon-carbon coupling catalysts.[9,13-16,56-59] The ability of the dendrimer template to retain oxidized Pd^{2+} ions, which can subsequently be reduced with H_2 gas, is a desirable characteristic that provides a means for reactivation and recycling (Figure 3.9). In contrast, many colloidal metallic catalysts deactivate when exposed to oxygen and cannot be reactivated.[72,73] The consequences of the oxidation of the dendrimer itself upon exposure

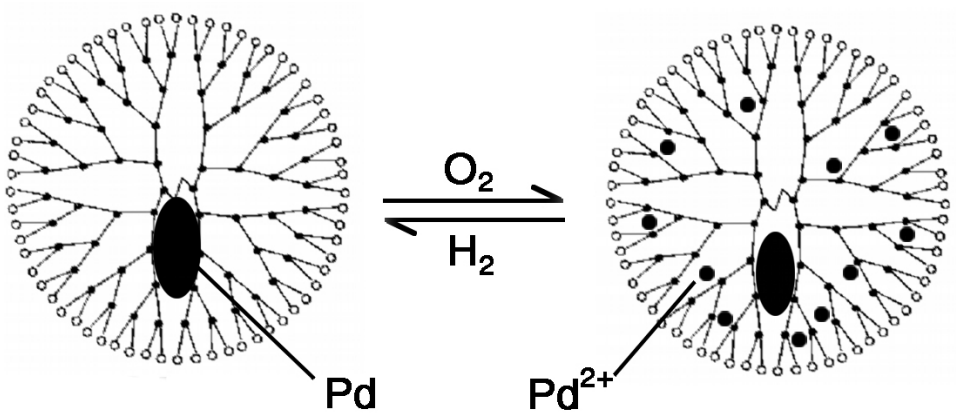

Figure 3.9. Schematic illustration of partial oxidation and re-reduction of DENs.

to O_2 need to be more fully explored, however.

3.5 Summary and Conclusions

This chapter has reported on the synthesis, physical and chemical properties, and stability of Pd DENs. This type of information is necessary for optimizing the catalytic properties of DENs so that their interesting properties can be fully exploited. We have shown that Pd DENs can be synthesized in both G4-OH and G4-NH_2 dendrimers, and that the loading of Pd ions into these dendrimers correlates, with a 1:1 stoichiometry, to the number of available interior amines present in the dendrimers. Pd DENs can be synthesized in G4-NH_2 dendrimers by selective protonation of the peripheral primary amine groups of the dendrimers. This is important because primary amines are more reactive than hydroxyl groups, and thus are better for linking DENs to surfaces, other polymers, and biological molecules. Pd DENs are stable in the absence of O_2, but oxidation occurs in air. Such oxidation can be minimized by dialysis of DEN solutions to remove excess coordinating ligands. The oxidation of Pd DENs is reversible: upon exposure to H_2 gas dendrimer-encapsulated metal ions are converted back to zerovalent Pd nanoparticles. The ability of the dendrimer template to retain oxidized Pd^{2+} ions, which can subsequently be reduced with H_2 gas in the presence of a zerovalent Pd seed, is a desirable characteristic that provides a means for reactivation and recycling.

CHAPTER IV

SYNTHESIS, CHARACTERIZATION, AND SURFACE IMMOBILIZATION OF PLATINUM AND PALLADIUM NANOPARTICLES ENCAPSULATED WITHIN AMINE-TERMINATED POLY(AMIDOAMINE) DENDRIMERS*

4.1 Synopsis

Platinum and palladium dendrimer-encapsulated nanoparticles (DENs) were prepared within commercially available, fourth-generation, amine-terminated poly(amidoamine) (PAMAM) dendrimers (G4-NH_2). The synthesis is carried out by selectively encapsulating metal complexes within the dendrimer, and then reducing the resulting composite. Intradendrimer complexation requires control over the solution pH to prevent attachment of the metal complexes to primary amine groups on the dendrimer periphery. That is, the surface primary amines of the dendrimer must be selectively protonated in the presence of the interior tertiary amines. The metal-ion encapsulation and reduction processes were characterized by UV-vis spectroscopy. 40-atom Pt and Pd DENs were examined by high-resolution transmission electron microscopy, which showed that the mean particle sizes were 1.4 nm and 1.5 nm, respectively, and that both were nearly monodisperse (standard deviation = 0.3 nm). The free amine groups on the dendrimer surface were used to link Pd DENs to monolithic Au surfaces via an intermediate self-assembled monolayer adhesion layer.

---

* Reprinted with permission from Ye, H.; Scott, R. W. J.; Crooks, R. M. *Langmuir* **2004**, *20*, 2915-2920: copyright 2004 American Chemical Society.

4.2 Introduction

This chapter reports the preparation of Pt and Pd nanoparticles encapsulated within fourth-generation, amine-terminated, poly(amidoamine) (PAMAM) dendrimers (G4-NH_2). These new results are significant because the dendrimers used as templates for the nanoparticle synthesis are commercially available, and because they have surface groups that provide a reactive handle for linking nanoparticles to surfaces and other polymers. We illustrate this point here by covalently attaching dendrimer-encapsulated nanoparticles (DENs) to a reactive self-assembled monolayer (SAM).[76] It should be possible to use this same basic strategy for linking DENs to a wide variety of substrates for heterogeneous catalysis, for linking DEN-based biomarkers to proteins and DNA,[77] and for creating new types of functional substrates that require highly monodisperse metal nanoparticles.

We and others previously reported the preparation and characterization of dendrimer-encapsulated Cu,[60] Pt,[7,56,78,79] Pd,[9,13,14,16,56-59,79-81] Au,[62,82-84] CdS,[64] and bimetallic[11,63] nanoparticles.[55,85] These materials are prepared by extracting metal ions into the interior of dendrimers, and then chemically reducing the metal ions to yield encapsulated nanoparticles. Although there are a few exceptions,[13,14,57-59,78,79,81] Pt and Pd DENs are normally prepared using PAMAM dendrimers terminated with hydroxyl groups.[7,9,16,56,60,80] There are two reasons for this. Foremost, hydroxyl groups are non-complexing toward most metal ions. This is important, because metal ions cross-link dendrimers terminated with good metal ligands and this leads to precipitation. Second,

both hydroxyl-terminated dendrimers and most metal ions and metal-ion complexes are water soluble.

We previously showed that monolayers of Pt DENs terminated with hydroxyl functional groups could be physisorbed to Au surfaces and used for the electrocatalytic reduction of O_2.[7] However, due to the low reactivity of the peripheral hydroxyl groups it was not possible to covalently link the dendrimer to the electrode surface, and consequently the stability of the dendrimer monolayer was poor under electrochemical conditions. In contrast, we knew from previous studies that amine-terminated dendrimers (without encapsulated nanoparticles) could be covalently attached to electrode surfaces to yield stable monolayers.[86,87] We reasoned that if DENs could be prepared within amine-terminated dendrimers, then the peripheral primary amines would form stable covalent bonds.

We previously described two approaches for preparing DENs in amine-terminated dendrimers. In one case, the dendrimer surface was partially quaternized.[79] This strategy takes advantage of the large number of functional groups on the dendrimer surface in that different fractions of the surface can be functionalized to perform specific tasks. Specifically, the unquaternized fraction of the periphery was shown to be reactive while positive charge on the quaternized fraction prevented agglomeration of DENs. While this approach is effective, it requires chemical modification of the dendrimer periphery. In the second case, we observed that the peripheral amines of PAMAM dendrimers could be selectively protonated by judicious control of solution pH, and that this provided a means for encapsulation of Pd nanoparticles.[57,58] The new results

provided here expand upon these preliminary findings. Specifically, we now describe optimal conditions for preparing both Pd and Pt DENs in amine-terminated dendrimers, fully characterize the resulting metal nanoparticles, and show that this family of DENs form stable, high-density monolayers on surfaces.

4.3 Experimental Section

Chemicals. G4-NH_2 was purchased as a 10-25% methanol solution (Dendritech, Inc., Midland, MI). Prior to use, the methanol was removed under vacuum. K_2PtCl_4, K_2PdCl_4 (Strem Chemicals, Inc.), and $NaBH_4$ (The Aldrich Chemical Company) were used without further purification. 11-mercaptoundecanoic acid, ethyl chloroformate, 4-methylmorpholine, dichloromethane (99.8%, anhydrous), and N,N-dimethylformamide (99.8%, anhydrous) were purchased from Aldrich and used for surface modification without further purification. 18 MΩ·cm Milli-Q deionized water (Millipore, Bedford, MA) was used to prepare aqueous solutions.

Characterization. Absorption spectra were obtained using a Hewlett-Packard HP8453 UV-vis spectrometer. The optical path length was 0.1 or 1.0 cm, and deionized water or aqueous dendrimer solutions were used as references. High-resolution transmission electron microscopy (HRTEM) images were obtained using a JEOL-2010 TEM having a point-to-point resolution of 0.19 nm. Samples were prepared by placing a drop of solution on a holey-carbon-coated grid and allowing the solvent to evaporate in air. Fourier transform infrared-external reflection spectroscopy (FTIR-ERS) was carried out using an FTS-6000 spectrometer (Bio-Rad, Cambridge, MA) equipped with a

Harrick Scientific Seagull reflection accessory (Ossing, NY) and a liquid-N_2-cooled, narrow-band MCT detector. The spectra were taken at 4 cm^{-1} resolution using *p*-polarized light at an 84^{o} angle of incidence with respect to the substrate normal.

Preparation of Pt and Pd Dendrimer-Encapsulated Nanoparticles (DENs). Dry G4-NH_2 was dissolved in sufficient deionized water (pH adjusted with HCl to ~5 for Pt DENs and ~3 for Pd DENs) to yield 2.5 - 50 μM dendrimer solutions, and then 30 or 40 mol equiv of aqueous 0.1 M K_2PtCl_4 or 0.1 M K_2PdCl_4 solution was added. Zerovalent Pt and Pd DENs were synthesized by slow addition of a 20–fold excess of 0.1 – 0.5 M $NaBH_4$ dissolved in deionized water. Following addition of $NaBH_4$, the solution pH was adjusted to 8 by addition of aqueous HCl, and then the DEN solution was dialyzed with a cellulose dialysis sack having a molecular weight cutoff of 12,000 (Sigma Diagnostics, Inc.) to remove impurities.[80]

Surface Immobilization of DENs. 11-mercaptoundecanoic acid (MUA) monolayers were prepared by immersing ozone-cleaned Au substrates into a 1 mM ethanolic solution of MUA for 24 h. The MUA substrates were then washed with ethanol, dried under flowing N_2 gas, and transferred to vials containing ethyl chloroformate and 4-methylmorpholine dissolved in DMF or CH_2Cl_2 for 1 h. This resulted in the formation of activated anhydride surfaces.[86-90] Next, the substrates were removed from solution, rinsed with DMF or CH_2Cl_2, and dried under flowing N_2 gas. The activated substrates were dipped into 10 mL of a Pd DEN solution (0.05 mM G4-NH_2 dendrimer) containing 0.1 mL of 4-methylmorpholine. As a control experiment to ensure covalent attachment to the surface, Pd DEN-modified substrates were prepared using the same procedure, but

in this case ethyl chloroformate was omitted. This prevents formation of a covalent bond.

4.4 Results and Discussion

Preparation of Pt DENs. Pt DENs were prepared by stirring aqueous pH 5 solutions containing G4-NH_2 and K_2PtCl_4 for 76 h and then reducing the encapsulated Pt metal complex with BH_4^-. The lengthy stirring time is required, because reaction between the interior amines of G4-NH_2 and Pt^{2+} (unless indicated otherwise, Pt^{2+} and Pd^{2+} are used to represent all possible complex ions of the two metals) is slow.[7,56] Because the exterior amines (pK_a = 9.2) are more basic than the interior amines (pK_a = 6.3),[68] metal ions selectively coordinate to the interior amines at pH 5. Slow addition of a 0.5 M aqueous $NaBH_4$ solution to the dendrimer/Pt^{2+} complex results in formation of a dark-brown, zerovalent Pt DEN solution. The solution pH increased to pH 8 - 9 after addition of $NaBH_4$ because of proton reduction. We have found that at pH > 8 these types of DENs aggregate after a few hours, and therefore the solution pH was adjusted back to pH 8 with HCl after reduction. We believe aggregate formation at high pH may be a consequence of DEN crosslinking facilitated by unreduced or re-oxidized metal ions, because after purification by dialysis for 24 h Pt DEN solutions do not precipitate at pHs as high as 10. Recent results from our group have shown that removal of complexing ligands from solution leads to much slower oxidation rates of Pd DENs.[80]

Figure 4.1 shows UV-vis absorbance spectra of pH 5 solutions of amine-terminated, fourth-generation PAMAM dendrimers containing, on average, 30 Pt^{2+} ions

($G4\text{-}NH_2(Pt^{2+})_{30}$) obtained over a 76 h period as well as shortly (15 min) after reduction with $NaBH_4$. The peak at 216 nm, which corresponds to a ligand-to-metal-charge-transfer band of $PtCl_4^{2-}$, decreases and shifts slightly to 220 nm.[91,92] Simultaneously the peak at 260 nm, which arises from coordination of the Pt complex to interior dendrimeric amines,[56,93] grows in intensity throughout the 3-day observation period. This suggests that a slow ligand-exchange reaction occurs between $PtCl_4^{2-}$ and the interior amine groups of the dendrimer.[94] The isosbestic point at 236 nm indicates that $PtCl_4^{2-}$ is exclusively converted to a single species, which we identify as amine-coordinated $PtCl_3^-$. We previously reported that Pt complexation with hydroxyl-terminated PAMAM dendrimers was complete within 45 h.[93] However, the solution was slightly basic in that case (because of the basicity of the PAMAM dendrimers); apparently, the reaction takes longer at lower pH because of proton competition for the interior amine sites.

Control experiments confirm that Pt salts coordinate with interior, rather than exterior, amines. For example, when a solution of K_2PtCl_4 is added to a dendrimer solution without pH control (slightly basic conditions), the solution precipitates after several hours. This is a consequence of interdendrimer crosslinking of the peripheral amines by the metal complex. Similarly, a Pt precipitate is observed when a solution of $G4\text{-}NH_2$ and K_2PtCl_4 are reduced at pH 5 prior to complete complexation of Pt with the interior dendrimer amines; that is, if less than 3 days is allotted for the complexation reaction.

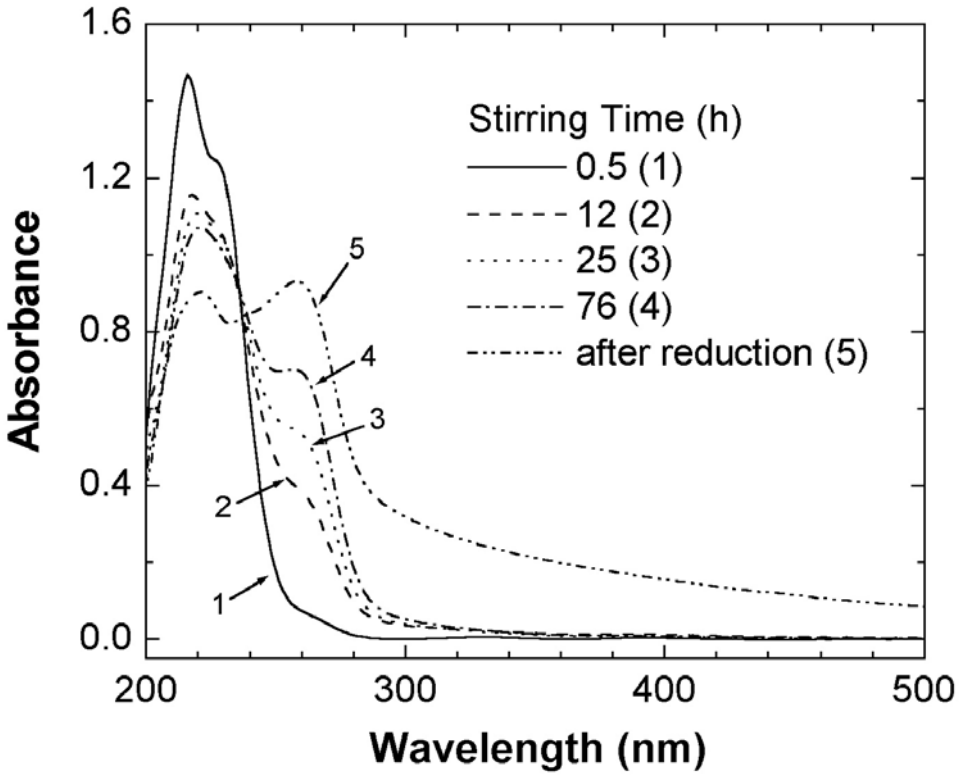

Figure 4.1. Time-resolved UV-vis absorbance spectra of G4-$NH_2(Pt^{2+})_{30}$ solutions (pH = 5) over a 76 h period and 15 min after reduction with $NaBH_4$ to yield G4-$NH_2(Pt_{30})$ (The solution pH increased to 8 after addition of $NaBH_4$). The final concentration of G4-NH_2 was 50 μM. The optical path length was 0.1 cm.

Chemical reduction of an aqueous solution of G4-$NH_2(Pt^{2+})_{30}$ with excess $NaBH_4$ yields Pt DENs, G4-$NH_2(Pt_{30})$. Figure 4.1 shows the UV-vis spectrum of the G4-$NH_2(Pt_{30})$ solution 15 min after reduction. The broad, featureless absorption at wavelengths >300 nm is consistent with the formation of colloidal Pt.[1,56,69,93] There are also two peaks (220 nm and 260 nm) present at low wavelength. Experimental observations and theoretical calculations have shown that the peak at 220 nm arises from absorbance of Pt nanoparticles in aqueous solution.[95,96] The peak at 260 nm is more difficult to assign, but it has been previously observed.[56,79] This peak may originate from unreduced Pt^{2+} still strongly bound to the tertiary amine groups of the dendrimers. To better understand the origin of the peak at 260 nm, the following experiments were performed. (1) For a constant dendrimer concentration, the absorbance of the peak at 260 nm is proportional to the amount of $PtCl_4^{2-}$ added. (2) The peak does not change even after adding more sodium borohydride and bubbling H_2 for 24 h. (3) The peak is absent if insufficient time is permitted for complete Pt^{2+} encapsulation. Specifically, the band at 260 nm is absent if the G4-$NH_2(Pt^{2+})_{30}$ is reduced just 1 h after mixing the dendrimer and the Pt complex. This peak is also absent if the reduction is carried out at very low pH, which prevents complexation of the Pt^{2+} complex with the dendrimer. In both cases, however, metal precipitates from solution. (4) The XPS spectrum of surface-confined G4-$NH_2(Pt_{30})$ (Figure 4.2) reveals a very small shoulder at 77.8 eV corresponding to $Pt^{2+}(4f_{5/2})$. These results lead us to conclude that the peak at 260 nm probably arises from unreduced Pt^{2+} still strongly bound to amine groups in dendrimers.

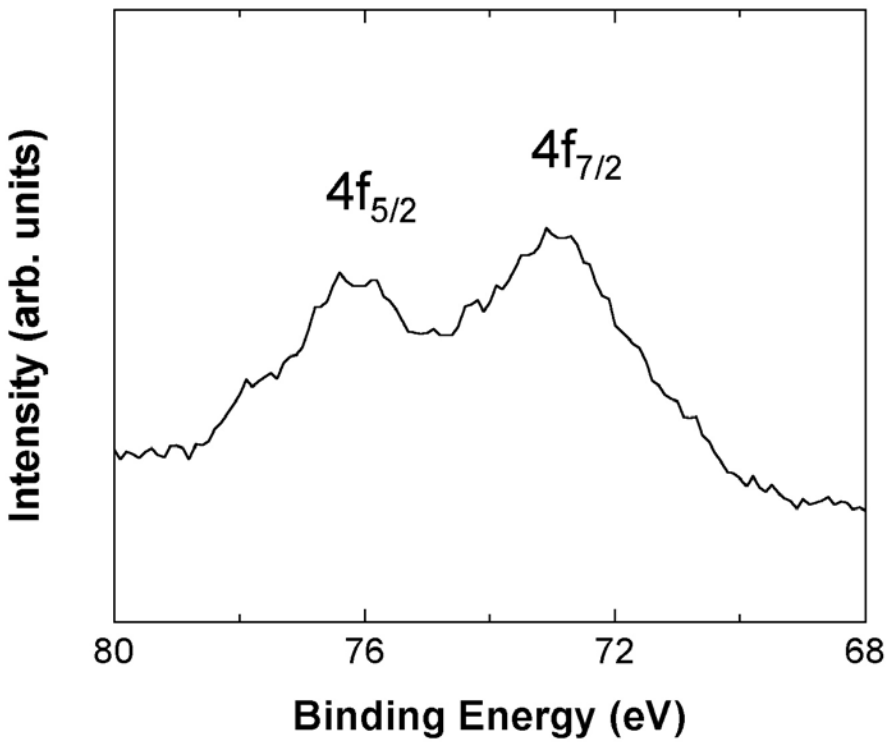

Figure 4.2. XPS spectrum of G4-NH_2(Pt_{30}). The data were acquired using an Axis HSi 165 Ultra Kratos instrument (Manchester, UK). The XPS positions were referenced to the Au ($4f_{7/2}$) peak at 83.8eV. Pt($4f_{7/2}$) and Pt($4f_{5/2}$) peaks are present at 73.0 eV and 75.9 eV, respectively, which is slightly higher binding energy than bulk platinum (71.2 eV).[97] This is probably a consequence of the small size of these nanoparticles and the presence of the dendrimeric ligands.[97-99]

Preparation of Pd DENs. The method used to prepare Pd DENs is very similar to that used for Pt DENs. Solutions of G4-NH_2 and K_2PdCl_4 are mixed together, stirred for 30 min at pH 3, and then reduced with BH_4^-. The kinetics of Pd^{2+} ion coordination with the interior amines are much faster than for Pt^{2+}, and therefore it was possible to use shorter reaction times and a lower pH. Figure 4.3a shows UV-vis spectra of an aqueous solution containing 2.5 μM G4-$NH_2(Pd^{2+})_{30}$ before reduction (at pH 3) and after reduction (at pH 8). Pd^{2+} coordination with the interior dendrimer amines is complete within 15 min, which is about 300 times faster than for Pt^{2+} coordination. The band at 221 nm corresponds to a ligand-to-metal charge transfer (LMCT) associated with complexation of Pd^{2+} to amine groups of the G4-NH_2 dendrimer.[80] We believe that complexation occurs via displacement of water from $PdCl_3(H_2O)^-$, which is the dominant Pd^{2+} species present under these conditions, followed by covalent reaction with the interior tertiary amines of the dendrimer.[80] After reduction the broad, featureless absorption at low energies, as well as the peak at 230 nm, arise from interband transitions of the intradendrimer Pd nanoparticle.[69,80,100,101]

The presence of Cl^- in solution is known to affect the way that dendrimers interact with Pd^{2+} complexes in two ways. First, it ensures that the dominant Pd^{2+} species in solution is $PdCl_4^{2-}$ rather than $PdCl_3(H_2O)^-$.[80,91] This is helpful for understanding the speciation of Pd^{2+}, because the Pd-Cl LMCT band for $PdCl_4^{2-}$ at 279 nm is well separated from the Pd-N LMCT band of G4-$NH_2(Pd^{2+})_{30}$ at 221 nm. In contrast, the LMCT band for $PdCl_3(H_2O)^-$ at 237 nm overlaps significantly with the Pd-N LMCT band.[91] Second, coordination of $PdCl_4^{2-}$ with intradendrimer tertiary amine ligands

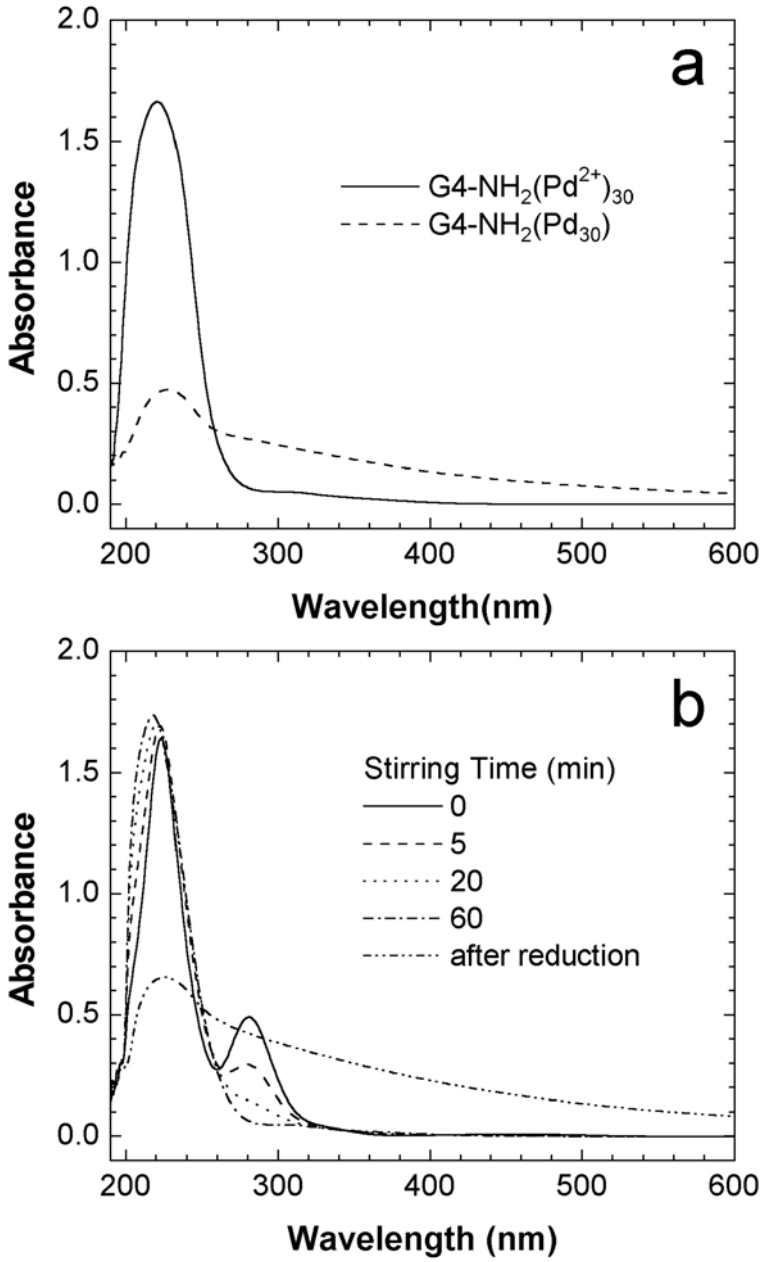

Figure 4.3. (a) UV-vis spectra of 2.5 μM solutions of G4-$NH_2(Pd^{2+})_{30}$ (pH = 3) and G4-$NH_2(Pd_{30})$ (pH = 8) solutions. (b) Time-resolved UV-vis spectra of G4-$NH_2(Pd^{2+})_{30}$ and G4-$NH_2(Pd_{30})$ solutions in the presence of 0.1 M KCl before (pH = 3) and after (pH = 8) reduction. The optical path length was 1.0 cm.

occurs more slowly than for $PdCl_3(H_2O)^-$. These two factors make it easier to follow the Pd^{2+} encapsulation reaction spectroscopically. Figure 4.3b shows that in the presence of 0.1 M KCl the LMCT of $PdCl_4^{2-}$ at 279 nm decreases within minutes of adding G4-NH_2 to the K_2PdCl_4 solution, and that this peak disappears completely after 1 h. The final spectrum is similar to that resulting from Pd^{2+} coordination to G4-NH_2 in the absence of KCl (Figure 4.3a). Reduction of the G4-$NH_2(Pd^{2+})_{30}$/KCl solution (Figure 4.3b) results in a spectrum that is nearly identical to that obtained in the absence of KCl.

It is interesting to note that very low pHs prevent complexation between the dendrimer and Pd^{2+}. Specifically, the absorbance spectrum of a K_2PdCl_4 solution in the absence of KCl did not change for at least 1 day when G4-NH_2 was added at pH 1.5. This means that a high proton concentration, which translates into protonation of all exterior and interior amines, completely prevents Pd^{2+} coordination to the dendrimer.

Spectrophotometric titrations were carried out to determine the maximum Pd^{2+} loading of G4-NH_2 at pH 3. Figure 4.4a shows UV-vis absorbance spectra for dilute aqueous solutions of K_2PdCl_4 in deionized water. The Pd complex has two strong LMCT bands at 207 nm and 237 nm, corresponding to literature values for the hydrolysis product $PdCl_3(H_2O)^-$.[91] Beer-Lambert plots obtained from these spectra at 221 and 237 nm are linear throughout the concentration range examined (Figure 4.4b). Figure 4.4c shows absorbance spectra for solutions containing both G4-NH_2 and K_2PdCl_4 at pH 3. Upon addition of K_2PdCl_4 to a 1.6 μM solution of G4-NH_2, a single, broad (FWHM = 45 nm at Pd^{2+}/G4-NH_2 = 40) absorption band is present at λ_{max} = 221 nm for Pd^{2+}/G4-NH_2 ratios of 60 and below. Recall that this is the LMCT associated with the Pd^{2+}/G4-NH_2

complex. Figure 4.4d shows that Beer-Lambert plots obtained for these solutions are linear only up to Pd^{2+}/G4-NH_2 ratios of approximately 60. Moreover, UV-vis spectra of G4-$NH_2(Pd^{2+})_{30}$ solutions before and after extended dialysis in water were identical, which means that Pd^{2+} is strongly bound to the dendrimers at low Pd^{2+}/G4-NH_2 ratios. That is, the amount of free $PdCl_3(H_2O)^-$ in solution is negligible in this range. At Pd^{2+}/G4-NH_2 ratios greater than 80, a shoulder becomes apparent at ~210 nm and the peak at 221 nm broadens (FWHM = 51 nm at Pd^{2+}/G4-NH_2 = 120). This is a consequence of the superposition of peaks corresponding to both dendrimer-encapsulated Pd^{2+} (221 nm) and free $PdCl_3(H_2O)^-$ in solution (207 and 237 nm) at Pd^{2+} concentrations exceeding the maximum capacity of the dendrimer interior. After extended dialysis in water, UV-vis spectra of solutions having Pd^{2+}/G4-NH_2 ratios above 60 revealed a significant decrease in absorbance in the 200-250 nm region, which confirms the presence of free $PdCl_3(H_2O)^-$ at high Pd^{2+}/G4-NH_2 ratios.

Extinction coefficients for $PdCl_3(H_2O)^-$ and G4-$NH_2(Pd^{2+})_n$ were obtained from the Beer-Lambert plots, and the relative concentration of each species was calculated using an appropriate analysis.[80] Figure 4.4e is a plot of calculated concentrations of free $PdCl_3(H_2O)^-$ and encapsulated Pd^{2+} vs. the Pd^{2+}/G4-NH_2 ratio in solution. These data indicate that there is a maximum loading of about 65 Pd^{2+} ions within the G4-NH_2 dendrimers at pH 3. This suggests that each Pd^{2+} is coordinated to about one of the 62 interior tertiary amine binding sites of G4-NH_2, and that there is little or no coordination between Pd^{2+} and the peripheral primary amine groups at this pH.

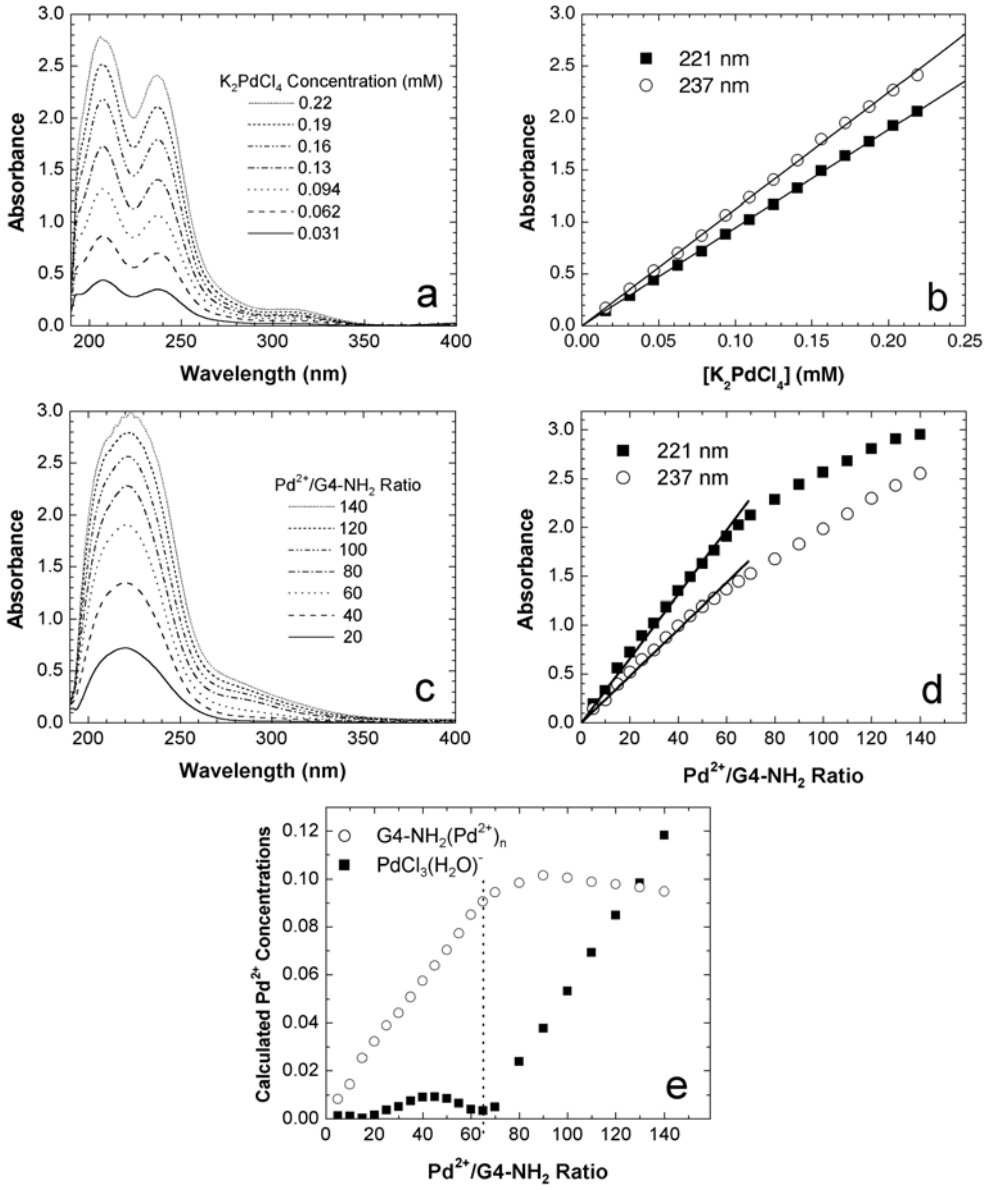

Figure 4.4. UV-vis spectra of (a) aqueous K_2PdCl_4 solutions and (c) G4-NH_2/K_2PdCl_4 solutions with [G4-NH_2] held constant at 1.6 μM. Each spectrum was obtained 15 min after addition of K_2PdCl_4. (b, d) Beer-Lambert plots over the concentration ranges shown in parts (a) and (c), respectively. (e) Titration plots (derived from part (b) and (d) showing the concentration of free $PdCl_3(H_2O)^-$ and dendrimer-encapsulated Pd^{2+} as a function of the Pd/G4-NH_2 mole ratio at pH = 3. The optical path length for UV-vis measurements was 1.0 cm.

Microscopy. Figure 4.5 shows HRTEM images and particle size distributions for G4-NH_2(Pt_{40}) and G4-NH_2(Pd_{40}) DENs. Analysis of 100 randomly selected particles shows that the average diameters for the Pt and Pd DENs are 1.4 ± 0.3 nm and 1.5 ± 0.3 nm, respectively. The size distributions, which in both cases correspond to $1\sigma = 0.3$ nm, are comparable to those obtained for Pd and Pt DENs prepared in hydroxyl-terminated PAMAM dendrimers ($1\sigma = 0.2$ - 0.3 nm).[9,56,93] Note, however, that the particle sizes are larger than the value of 1.1 nm calculated for a Pd or Pt particle containing 40 atoms with face-centered cubic packing.[56,93] We[1,56,93] and others[16,59,102] always observe that Pt and Pd DENs appear to be too large in HRTEM micrographs, even though the calculated and measured sizes of Au DENs are always self-consistent.[82] At present, we do not understand this apparent inconsistency, but it is possible that Pt and Pd DENs have irregular shapes (*i.e.* non-close packed geometries), which causes them to appear too large in the two-dimensional HRTEM projections.[1,9,93]

Synthesis and Characterization of DEN Thin Films. We are interested in using thin films of DENs as heterogeneous catalysts, and therefore we examined the feasibility of attaching DEN monolayers to surfaces. Specifically, G4-NH_2(Pd_{30}) was covalently linked to a monolithic Au surface using an intermediate 11-mercaptoundecanoic acid (MUA) self-assembled monolayer (SAM) adhesion layer. To gauge the strength of the attachment, we evaluated the stability of DEN monolayers prepared with and without activation of the MUA acid groups. Spectrum 1 in Figure 4.6a was obtained following coupling of G4-NH_2(Pd_{30}) to an activated MUA SAM and subsequent sonication in water for 30 s. The amide I and II bands present at 1665 cm^{-1}

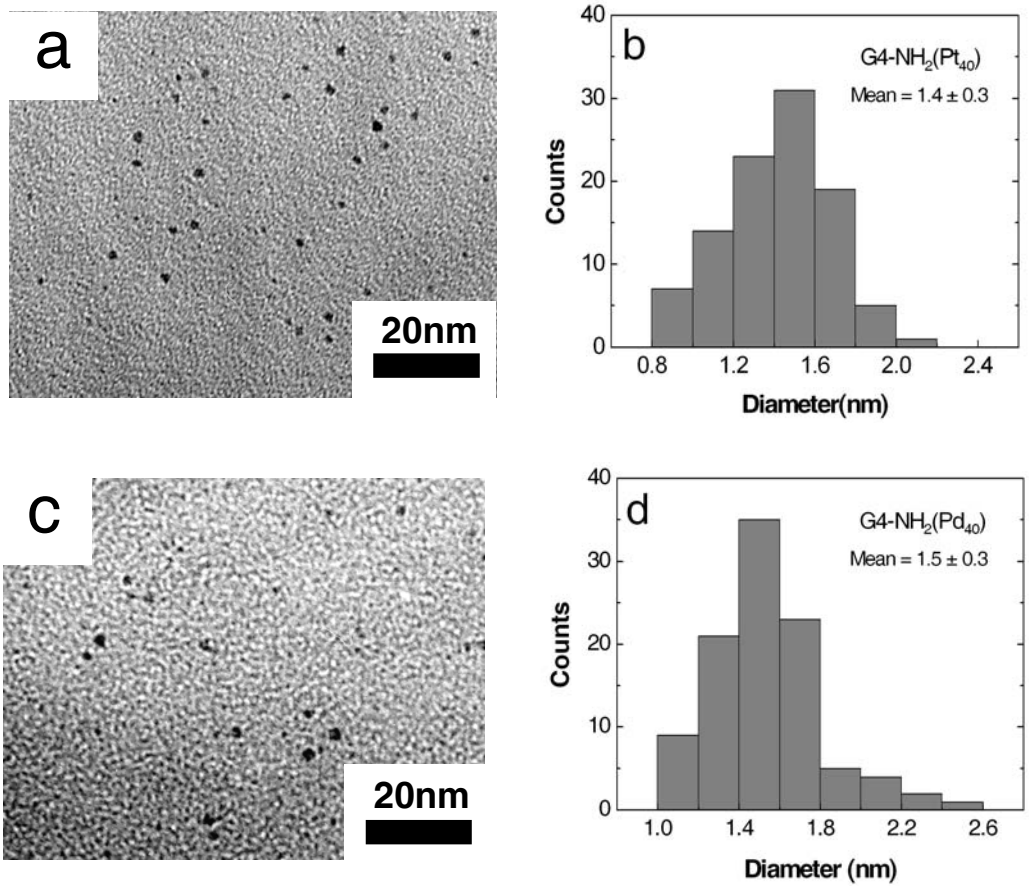

Figure 4.5. HRTEM images and particle size distribution of (a) G4-$NH_2(Pt_{40})$ (b) G4-$NH_2(Pd_{40})$. Particle size distributions are based on 100 randomly selected particles.

and 1550 cm^{-1}, respectively, indicate that the dendrimer is present on the surface.[86,103] The height of amide I band is 0.0035. This value is comparable with previous studies of dendrimer monolayer films in which no metal was encapsulated within the dendrimer,[87,103] and it is about 2.5 times higher than DEN films prepared using partially quaternized dendrimers.[79] Spectrum 2 was obtained using the same film, but after sonication in water for 5 min at pH 2. Analysis of the height of the amide I bands before and after sonication in acid indicates that 94% of the DEN film remains on the surface.

Figure 4.6b shows an analogous experiment carried out using an unactivated MUA SAM. In this case, the DENs are likely attached to the surface via electrostatic interactions between the acid terminal groups of MUA and the peripheral primary amines of the dendrimer. Physisorption (van der Waals interactions) may also play a role. After sonicating this film in water for 5 min at pH 2, only 78% of the amide I peak remains. These results suggest that Pd DEN monolayers prepared on activated MUA surfaces form covalent bonds and remain robust even under aggressive conditions intended to desorb the dendrimer. However, DENs bound to the unactivated surface are also surprisingly stable.

Unfortunately, there is no unique IR signature that would definitively prove covalent attachment of the DENs to the activated MUA SAM. Note, however, that after sonication in acid only the unactivated film (spectrum 2, Figure 4.6b) reveals a distinct shoulder at 1726 cm^{-1}. This band corresponds to the terminal carboxylic acid groups of the MUA SAM, and it indicates that many of the acid groups are protonated after acid treatment. The absence of this band in Figure 4.6a indicates the absence of free acid

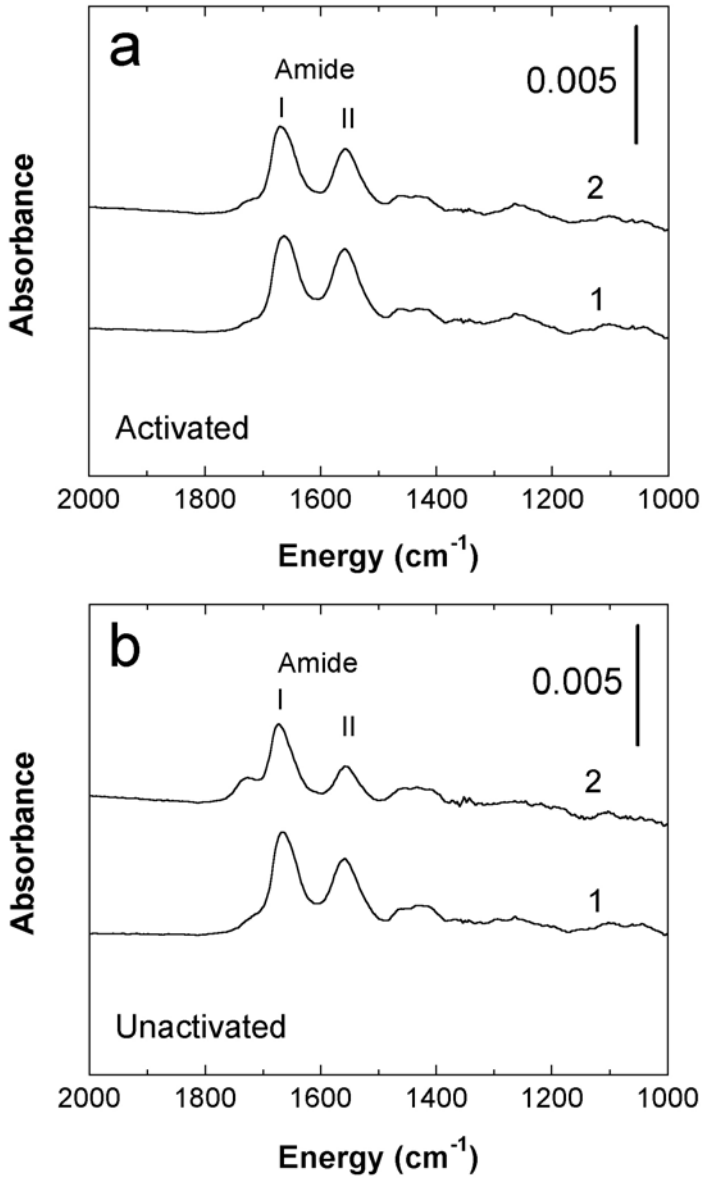

Figure 4.6. FTIR-ERS spectra of a Pd DEN film attached to a MUA SAM (a) with and (b) without activation of the SAM. In both (a) and (b), spectrum 1 was obtained after sonication in water at pH 7 for 30 s and spectrum 2 was obtained after sonication in water at pH 2 for 5 min.

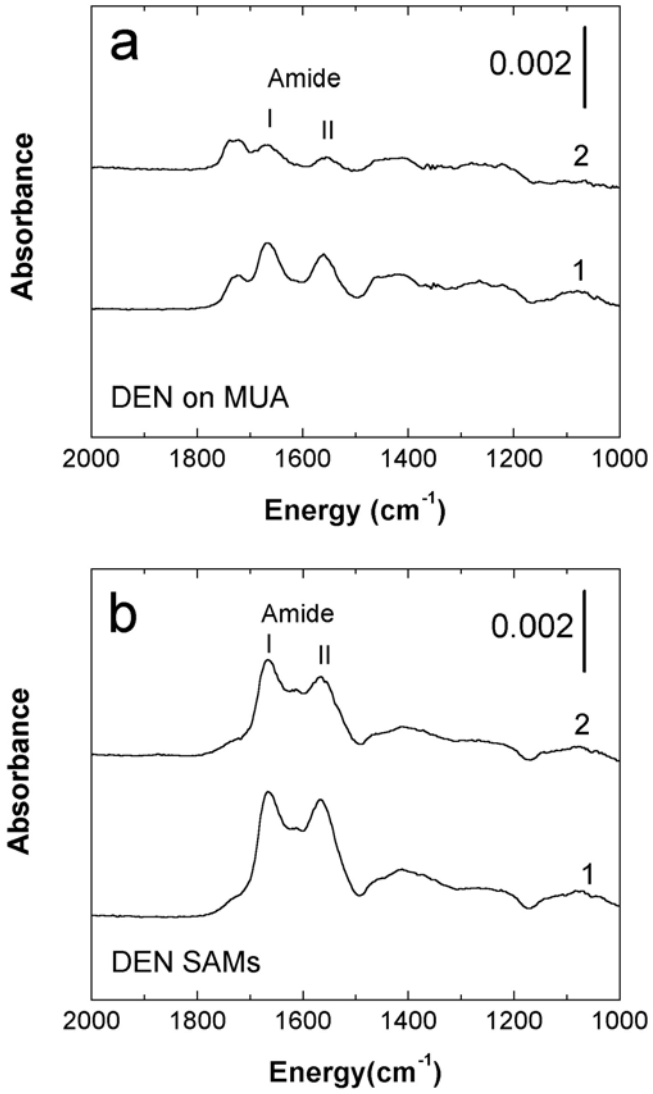

Figure 4.7. FTIR-ERS spectra of (a) G4-OH(Pd_{30}) electrostatically linked to MUA monolayers on a Au substrate; (b) G4-OH(Pd_{30}) physisorbed directly onto a Au substrate. The amide I and II peaks, which are characteristic of the surface-confined dendrimer, are present at 1665 cm^{-1} and 1567 cm^{-1}, respectively. In both (a) and (b), spectrum 1 was obtained after sonication in water at pH 7 for 30 s and spectrum 2 was obtained after sonication in water at pH 2 for 5 min.

groups, and this in turn suggests nearly complete conversion of the acid to amide linkages between the dendrimer and the SAM. Although the IR data do not provide definitive proof for covalent attachment, they are suggestive. The important point is that regardless of how the G4-NH_2(Pd_{30}) monolayer is prepared, it provides a significantly more robust film and higher coverage than a G4-OH(Pd_{30}) monolayer prepared on either a naked Au substrate or a MUA SAM (see Figure 4.7).

Because of spectral interferences it was not possible to confirm the presence of Pd on the Au surface by X-ray photoelectron spectroscopy (XPS). However, an experiment was carried out to couple Pt DENs to an activated MUA surface following the procedure described for Pd DENs, and the result definitively showed zerovalent Pt on the surface (see Figure 4.2).

4.5 Summary and Conclusions

We have shown that Pt and Pd nanoparticles can be prepared within amine-terminated PAMAM dendrimers by selective protonation of the terminal amine groups and selective metal-ion complexation with interior amine groups. The properties of the metal nanoparticles are about the same as those we have previously prepared within hydroxyl-terminated PAMAM dendrimers, but the presence of the amine groups provides a reactive handle for linking DENs to surfaces, polymers, or other molecules. This approach complements another strategy we previously described for preparing reactive DENs.[79] The approach described here uses commercially available dendrimers and yields higher coverages of DENs on surfaces, but there are strict pH conditions

required for DEN synthesis. The partially quaternized DENs[79] require custom synthesis of the dendrimer and yield lower-coverage films, but there are no special pH requirements for DEN synthesis.

CHAPTER V

ELECTROCATALYTIC O_2 REDUCTION AT GLASSY CARBON ELECTRODES MODIFIED WITH DENDRIMER-ENCAPSULATED Pt NANOPARTICLES*

5.1 Synopsis

Platinum dendrimer-encapsulated nanoparticles (DENs) were prepared within fourth-generation, hydroxyl-terminated, poly(amidoamine) dendrimers and immobilized on glassy carbon electrodes using an electrochemical immobilization strategy. X-ray photoelectron spectroscopy, electron microscopy, and electrochemical experiments confirm that the Pt DENs are about 1.4 nm in diameter and that they remain within the dendrimer following surface immobilization. The resulting Pt DEN films are electrocatalytically active for the oxygen reduction reaction. The films are also robust, surviving up to 50 consecutive cyclic voltammograms and sonication.

5.2 Introduction

Here we show that dendrimer-encapsulated Pt nanoparticles of uniform size can be immobilized on glassy carbon electrodes (GCEs) and that they are electrocatalytically active for the O_2 reduction reaction (ORR) (Figure 5.1).[4] This is a significant finding, because there are few alternative methods for immobilizing highly uniform nanoparticle catalysts on electrode surfaces. Therefore, the approach described in this chapter will

---

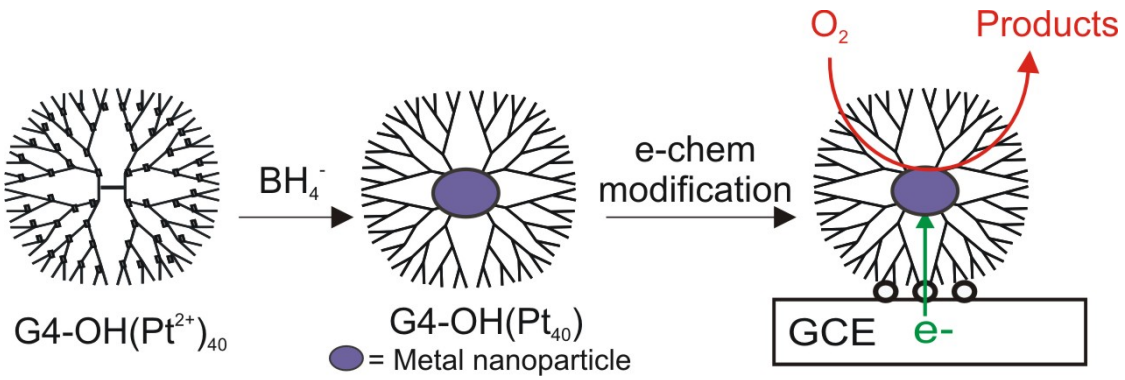

Figure 5.1. Schematic illustration of ORR on GCEs modified with Pt DENs.

provide a convenient model system for correlating the size, composition, and structure of nanoparticles to their electrocatalytic activity.

Dendrimer-encapsulated nanoparticles (DENs) are prepared by a two-step process.[2] First, metal ions are extracted into dendrimers where they coordinate in fixed stoichiometries with interior functional groups. Second, the metal-ion/dendrimer composites are reduced to yield encapsulated nanoparticles. This process leads to stable, nearly size-monodisperse, catalytically active nanoparticles composed of Pt,[7,56,78,79,104] Pd,[9,13,14,16,56-59,79-81,104] Au,[62,82-84] or Cu.[60] It is also possible to prepare alloy[6,11,12,63] and core/shell[6,12] bimetallic nanoparticles using a slight variation on this basic synthetic scheme. Monometallic and bimetallic DENs have previously been shown to be catalytically active for homogeneous hydrogenation and carbon-carbon coupling reactions[8] as well as for heterogeneous catalytic reactions.[19,20] We have also shown that it is possible to physisorb DENs onto Au electrodes and use them to electrocatalytically reduce O_2.[7] However, adhesion of the DENs to the electrode surface was poor and catalytic activity deteriorated quickly. We attempted to improve stability by covalently linking the terminal amine groups of the dendrimers to an *n*-alkanethiol monolayer having a distal acid group,[79,104] but the distance between the Pt nanoparticle and the electrode was too large and no catalytic current was observed.

In this chapter we report a new strategy for DEN immobilization on GCEs that is simple, and that leads to robust, electrocatalytically active DEN monolayers. The approach involves preparation of DENs within hydroxyl-terminated dendrimers and subsequent coupling of the dendrimer to the GCE surface via an electrooxidation

reaction. Similar electrochemical immobilization strategies have been reported for the oxidation of amines,[105] arylacetates,[106] and alcohols,[107] as well as for the reduction of aryl diazonium cations.[108-110] Here, we are particularly interested in prior examples of the electrooxidation of alcohols, because the dendrimers used in this study have multiple hydroxyl groups on their periphery. Specifically, Ohmori and coworkers reported that various alcohols can be electrochemically attached to GCEs via ether bonds in anhydrous alcohol solutions.[107,111] They also reported that triethylene glycol could be oxidatively coupled to GCEs.[112]

There are three general approaches for immobilization of electrocatalytic nanoparticles onto electrode surfaces. The first involves two steps: synthesis of the nanoparticles followed by surface immobilization.[7,31,113-117] This includes the most common method for preparing electrocatalysts: physical deposition of a mixture of carbon-supported metal nanoparticles and Nafion onto an electrode surface.[31,113-115] The dendrimer-based approach reported here also fits into this category. In the second family of methods, nanoparticle formation and immobilization occur simultaneously. This approach includes electrodeposition of metal particles onto electrodes modified with polymer films,[118-122] vacuum evaporation,[123] and electroless deposition.[124-126] The third approach involves immobilization of metal ions, usually within a polymer, and then reduction to metal nanoparticles.[127-129]

In this chapter, we report the preparation of Pt nanoparticles within fourth-generation, hydroxyl-terminated, poly(amidoamine) (PAMAM) dendrimers (G4-OH) and the subsequent electrooxidative coupling of the composite to GCEs in an aqueous

0.1 M $LiClO_4$ electrolyte solution. The Pt electrocatalysts contain an average of 40 atoms each and have a diameter of 1.4 ± 0.3 nm.[7,56] Electrodes modified with these Pt DENs are electrocatalytically active for oxygen reduction, implying that the encapsulated Pt nanoparticles are within tunneling distance of the GCE surface. Moreover, the Pt DEN monolayers are robust, surviving up to 50 consecutive electrochemical scans through the O_2 reduction process and sonication for up to 10 min in 0.5 M H_2SO_4 with no significant change in activity.

5.3 Experimental Section

Chemicals. G4-OH dendrimers were purchased as a 10-25% methanol solution (Dendritech, Inc., Midland, MI). Prior to use, the methanol was removed under vacuum. K_2PtCl_4 (Strem Chemicals, Inc.), $NaBH_4$, $LiClO_4$, CH_2Cl_2, 1-dodecanethiol (The Aldrich Chemical Co.), and H_2SO_4 (EMD Chemicals, Inc.) were used without further purification. 18 MΩ·cm Milli-Q deionized water (Millipore, Bedford, MA) was used to prepare aqueous solutions.

Preparation of Pt DENs. Pt DENs were prepared according to a previously published procedure.[7,56] Briefly, 40 mol equiv of an aqueous 0.1 M K_2PtCl_4 solution was added to a 50 μM aqueous G4-OH solution. The mixture was stirred for 48 h to allow the Pt ions to complex with the interior amines of the dendrimers. Zerovalent Pt DENs (G4-OH(Pt_{40})) were synthesized by slow addition of a 10–fold excess of an aqueous 0.5 M $NaBH_4$ solution. This Pt DEN solution was allowed to stand in a closed vial for 5 h to ensure complete reduction of Pt. Finally, the solution was dialyzed using a cellulose

dialysis sack having a molecular weight cutoff of 12,000 (Sigma Diagnostics, Inc.) to remove impurities.[80] The resulting Pt DENs were examined by transmission electron microscopy (TEM), which showed that the mean particle size was 1.4 ± 0.3 nm (Figure 5.2). This result is comparable to our previous results.[7,56]

Electrode Preparation. Glassy carbon (GC) disks (Bioanalytical Systems, Inc., 3.0 mm diameter) and GC plates (Tokai Carbon Co., grade GC-20,) were used as electrodes. GC plates were obtained as 10 cm x 10 cm x 0.3 cm plates and cut into 2 cm x 1 cm x 0.3 cm pieces before use. Both types of GCEs were prepared by polishing with 1.0 and 0.3 μm alumina powder on a polishing cloth (Buehler) followed by sonication in water for 10 min. The electrodes were then rinsed with water and ethanol and dried under flowing N_2 gas. All electrochemical experiments were performed in a single-compartment, glass cell using a standard three-electrode configuration with a Pt-gauze counter electrode and a Ag/AgCl (3 M NaCl) reference electrode (Bioanalytical Systems, Inc.). Cyclic voltammetry was performed using a Pine AFRDE4 potentiostat configured with an X-Y recorder.

Characterization. X-ray photoelectron spectroscopy (XPS) data were acquired using an Axis His 165 Ultra Kratos instrument (Manchester, UK) with a Mg $K_{\square}$ X-ray source. The XPS positions were referenced to the C(1s) peak at 284.5 eV. TEM images were obtained using a JEOL-2010 TEM having a point-to-point resolution of 0.19 nm. Samples were prepared by placing a drop of solution on a holey-carbon-coated grid and allowing the solvent to evaporate in air. Field-emission scanning electron microscopy (FESEM) images were obtained using a Zeiss VP1530 microscope.

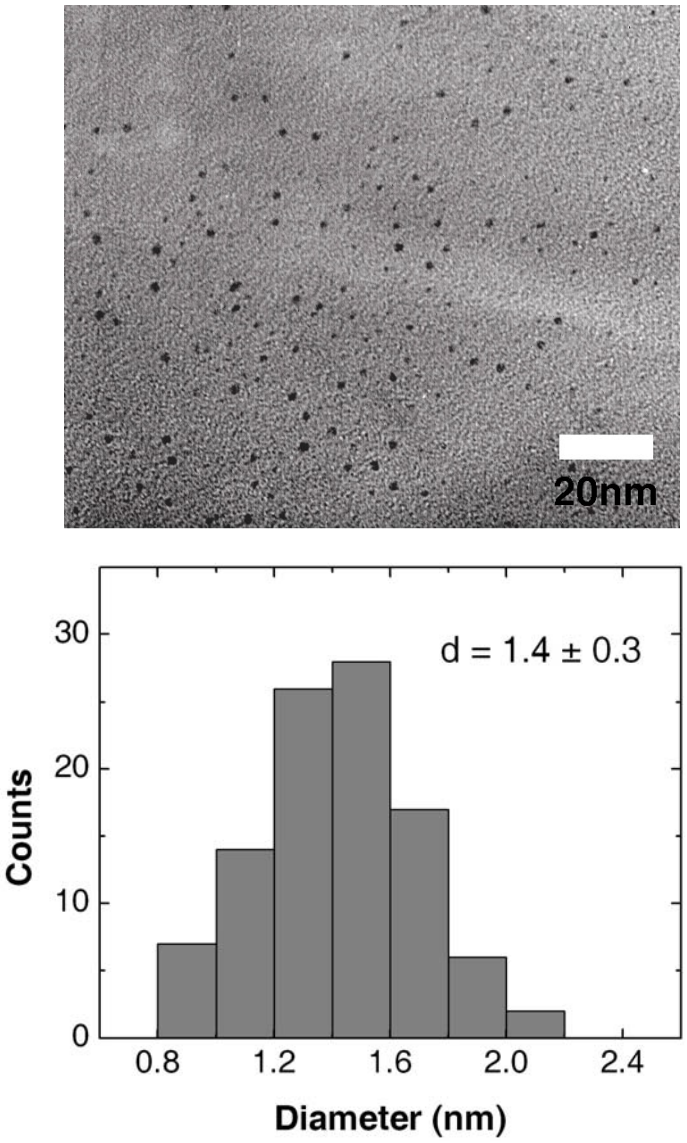

Figure 5.2. TEM image and particle-size distribution for the G4-OH(Pt_{40}) DENs used in the catalysis experiments. Particle-size distributions are based on 100 randomly selected particles.

5.4 Results and Discussion

Immobilization of Pt DENs on GCEs. The immobilization of Pt DENs on GCEs was carried out using a procedure similar to that reported by Ohmori and coworkers for the modification of GCEs with alcohols.[107,111] A freshly polished GCE was placed in an aqueous 20 μM G4-OH(Pt_{40}) solution containing 0.1 M $LiClO_4$, and then the potential of the electrode was scanned three times between 0 V and 1.0 V (vs. Ag/AgCl, 3 M NaCl). This resulted in robust immobilization of the Pt DENs. Figure 5.3a shows three cyclic voltametric background scans obtained in a DEN-free electrolyte solution. Only a small background current is observed. The data in Figure 5.3b were obtained under the same conditions as Figure 5.3a, but in the presence of Pt DENs. An irreversible oxidation wave appears at potentials > 0.6 V. For alcohols, the current associated with this wave has previously been attributed to electrochemical oxidation of the GCE, which is followed by nucleophilic attack on hydroxyl groups.[107,111] However, this mechanism is speculative and the details remain to be worked out. After the first scan, the current decreases and then remains approximately constant for the third scan. We believe the decrease in the oxidation wave is mainly attributable to the irreversible immobilization of Pt DENs onto the GCE after the first scan.

XPS measurements confirmed the presence of both the dendrimer and Pt on the GCE after electrochemical immobilization of the DENs. Figure 5.4a shows the XPS spectrum of a Pt DEN-modified GCE electrode. The N(1s) peak at 399.8 eV confirms the presence of the PAMAM dendrimers, while the Pt(4d) and Pt(4f) peaks confirm the presence of Pt. The Pt($4f_{7/2}$) and Pt($4f_{5/2}$) peaks are present at 75.3 eV and 72.1 eV,

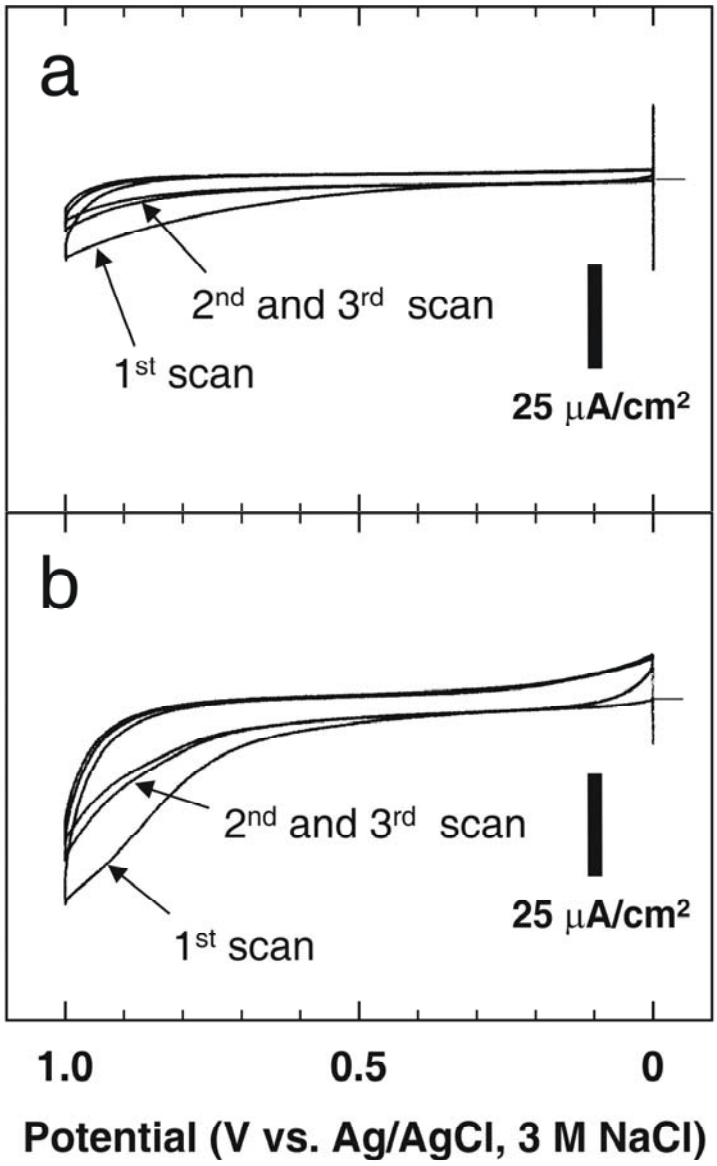

Figure 5.3. Three consecutive cyclic voltammograms obtained using a freshly polished GCE in (a) electrolyte solution only; (b) electrolyte solution plus 20 μM G4-OH(Pt_{40}). The aqueous electrolyte solution contained 0.1 M $LiClO_4$. The scan rate was 10 mV/s.

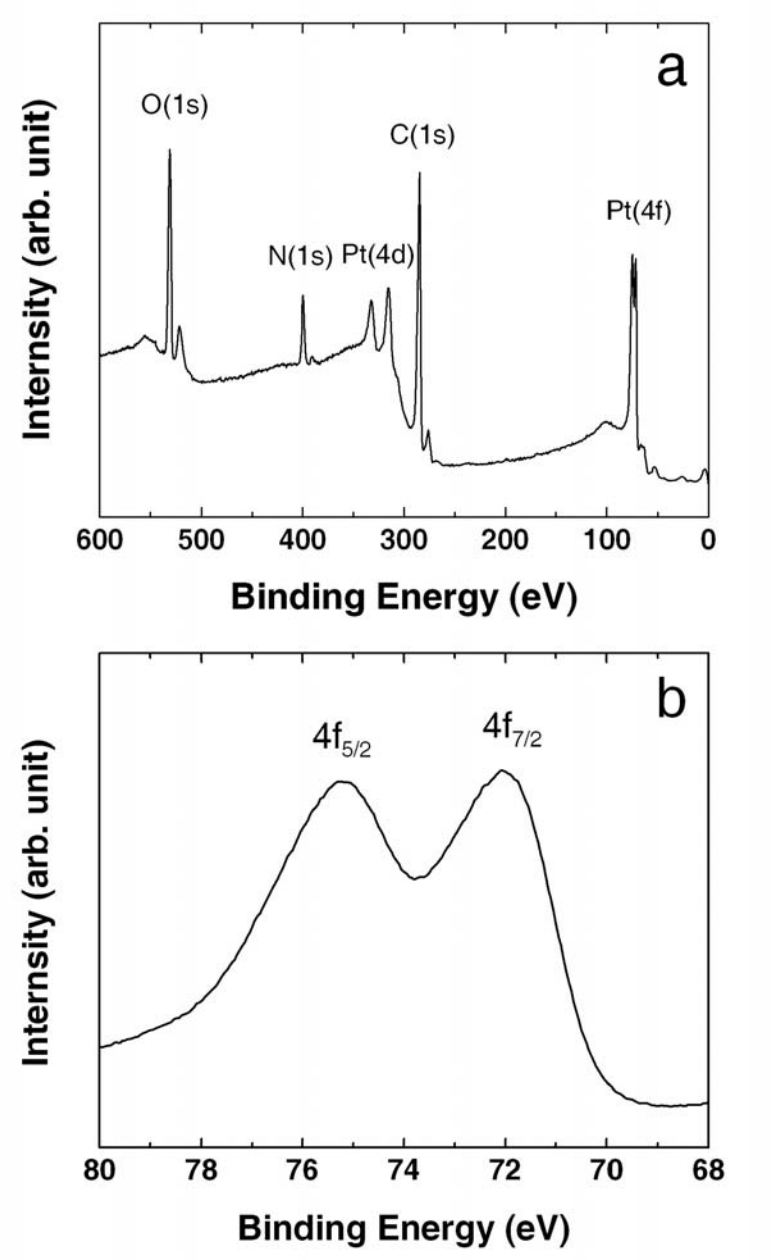

Figure 5.4. (a) An XPS spectrum of a G4-OH(Pt_{40}) film electrochemically immobilized on a GCE. (b) A high-resolution XPS spectrum in the Pt(4f) region for the same film. The electrode was cut from a sheet of glassy carbon, as described in the Experimental Section.

respectively, which is slightly higher than would be observed for bulk Pt (71.2 eV for Pt($4f_{5/2}$)). However, this result agrees with previous XPS investigations of Pt DENs and is probably a consequence of the small size of these nanoparticles and the presence of the dendrimeric ligands.[97-99]

To confirm that the Pt DENs described in the previous paragraph are not just physisorbed to the electrode surface, we performed a control experiment in which a GCE was soaked in a Pt DEN solution for 15 min but with no potential applied. The GCE prepared using this method also revealed the presence of Pt and N peaks in the XPS spectra (Figure 5.5), but they were substantially lower (31 and 42%, respectively) than those obtained using electrochemically modified GCEs. This is the anticipated result, because PAMAM dendrimers physisorb to nearly all surfaces including Au,[7,103] mica,[130] and highly oriented pyrolytic graphite (HOPG).[130] We also examined a GCE modified exactly as described for Figure 5.4, except in this case only the dendrimer was immobilized (no Pt DEN). The resulting XPS spectrum (Figure 5.5) indicated the presence of N and the absence of Pt. Interestingly, the peak intensity of N was only 50% as intense as that shown in Figure 5.4a. This might suggest that the encapsulated Pt nanoparticles catalyze linking of the dendrimer onto the GCE surface.[131]

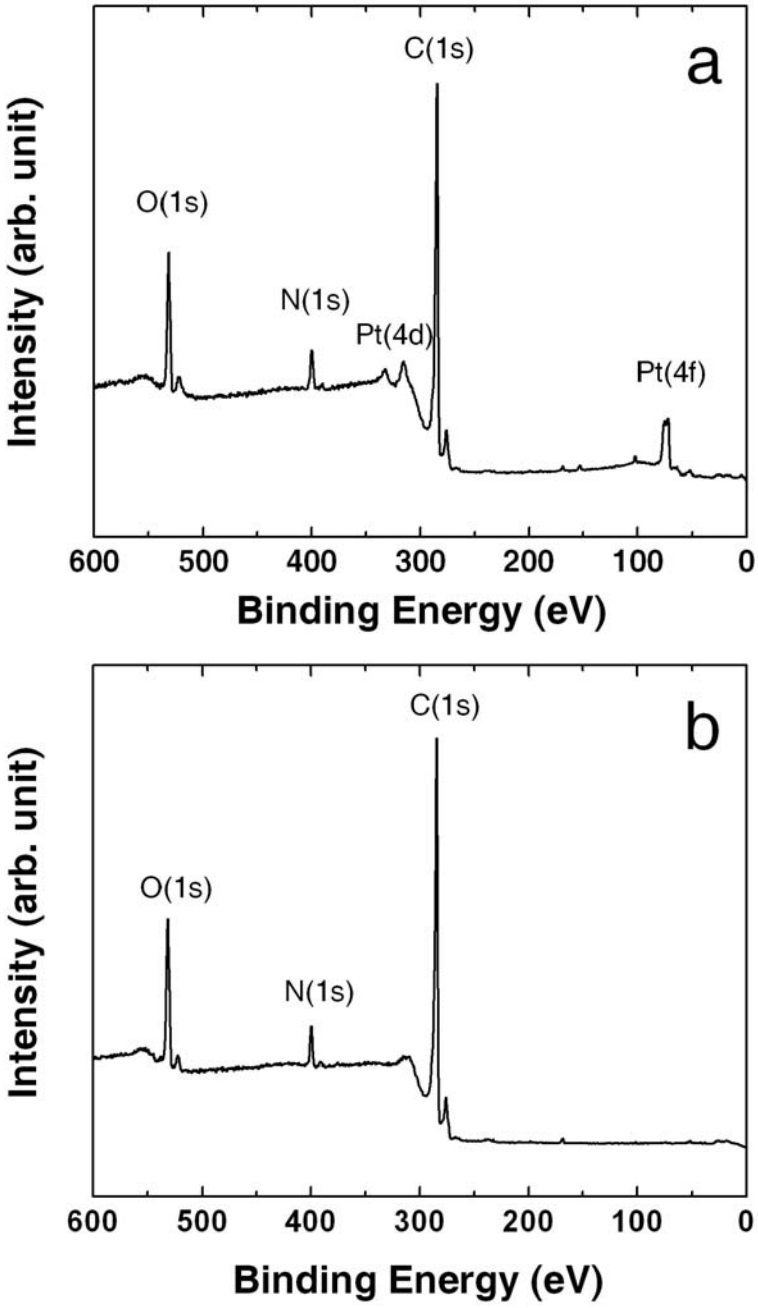

Figure 5.5. (a) XPS spectrum of a GCE treated identically to that described for Figure 5.4, except: (a) without applying an electrochemical potential and (b) in the presence of Pt-free G4-OH dendrimers.

The size of the immobilized DENs was examined by TEM and FESEM. TEM micrographs were obtained by scraping Pt DENs off the electrode surface and examining the powder. The results indicated that the particle size was 1.6 ± 0.4 nm (Figure 5.6), which is just slightly larger than the diameter of the DENs prior to immobilization (1.4 ± 0.3 nm). FESEM has a resolution of 2.1 nm, and there were no observable differences between micrographs obtained from unmodified (naked) GCEs and GCEs modified with Pt DENs. This indicates that there are no Pt aggregates > ~10 nm in diameter present on the GCE surface (Figure 5.7).

Electrocatalytic O_2 Reduction. Figure 5.8 shows cyclic voltammograms (CVs) for the reduction of O_2 at a naked GCE, a GCE modified with Pt-free G4-OH dendrimers, and a GCE modified with G4-OH(Pt_{40}) DENs. All three CVs were obtained in an O_2-saturated aqueous electrolyte solution containing 0.5 M H_2SO_4. Reduction at the naked GCE begins at a potential of about -0.1 V, and there is a well-defined peak at –0.39 V attributable to O_2 reduction. The electrochemical behavior at a GCE modified with G4-OH (but no Pt DENs) is similar to the naked GCE. However, the G4-OH(Pt_{40})-modified GCE exhibits an onset current of about 0.5 V and a well-defined peak at 0.22 V. The ~600 mV positive shift in the O_2 reduction peak for the Pt DENs indicates a significant electrocatalytic effect. It also demonstrates that the Pt DENs are within electron tunneling distance of the GCE surface, and that O_2 is able to penetrate the G4-OH dendrimer, encounter the encapsulated Pt nanoparticle, and that the product of the reaction is able to escape the dendrimer interior.

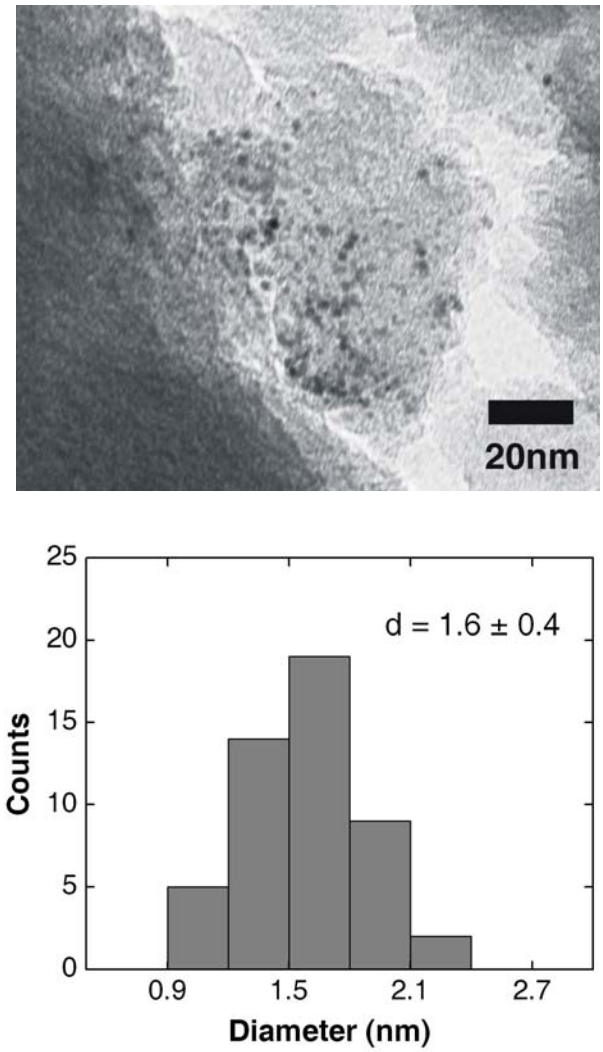

Figure 5.6. TEM image and particle-size distribution for G4-OH(Pt_{40}) DENs immobilized on a GC plate using the electrochemical method described in the text. The sample was prepared as follows. The Pt-DEN-modified GC plate was ground gently with an abrasive strip (Buehler, 600 grit), the resulting powder, consisting of GC particles, DENs, and grit from the abrasive, was dispersed in ethanol, and then a few drops of the suspension were placed on a TEM grid and allowed to dry. The particle-size distribution is based on 50 randomly selected particles.

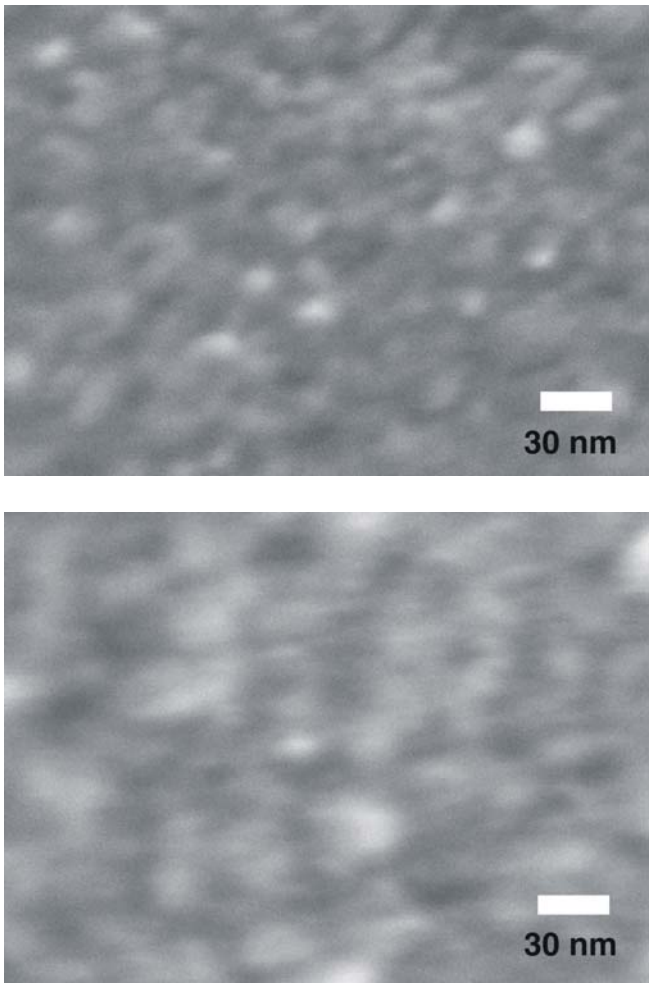

Figure 5.7. FESEM images of (top) a G4-OH(Pt_{40})-modified GC plate and (bottom) a naked GC plate. There is no detectable difference between the two images, suggesting that large aggregates (> 10 nm) of Pt are not present on the surface. The resolution of the microscope is 2.1 nm.

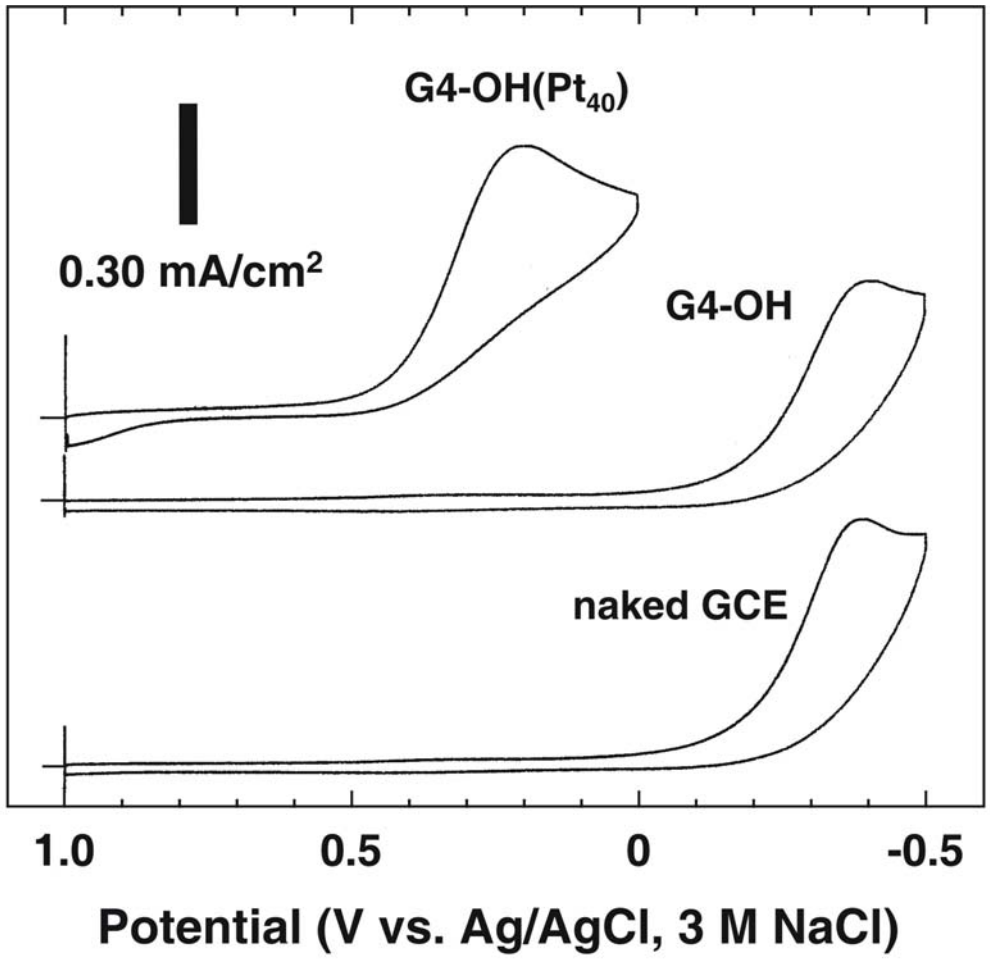

Figure 5.8. CVs for the reduction of O_2 using (top to bottom) a GCE modified with G4-OH(Pt_{40}) DENs, a GCE modified with Pt-free G4-OH dendrimers, and a naked GCE. The data were obtained in an aqueous 0.5 M H_2SO_4 electrolyte solution saturated with O_2. The scan rate was 50 mV/s.

The electrocatalytic properties of GCEs modified with physisorbed Pt DENs (no electrochemical linking to the GCE) were also examined. These surfaces were found to be less catalytically active than the electrochemically linked films (Figure 5.9). For example, the O_2 reduction peak had a poorly defined shape and was shifted 140 mV negative compared to the uppermost CV shown in Figure 5.8. Control experiments corresponding to the three CVs in Figure 5.8, but carried out in O_2-free electrolyte solutions, were also performed. They revealed only a small background current (Figure 5.10). This result confirms our contention that the peaks in Figure 5.8 arise from O_2 reduction.

Stability of G4-OH(Pt_{40})-modified GCEs. The stability of the G4-OH(Pt_{40}) films on GCEs was tested by repetitive cycling between 1.0 V and 0 V. Even after 50 scans, no significant change in the O_2 reduction peak current or position was observed (Figure 5.11). As a further test of stability, a G4-OH(Pt_{40})-modified GCE was sonicated in a 0.5 M H_2SO_4 solution for 10 min, and afterwards the resulting voltammetry indicated no significant change of the O_2 reduction peak current or position compared to a CV obtained prior to sonication (Figure 5.11). XPS measurements were also performed to verify the presence of the dendrimer and Pt after both of these stability tests. The resulting XPS spectra showed no significant change of the N and Pt bands compared to the freshly prepared G4-OH(Pt_{40}) films. These results support the presence of a robust link between the dendrimer and the GCE, and an equally durable attachment of the Pt nanoparticle within the dendrimers.

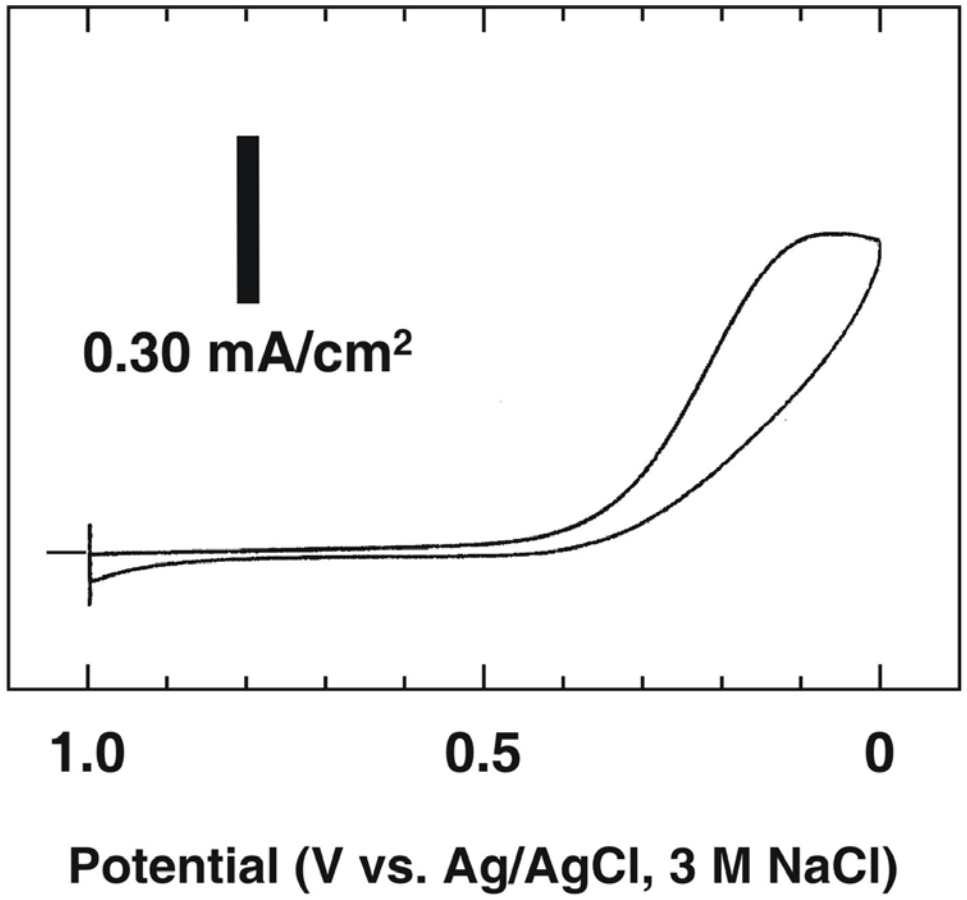

Figure 5.9. CV of a GCE prepared as in Figure 5.5a and obtained in an O_2-saturated 0.5 M H_2SO_4 electrolyte solution. The scan rate was 50 mV/s.

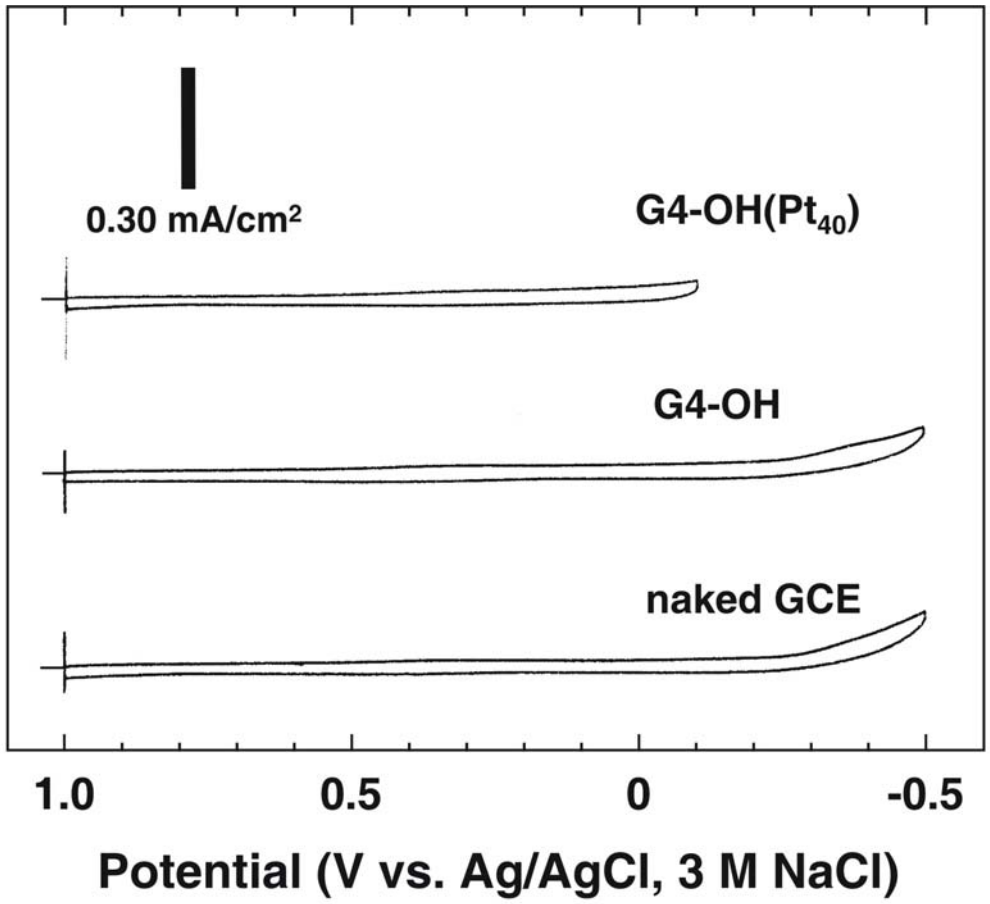

Figure 5.10. CVs obtained in N_2-saturated 0.5 M H_2SO_4 electrolyte solution using (top to bottom) a GCE modified with G4-OH(Pt_{40}) DENs, a GCE modified with Pt-free G4-OH dendrimers, and a naked GCE. The scan rate was 50 mV/s.

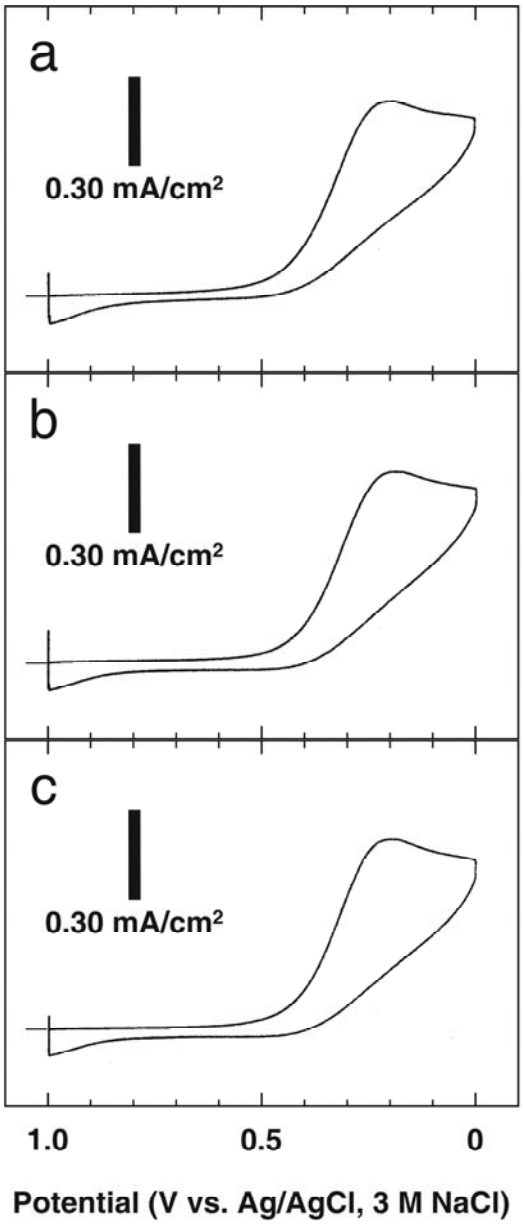

Figure 5.11. CVs obtained using a GCE modified with G4-OH(Pt_{40}) DENs. (a) 1st scan, (b) 50th scan, and (c) after sonicating for 10 min in 0.5 M H_2SO_4 solution. Data were obtained in an O_2-saturated 0.5 M H_2SO_4 electrolyte solution. The scan rate was 50 mV/s. There is no measurable difference between the CVs, indicating robust attachment to the GCE.

Location of the Pt Nanoparticles. Thus far, we have assumed that the Pt nanoparticles remain within the dendrimers during immobilization. However, the data presented up to this point does not exclude the possibility that the Pt DENs are somehow extracted from within the dendrimers and present as naked nanoparticles, possibly as aggregates having diameters below the resolution of FESEM (~10 nm), sorbed to the GCE surface (Figure 5.12). While we view this scenario as unlikely, it is fundamental to the central claim of this chapter (Figure 5.1) and therefore needs to be addressed.

To verify that the Pt nanoparticles remain within the dendrimers during the electrochemical immobilization procedure, we performed a selective Pt DEN poisoning experiment using 1-dodecanethiol (C12SH) dissolved in either ethanol or CH_2Cl_2. Because ethanol is a good solvent for PAMAM dendrimers, we hypothesized that the dendrimer would have an open structure in ethanol. Therefore, C12SH should easily penetrate the outer branches of the dendrimer, adsorb to the surface of the encapsulated Pt nanoparticle, and reduce its subsequent electrocatalytic activity.[132,133] In contrast, we reasoned that the dendrimer would collapse around the Pt nanoparticles in CH_2Cl_2, which is a poor solvent for PAMAM dendrimers, and thereby protect the encapsulated DENs from C12SH adsorption. This hypothesis is based on existing literature demonstrating that the dendrimer branches can act as selective gates that modulate substrate access to DENs.[9] Additionally, it has previously been shown that in air, which of course is a very poor solvent for PAMAM dendrimers, the dendrimeric branches completely collapse around DENs and render them totally inaccessible to substrates.[18,19]

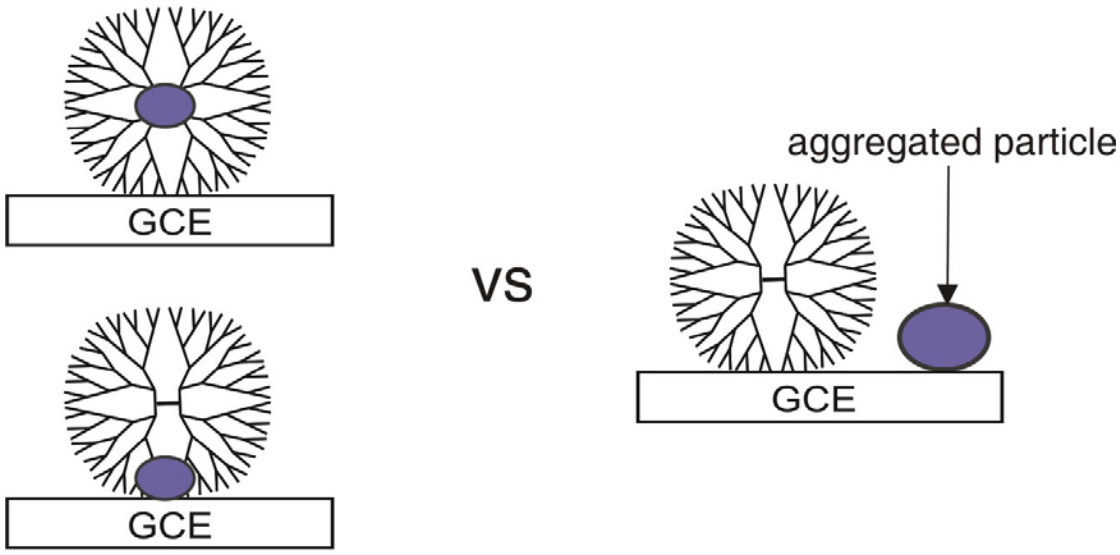

Figure 5.12. Possible forms of Pt DENs on GCEs after electrochemical immobilization.

After exposing Pt DEN-modified GCEs to 3 mM C12SH solutions in either ethanol or CH_2Cl_2 for 20 min and then rinsing in solvent and water, the CVs shown in Figure 5.13 were obtained in an O_2-saturated electrolyte solution. The top CV corresponds to C12SH treatment in CH_2Cl_2. This CV is only slightly changed compared to the corresponding CV shown in Figure 5.8, suggesting that during exposure to C12SH the dendrimer protected the nanoparticle against poisoning. In contrast, when the poisoning experiment was carried out in ethanol, the subsequent CV indicated extensive surface passivation of the Pt DENs. No change in electrocatalytic activity was observed for Pt DEN-films exposed to ethanol or CH_2Cl_2 in the absence of C12SH, which indicates that the differences in the two CVs shown in Figure 5.13 are not attributable to solvent (ethanol or CH_2Cl_2) poisoning. Based on these results, we concluded that Pt nanoparticles are present within the dendrimers (left side of Figure 5.12) even after the electrochemical immobilization process. Otherwise, there would be no effect of solvent on the accessibility of the naked Pt surface toward C12SH. Taken together with the microscopy results discussed earlier, which showed no evidence of metal aggregation, we are confident in concluding that the model of an intact, surface-immobilized Pt DEN catalyst is correct.

5.5 Summary and Conclusions

We have shown that Pt DENs prepared within hydroxyl-terminated PAMAM dendrimers can be immobilized on GCEs using an electrochemical attachment method. The resulting films are electrocatalytically active for O_2 reduction, and they are

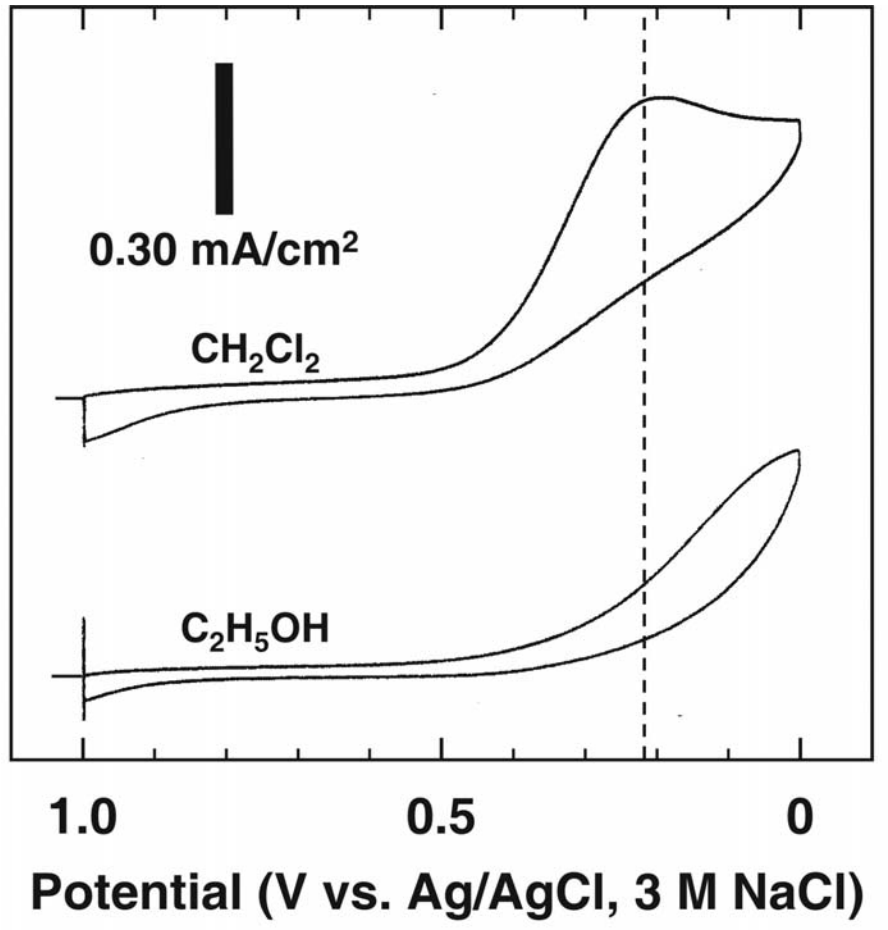

Figure 5.13. CVs obtained using G4-OH(Pt_{40})-modified GCEs. Prior to obtaining the CVs, the modified electrodes were exposed to C12SH dissolved in either CH_2Cl_2 (top) or ethanol (bottom) for 20 min. The CVs were obtained in an aqueous 0.5 M H_2SO_4 electrolyte solution saturated with O_2. The dashed line shows the position of O_2 reduction peak before the modified electrodes were exposed to C12SH solution. The scan rate was 50 mV/s.

remarkably stable, retaining their electrocatalytic properties even after 50 consecutive cyclic voltammetric scans through the O_2 reduction wave. Selective thiol poisoning experiments demonstrate that the Pt nanoparticles are retained within the dendrimers after electrochemical immobilization. Future studies will involve the use of electrochemical generation-collection experiments to quantitatively assess the electrocatalytic activity of the metal nanoparticles,[113,114] including alloy and core-shell bimetallic DENs,[6] as a function of the size and elemental composition of the DENs.[31]

CHAPTER VI

THE EFFECT OF ELEMENTAL COMPOSITION OF 180-ATOM PtPd BIMETALLIC NANOPARTICLES ON THE KINETICS OF THE ELECTROCHEMICAL OXYGEN REDUCTION REACTION*

6.1 Synopsis

PtPd bimetallic nanoparticles containing an average of 180 atoms and composed of seven different Pt:Pd ratios have been prepared within sixth-generation, hydroxyl-terminated, poly(amidoamine) dendrimers. Transmission electron microscopy indicates that the sizes of all seven nanoparticle compositions are within ±0.2 nm of one-another and the calculated size. Single-particle energy dispersive spectroscopy shows that the elemental composition is determined by the ratio of the Pt and Pd precursor salts used to prepare the nanoparticles. Cyclic voltammetry and rotating disk voltammetry measurements show that the Pt:Pd ratio of the nanoparticles determines their efficiency for the oxygen reduction reaction (ORR). The maximum rate for the ORR occurs at a Pt:Pd ratio of 5:1, which corresponds to a relative mass activity enhancement of 2.5 compared to otherwise identical monometallic Pt nanoparticles.

6.2 Introduction

In this chapter we demonstrate that well-defined PtPd bimetallic catalysts prepared by dendrimer templating can be used to precisely correlate the effect of catalyst

---

* Reprinted with permission from Ye, H.; Crooks, R. M. *J. Am. Chem. Soc.* **2006**, submitted for publication: unpublished work copyright 2006 American Chemical Society.

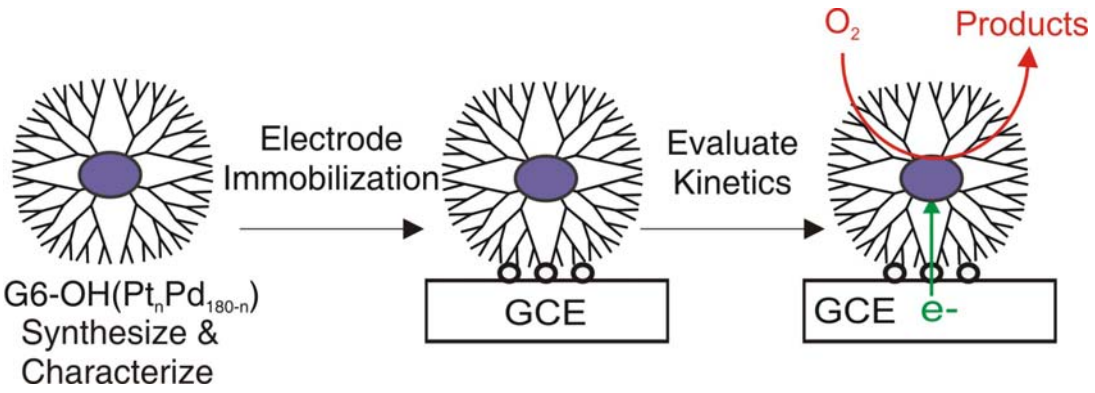

Figure 6.1. Schematic illustration of ORR on GCEs modified with PtPd DENs.

composition to the efficiency of the oxygen reduction reaction (ORR) (Figure 6.1). This is a significant finding for two reasons. First, dendrimer templating is the only method we are aware of for preparing very well defined, electrocatalytically active bimetallic nanoparticles in the < 3 nm size range. Here, 'well-defined' means size distributions having standard deviations of ±0.3 nm and particle-to-particle elemental compositional variations of $\leq 7\%$. Second, dendrimer-encapsulated catalysts can be characterized prior to electrode immobilization, using, for example, methods like transmission electron microscopy (TEM) and single-particle energy dispersive spectroscopy (EDS). This ensures that catalytic performance is not dominated by a small number of unique particles, which in turn makes it possible to directly correlate the elemental composition of the particles to their catalytic function. The results of this study indicate that certain bimetallic compositions of Pt and Pd exhibit more favorable kinetics for the ORR than particles of identical size but composed exclusively of Pt.

DENs are prepared in two-steps.[2] First, metal ions are extracted into dendrimers and coordinate in fixed stoichiometries with interior functional groups. Second, the intradendrimer metal ions are reduced to yield dendrimer-encapsulated nanoparticles (DENs). This process leads to stable, nearly size-monodisperse, catalytically active nanoparticles composed of Pt,[7,56,78,79,104,134] Pd,[9,10,13,14,16,17,56-59,79-81,104] Au,[62,82-84] or Cu.[60] It is also possible to prepare alloy[6,11,12,63] and core/shell[6,12] bimetallic DENs using a slight variation of this basic approach. Monometallic and bimetallic DENs have previously been shown to be catalytically active for homogeneous hydrogenation and carbon-carbon coupling reactions[8] as well as for heterogeneous catalytic reactions.[19,20]

Finally, we recently reported that Pt-only monometallic DENs can be immobilized on glassy carbon electrodes and that the resulting DEN monolayers are stable and electrocatalytically active for the ORR.[134]

Efficient O_2 reduction is a requirement for H_2/O_2 fuel cells. At present, only Pt is viewed as a viable metal catalyst for the ORR. However, even Pt suffers from a number of serious problems. First, the cost of Pt is too high for worldwide implementation of H_2/O_2 fuel cells. Second, the overpotential for the ORR is large even on Pt catalysts, and therefore most of the power loss in a H_2/O_2 fuel cells occurs at the cathode.[3] Accordingly, there has been a considerable amount of effort directed toward the discovery of alternative ORR catalysts. At present, many of these studies are focused on discovering multimetallic catalysts that contain some Pt plus an additional element or two that impart superior performance compared to Pt only. For example, the performance of bulk alloy electrodes[22,23,135] and thin alloy films[24,25,136] have been evaluated for the ORR. However, improvements in ORR activity have been most commonly associated with nanophase multimetallic alloys, such as Pt-Co,[30-32,37,137] Pt-Ni,[30,31,35] Pt-Cr,[30,34] and Pt-Fe[26,32,37], supported on carbon electrodes. Adzic and coworkers have reported a particularly interesting approach for preparing structured nanophase catalysts via deposition of catalytically active metals over a nonnoble core.[138] These materials, as well as related nonparticulate thin films,[38,139] have been shown to possess very high mass activities for the ORR. There have also been recent efforts to eliminate Pt from ORR catalysts altogether, and a number of materials have been reported that have ORR activities approximating that of Pt.[43-45] Finally, a number of theoretical studies have appeared that

provide insight into the origin of the activity enhancements in multimetallic ORR catalysts.[37-42]

In this chapter, we report the synthesis of well-defined bimetallic PtPd electrocatalysts containing 180 total atoms (~1.8 nm in diameter) but seven different ratios of Pt:Pd. TEM and EDS indicate that individual nanoparticles having particular Pt:Pd ratios are remarkably uniform in size and composition. Following complete characterization of these ORR catalysts, they were immobilized onto the surface of a glassy carbon electrode and their effectiveness evaluated as a function of composition using cyclic voltammetry and rotating disk voltammetry. The results indicated that PtPd bimetallic DENs of most compositions enhance the catalytic activity of the ORR. The maximum kinetic enhancement of 250% (vs. the equivalent monometallic Pt DEN catalyst) occurs for bimetallic nanoparticles containing 17% Pd.

6.3 Experimental Section

Chemicals. G6-OH dendrimers were purchased as an 11.46 % methanol solution (Dendritech, Inc., Midland, MI). Prior to use, the methanol was removed under vacuum. K_2PdCl_4 (Strem Chemicals, Inc., Newburyport, MA), K_2PtCl_4, $NaBH_4$, $LiClO_4$ (Sigma-Aldrich, Inc.), and H_2SO_4 (J.T.Baker, Ultrex II) were used without further purification. 18 MΩ·cm Milli-Q deionized water (Millipore) was used to prepare aqueous solutions. Research-grade O_2 gas (Praxair, 99.999%) was used for the ORR.

Preparation of PtPd DENs. PtPd DENs were prepared according to a previously published procedure.[11] Briefly, an aqueous solution containing K_2PtCl_4 and

K_2PdCl_4 prepared freshly (within 5 min) was added to a 10 μM aqueous G6-OH solution. The final metal-to-dendrimer ratio was fixed at 180 to 1 and the Pt:Pd ratio was adjusted to n:(180-n) where n = 180, 150, 120, 90, 60, 30, and 0. The metal complex/dendrimer solution was stirred for 72 h to allow the Pt and Pd ions to fully complex with the interior amines of the dendrimers.[7,56,104] Zerovalent PtPd DENs (G6-OH(Pt_nPd_{180-n})) were produced by slow addition of a 10–fold molar excess of aqueous 0.5 M $NaBH_4$ to this solution. The resulting PtPd DEN solutions were allowed to stand in a closed vial for 24 h to ensure complete reduction. Finally, the solution was dialyzed for 24 h using a cellulose dialysis sack having a molecular weight cutoff of 12,000 (Sigma-Aldrich, Inc.) to remove impurities.[80]

Electrochemistry. Glassy carbon (GC) disks (Pine Instruments, 5.0 mm diameter) were used as electrodes. Glassy carbon electrodes (GCEs) were prepared by successive polishing with 1.0 and 0.3 μm alumina powder on a polishing cloth (Buehler) followed by sonication in water for 5 min. The electrodes were then rinsed with water and dried under flowing N_2 gas. All electrochemical experiments were performed in a single-compartment, glass cell using a standard three-electrode configuration with a Pt-gauze (DEN immobilization) or an Au coil (ORR experiments) counter electrode and a mercury/mercurous sulfate reference electrode (CH Instruments, Inc., Austin, TX). For convenience, measured potentials are reported versus the Reversible hydrogen electrode (RHE). Cyclic voltammetry and rotating disk voltammetry were performed using a computer-controlled Pine Instruments (Grove City, PA) AFRDE4 potentiostat and ASR rotator. All electrochemical experiments were performed at 22 ± 1 °C.

Characterization. X-ray photoelectron spectroscopy (XPS) data were acquired using an Axis His 165 Ultra (Kratos, Manchester, UK) with a Mg K_α X-ray source. The XPS positions were referenced to the C(1s) peak at 284.5 eV. Instead of using GC disks, GC plates (Tokai Carbon Co., grade GC-20) were used as electrodes for XPS measurements. TEM and EDS measurements were performed using a JEOL-2010F TEM configured with an Oxford INCA energy dispersive spectrometer. Samples were prepared by placing several drops of solution on a carbon-coated Cu TEM grid and allowing the solvent to evaporate in air.

6.4 Results and Discussion

Characterization of Bimetallic DENs. Seven different G6-OH(Pt_nPd_{180-n})(n = 180, 150, 120, 90, 60, 30, and 0) DENs were synthesized and then characterized by TEM to determine their average size and size distribution (Figure 6.2, Figure 6.3, and Table 6.1). Assuming a spherical geometry, the calculated diameter of G6-OH(Pt_nPd_{180-n}) DENs is 1.7 nm. The average measured diameters for the seven different compositions used in this study ranged from 1.7 - 1.9 nm.

Previously we found that the molar ratio of metal salts or complexes (in this case K_2PdCl_4 and K_2PtCl_4) used to prepare bimetallic DENs is reflected in the nanoparticle composition after reduction.[11,12] To confirm that this is true in the present case, single-particle EDS analysis was performed for three of the DEN composition: (G6-OH($Pt_{120}Pd_{60}$), G6-OH($Pt_{90}Pd_{90}$), and G6-OH($Pt_{60}Pd_{120}$). Five particles selected randomly from each of these compositions were analyzed, and the results are provided in

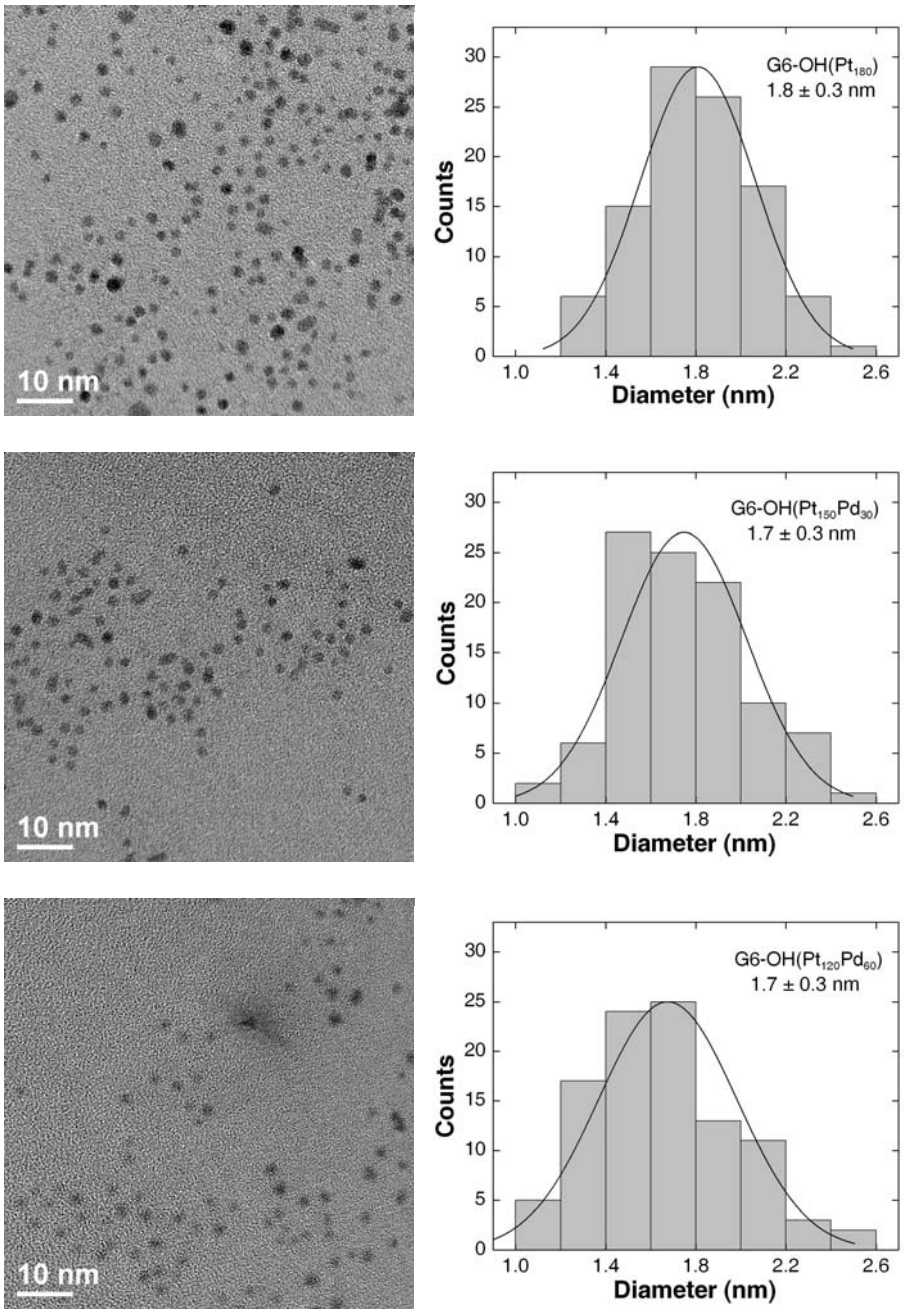

Figure 6.2. TEM images and particle-size distributions for G6-OH(Pt_{180}), G6-OH($Pt_{150}Pd_{30}$), and G6-OH($Pt_{120}Pd_{60}$) DENs. Particle-size distributions are based on 100 randomly selected particles.

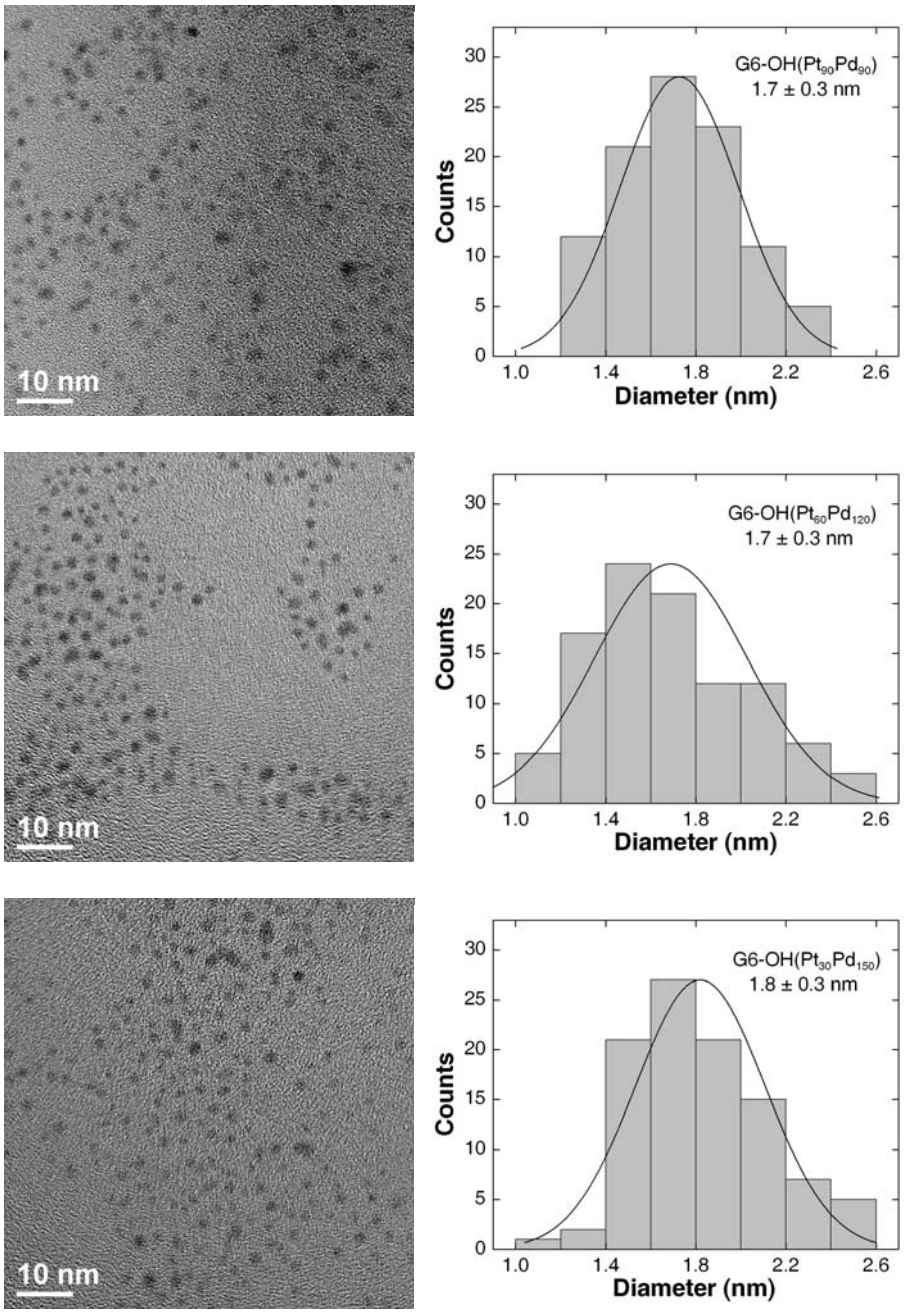

Figure 6.3. TEM images and particle-size distributions for G6-OH($Pt_{90}Pd_{90}$), G6-OH($Pt_{60}Pd_{120}$), and G6-OH($Pt_{30}Pd_{150}$) DENs. Particle-size distributions are based on 100 randomly selected particles.

Table 6.1. Measured and calculated particle sizes for Pt, PtPd, and Pd DENs

Sample	Average Particle Size	Calculated Size[a]
G6-OH(Pt_{180})	1.8 ± 0.3 nm	1.73 nm
G6-OH($Pt_{150}Pd_{30}$)	1.7 ± 0.3 nm	
G6-OH($Pt_{120}Pd_{60}$)	1.7 ± 0.3 nm	
G6-OH($Pt_{90}Pd_{90}$)	1.7 ± 0.3 nm	
G6-OH($Pt_{60}Pd_{120}$)	1.7 ± 0.3 nm	
G6-OH($Pt_{30}Pd_{150}$)	1.8 ± 0.3 nm	
G6-OH(Pd_{180})	1.9 ± 0.3 nm	1.72 nm

[a] Calculated using the equation $n = 4\pi r^3/3V_g$, where n is the number of Pt or Pd atoms, r is radius of the Pt or Pd nanoparticle, and V_g is the volume of one Pt (15.1 $Å^3$) or Pd (14.7 $Å^3$) atom calculated from the molar volume.[140]

Table 6.2. Additionally, the figure 6.4 provides a typical single-particle EDS spectrum for G6-OH($Pt_{90}Pd_{90}$). The EDS results indicate that the measured Pt:Pd ratios agree very well with the anticipated values (in parentheses) based on the ratios of the metal complexes used for the synthesis: G6-OH($Pt_{120}Pd_{60}$), 2.2 (2.0); G6-OH($Pt_{90}Pd_{90}$), 1.0 (1.0); and G6-OH($Pt_{60}Pd_{120}$), 0.6 (0.5). On the basis of the average compositions and sizes of the PtPd DENs, and the modest particle-to-particle variations in size and composition, we conclude that the O_2 reduction kinetics discussed later can be directly correlated to the composition of the DENs. That is, the electrochemical results are unlikely to be dominated by small populations of particles having unanticipated sizes or compositions. Indeed, the ability to correlate a population of particles having uniform structures to their catalytic function is the main point of this study.

Immobilization of Pt and PtPd DENs on GCEs. The immobilization of Pt and PtPd DENs on GCEs was carried out using a previously published procedure.[134] Briefly, a freshly polished GCE was placed in an aqueous 10 μM Pt or PtPd DEN solution containing 0.1 M $LiClO_4$, and then the electrode potential was scanned three times between 0.50 V and 1.40 V (vs. RHE) at a scan rate of 10 mV/s. Next, the electrode was rinsed with water, sonicated in water for 5 min, dried under flowing N_2 gas, and then immediately placed in the electrolyte solution used for ORR experiments. We have previously shown that this procedure results in robust immobilization of the dendrimer and that the DENs are in electrical communication with the electrode surface.[134] We have also demonstrated that the nanoparticles are retained within the dendrimers following electrode immobilization.[134] To confirm that the electrode coverage of DENs

Table 6.2. Atomic% analysis of individual G6-OH($Pt_{120}Pd_{60}$), G6-OH($Pt_{90}Pd_{90}$), and G6-OH($Pt_{60}Pd_{120}$) DENs.

Particle	G6-OH($Pt_{120}Pd_{60}$)		G6-OH($Pt_{90}Pd_{90}$)		G6-OH($Pt_{60}Pd_{120}$)	
	Pt (%)	Pd (%)	Pt (%)	Pd (%)	Pt (%)	Pd (%)
#1	72	28	50	50	36	64
#2	71	29	41	59	43	57
#3	71	29	52	48	38	62
#4	63	37	61	39	40	60
#5	69	31	46	54	41	59
Average	69 ± 4	31 ± 4	50 ± 7	50 ± 7	39 ± 3	61 ± 3

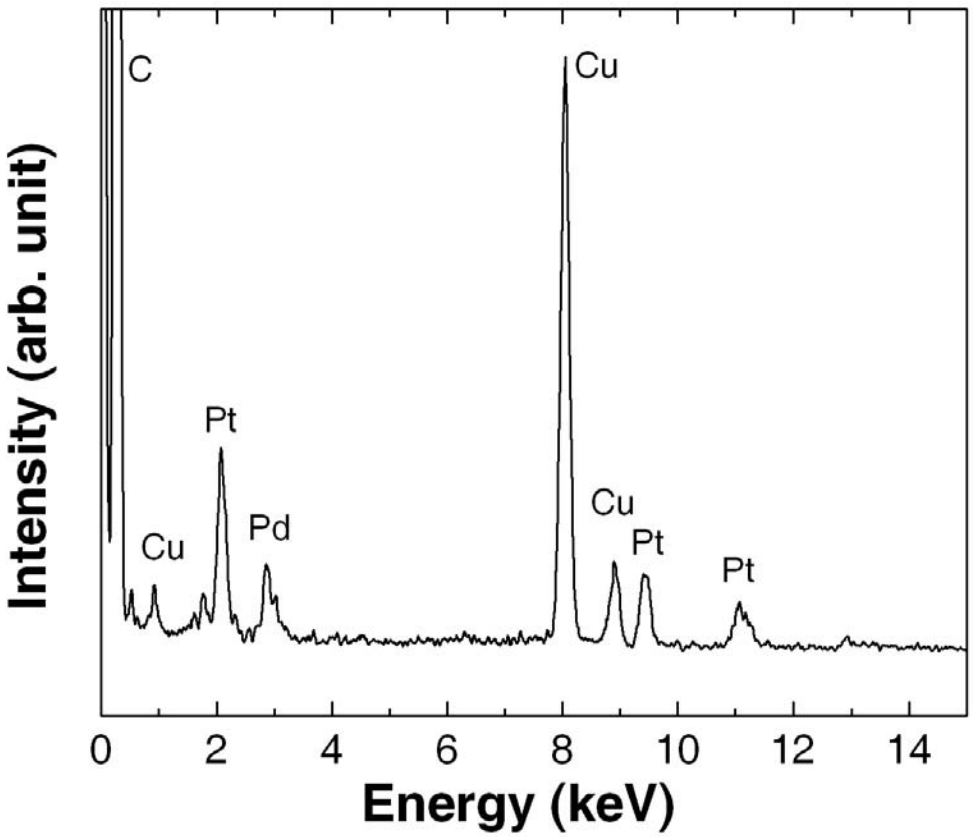

Figure 6.4. A single-particle EDS spectrum for G6-OH($Pt_{90}Pd_{90}$). The Cu and C signals are due to the TEM grid.

is independent of the type of encapsulated metal, we carried out the following experiment. An equimolar mixture of G6-OH(Pt_{180}) and G6-OH(Pd_{180}) DENs was immobilized on a GCE using the just-described electrochemical anchoring method, and then the elemental composition of the electrode surface was evaluated by XPS (Figure 6.5). The resulting XPS spectrum revealed that the atomic percentages of Pt and Pd on the surface were the same, indicating that the identity of the encapsulated nanoparticle does not bias the surface composition of DENs. We have previously shown that dendrimers adsorb onto surfaces at a constant number density that depends only on the generation of the dendrimer.[103] We infer from that study that the catalytic results reported next are not influenced by differences in the surface concentration of DENs.

Cyclic Voltammetry. Electrodes modified with seven different types of DENs (G6-OH(Pt_nPd_{180-n}), n = 180, 150, 120, 90, 60, 30, and 0) were prepared as described in the previous section, and their electrocatalytic properties were qualitatively evaluated using cyclic voltammetry. Figure 6.6a shows a series of seven cyclic voltammograms (CVs) obtained using electrodes modified with DENs having the same number of atoms but different Pt:Pd ratios. All CVs were acquired in an O_2-saturated aqueous electrolyte solution containing 0.5 M H_2SO_4 and using a scan rate of 50 mV/s. Before the CVs were obtained, the electrodes were activated by scanning the potential between 0.95 V and 0 V two times in the same electrolyte solution. Each CV (except G6-OH(Pd_{180})) exhibits a well-defined peak between 0.70 and 0.55 V that corresponding to the ORR. For example, the peak current for the electrode modified with G6-OH(Pt_{180}) is found at 0.67 V, but the electrodes coated with bimetallic PtPd DENs having low percentages of Pd exhibit ORR

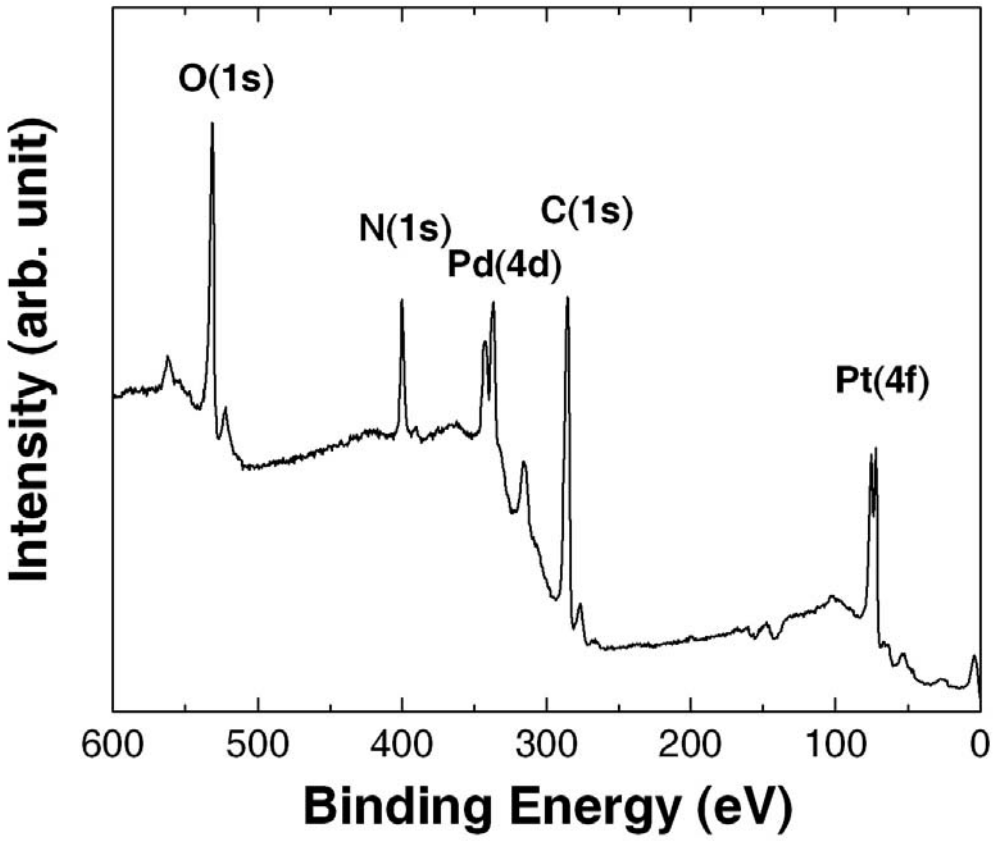

Figure 6.5. XPS spectrum of a mixed G6-OH(Pt_{180})/G6-OH(Pd_{180}) DEN film prepared from an equimolar solution of the two DENs.

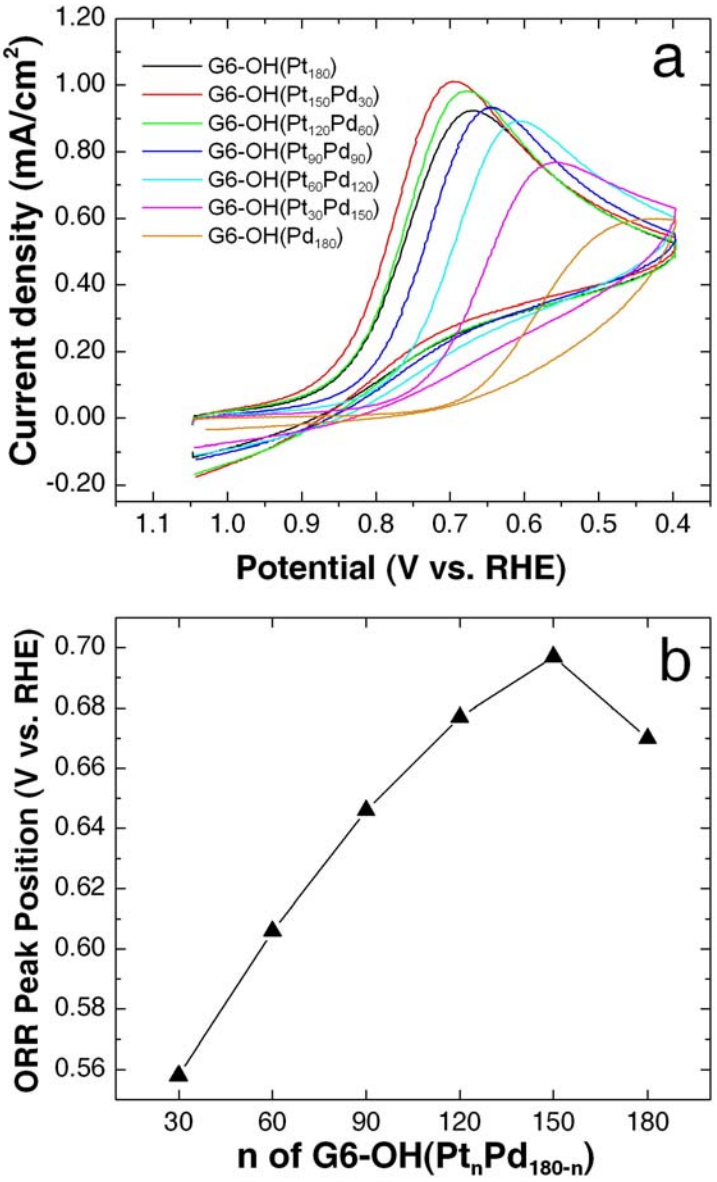

Figure 6.6. (a) Cyclic voltammograms of G6-OH(Pt_nPd_{180-n})(n = 180, 150, 120, 90, 60, 30, and 0). (b) A plot of the peak current position for the ORR as function of n of G6-OH(Pt_nPd_{180-n}). Scan rate: 50 mV/s; electrolyte solution: aqueous 0.5 M H_2SO_4 saturated with O_2.

peaks at more positive potentials (e.g., 0.70 V and 0.68 V for G6-OH($Pt_{150}Pd_{30}$) and G6-OH($Pt_{120}Pd_{60}$), respectively). This suggests that these bimetallic PtPd DENs have enhanced electrocatalytic ORR activity. Figure 6.6b summarizes the CV data by showing the potential of the peak current for the ORR as a function of increasing Pt percentage in each electrocatalytic particle. From these data it is clear that the maximum catalytic activity is achieved for G6-OH($Pt_{150}Pd_{30}$).

For electrocatalytic reactions, it is important to know the active surface area of the catalyst. We determined this value experimentally using the hydrogen adsorption/desorption method.[141,142] Figure 6.7 shows CVs of G6-OH(Pt_nPd_{180-n}) (n = 180, 150, 120, and 90) and a voltammogram obtained using an electrode modified with G6-OH only (no metal particles). CVs of DEN-modified electrodes exhibit broad peaks between 0.05 and 0.3 V that are characteristic of hydrogen adsorption and desorption. Small shoulders characteristic of hydrogen adsorption on bulk Pt[141] are only just noticeable in the CV of G6-OH(Pt_{180}), but as the Pd content increases these features are lost and the total charge associated with hydrogen increases slightly. These latter two changes probably arise from differences in adsorption characteristics of hydrogen on the bimetallic surface and possibly because of some insertion of hydrogen into the interior of the Pd-containing bimetallics (absorption). Additionally, the total charge associated with the hydrogen adsorption/desorption region of the CVs decreases significantly during continuous voltammetric scanning for PtPd DENs containing more than 60 atoms of Pd. We calculated the active surface area of the stable G6-OH(Pt_{180}) catalyst based on the charge associated with the hydrogen desorption region (anodic current between 0.05 and

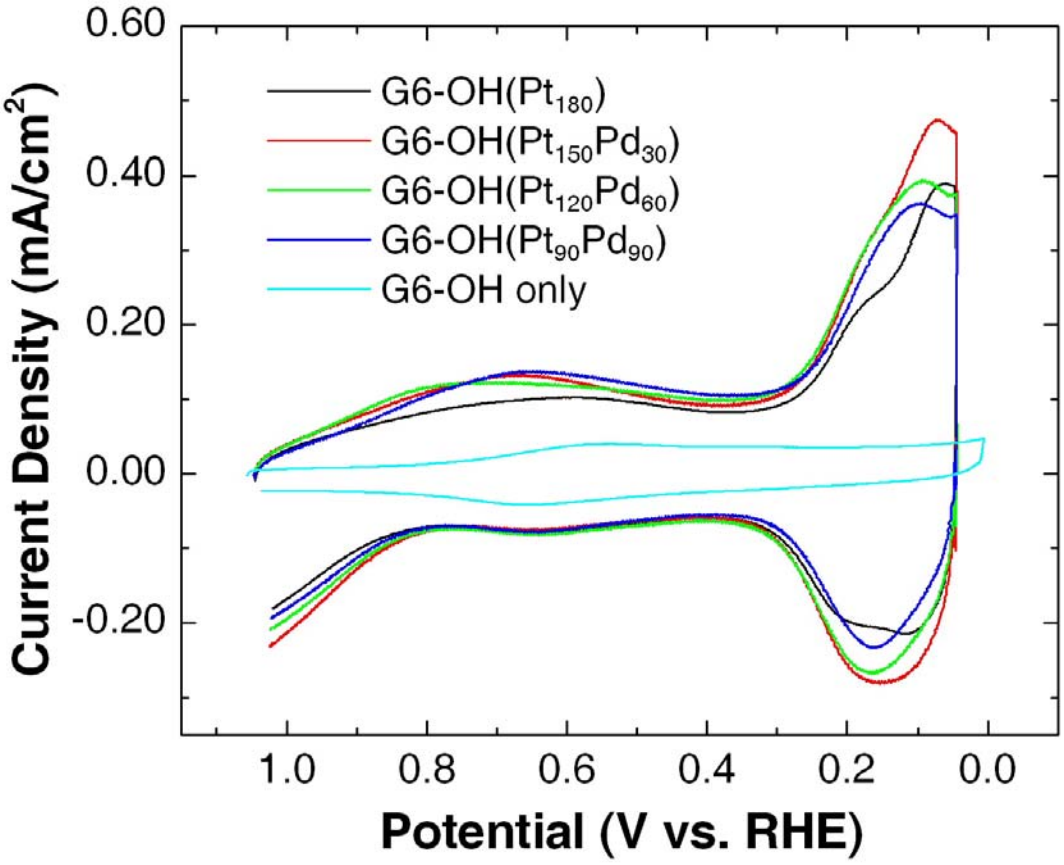

Figure 6.7. Cyclic voltammograms of G6-OH(Pt_nPd_{180-n})(n = 180, 150, 120, and 90) in N_2-saturated, 0.5 M H_2SO_4 electrolyte solution. A cyclic voltammogram of an electrode modified only with G6-OH is also shown. Scan rate: 100 mV/s. The initial potential was 1.05 V.

0.3 V). After subtraction of the background charge, the total charge was found to be 46 μC, which correspond to 0.22 cm^2 of active surface area assuming that hydrogen desorption yields 210 μC/cm^2 of Pt surface area.[141]

It is also possible to estimate the surface area of the Pt and PtPd DENs with a simple calculation and appropriate assumptions. We have previously shown that dendrimers form near-monolayer coverages on most surfaces.[103] Thus, assuming monolayer coverage, a projected area for each dendrimer of 35 nm^2, that one nanoparticle is encapsulated within each dendrimer, that each nanoparticle is a sphere having a diameter of 1.8 nm, and that the roughness factor of GC surfaces is 2.4, which is an average value from the literature (range: 1.3 – 3.5),[143-145] we calculate a total metal surface area of 0.14 cm^2 for G6-OH(Pt_{180}). This value is in reasonable agreement with the experimentally determined value obtained by hydrogen desorption for G6-OH(Pt_{180}) of 0.22 cm^2. The mass of Pt corresponding to the total Pt surface area of 0.14 cm^2 is 0.088 μg, or 0.45 μg/cm^2 when normalized to the projected surface area of the electrode.

Rotating Disk Voltammetry. The electrocatalytic activity of PtPd DENs was quantitatively examined as a function of catalyst composition using rotating disk voltammetry.[5,31,114] The rotating disk electrodes (RDEs) were modified with DENs following the same procedure used for the CV experiments. Figure 6.8a shows a family of rotating disk voltammograms (RDVs) for the G6-OH(Pt_{180}) electrocatalyst obtained at rotation rates ranging from 200 to 2500 rpm. These RDVs were measured using electrolyte solutions having the same composition as that used for the CVs, and the potential was scanned from 0.95 V to 0.15 V at 10 mV/s. Figure 6.8a only shows the

forward-going scan, but a comparison of the forward and reverse scans is provided in Figure 6.9. The amount of hysteresis is about 45 mV, which is typical for all the RDVs described here.

The RDVs in Figure 6.8a exhibit onset currents at about 0.80 V and attain mass-transfer-limited values that are a function of the rotation rate. The observed current is attributable to O_2 reduction, because no measurable current was observed when an N_2-saturated electrolyte solution was scanned in this same potential window. The G6-OH($Pt_{150}Pd_{30}$)-modified RDE shows slightly different results (Figure 6.10a). The shape of voltammograms is same as in Figure 6.8a, but the RDVs are shifted to a more positive potential. For example, the RDV obtained at 900 rpm for the G6-OH(Pt_{180}) catalyst attains a current density of 2.0 mA/cm^2 at 0.64 V while the G6-OH($Pt_{150}Pd_{30}$) catalyst exhibits this same current density at 0.69 V. This means that the G6-OH($Pt_{150}Pd_{30}$) DENs are more active ORR catalysts than the G6-OH(Pt_{180}) DENs. The potentials of the RDVs are reproducible (± 10 mV) for independently synthesized G6-OH(Pt_{180}) and G6-OH($Pt_{150}Pd_{30}$) electrocatalysts immobilized on independently prepared electrodes. As the percentage of Pd in the DEN electrocatalysts increases, the RDVs retain a similar appearance, except that they shift to more negative potentials compared to G6-OH($Pt_{150}Pd_{30}$), indicating that they have inferior catalytic properties. These additional RDVs are provided in Figure 6.11. Importantly, the CVs and RDVs provide consistent information: maximum catalytic activity is observed for G6-OH($Pt_{150}Pd_{30}$), and as the percentage of Pd increases, the catalytic performance monotonically decreases.

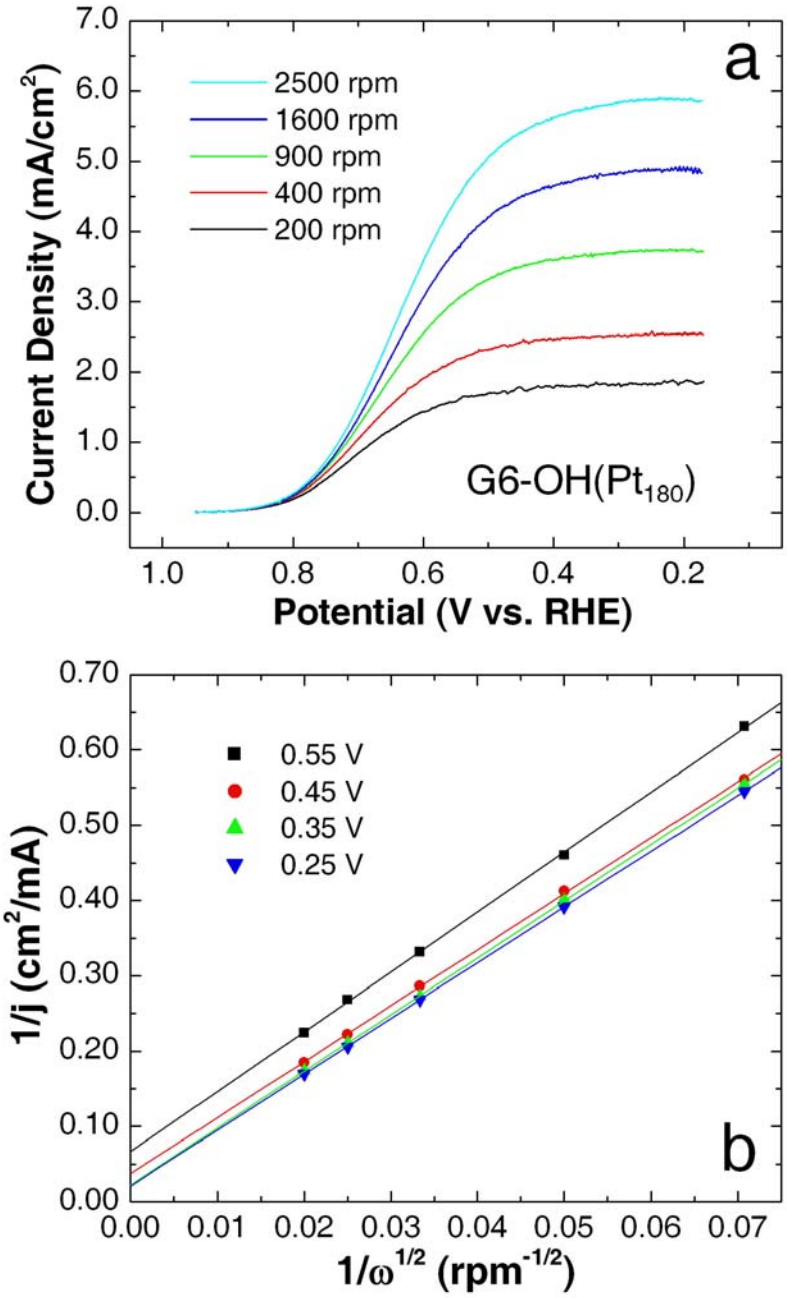

Figure 6.8. (a) Rotating disk voltammograms for a G6-OH(Pt_{180})-modified GCE. (b) Plots of $1/j$ vs. $1/\omega^{1/2}$ derived from the RDVs in (a). Scan rate: 10 mV/s; electrolyte solution: aqueous 0.5 M H_2SO_4 saturated with O_2.

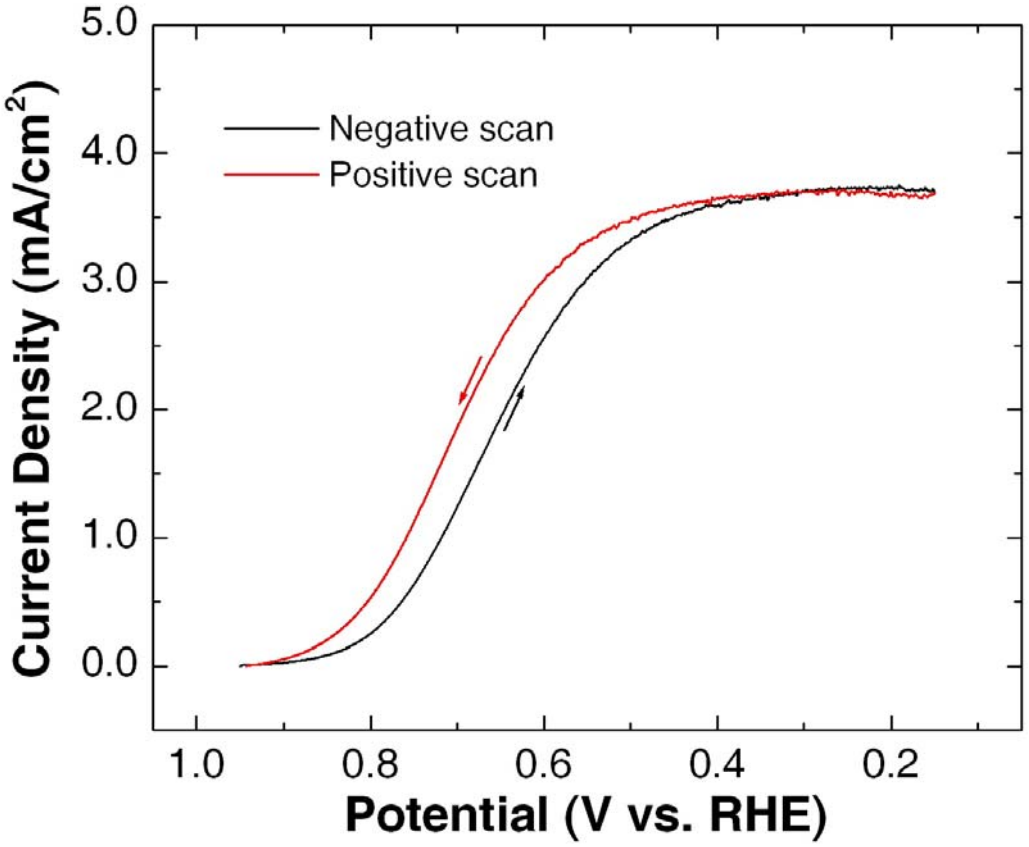

Figure 6.9. Forward (black) and reverse (red) RDVs (at 900 rpm) obtained at a G6-OH(Pt_{180})-modified GCE. Scan rate: 10 mV/s; electrolyte solution: aqueous 0.5 M H_2SO_4 saturated with oxygen.

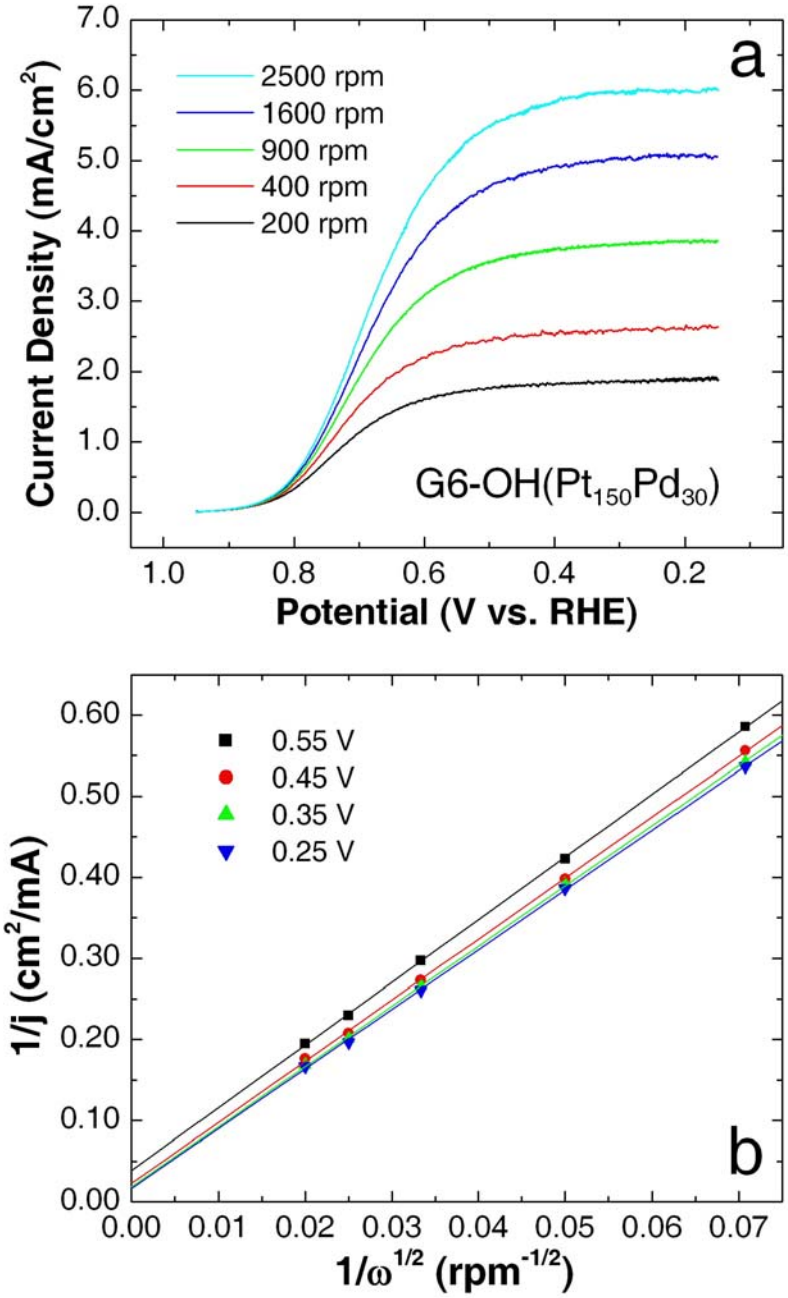

Figure 6.10. (a) Rotating disk voltammograms for a G6-OH($Pt_{150}Pd_{30}$)-modified GCE. (b) Plots of $1/j$ vs. $1/\omega^{1/2}$ derived from the RDVs in (a). Scan rate: 10 mV/s; electrolyte solution: aqueous 0.5 M H_2SO_4 saturated with O_2.

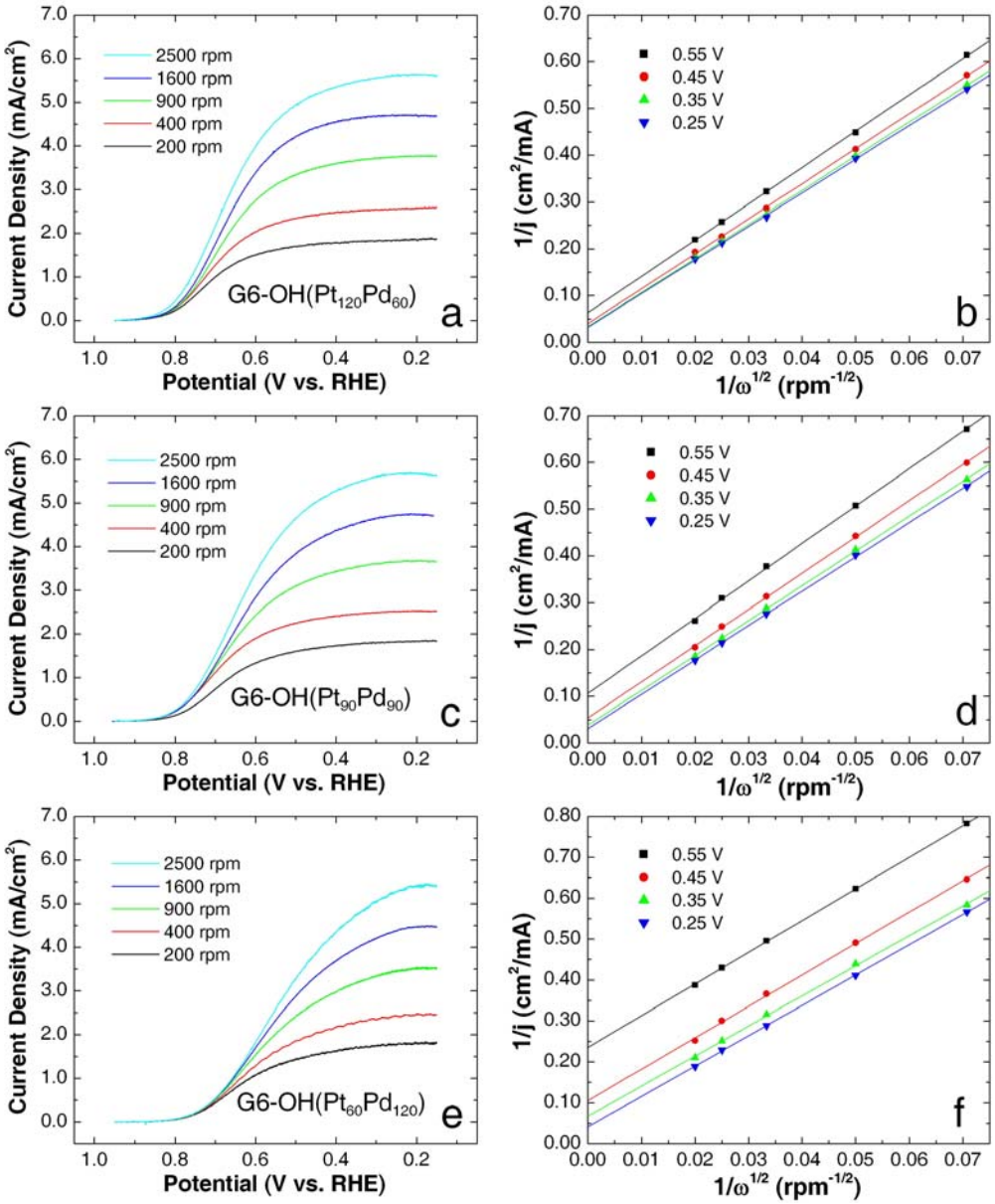

Figure 6.11. RDVs obtained using a GCE modified with (a) G6-OH($Pt_{120}Pd_{60}$), (c) G6-OH($Pt_{90}Pd_{90}$), and (e) G6-OH($Pt_{60}Pd_{120}$) DENs. (b), (d), and (f) Plots of $1/j$ vs. $1/\omega^{1/2}$ as a function of potential derived from the RDVs. RDVs for G6-OH($Pt_{30}Pd_{150}$) and G6-OH(Pd_{180}) are not shown, because the results was not sufficiently reproducible. Scan rate: 10 mV/s; electrolyte solution: aqueous 0.5 M H_2SO_4 saturated with oxygen.

Figures 6.8b and 6.10b are Koutecky-Levich plots[146] ($1/j$ vs. $1/\omega^{1/2}$) as a function of potential for the G6-OH(Pt_{180}) and G6-OH($Pt_{150}Pd_{30}$) DENs, respectively. We compared the slopes of these Koutecky-Levich plots with the theoretically calculated values for the 4-electron O_2 reduction using Eq. 6.1.

$$\frac{1}{j} = \frac{1}{j_K} + \frac{1}{0.20nFD_O^{2/3}\omega^{1/2}\nu^{-1/6}C_O} = \frac{1}{j_K} + \frac{1}{B\omega^{1/2}} \tag{6.1}$$

Here, j is the measured current density, j_K is kinetic current density, F is the faraday constant, D_O is the diffusion coefficient of O_2 (1.9×10^{-5} cm^2/s), ω is electrode rotation rate in unit of rpm, ν is kinematic viscosity of water (1.0×10^{-2} cm^2/s), and C_O is the concentration of O_2 in dilute, aqueous sulfuric acid (1.1×10^{-6} mol/cm^3).[147,148] Using appropriate numerical values, the calculated B value is 0.13 $mA/cm^2rpm^{1/2}$. This value can be compared to the measured B values obtained from the slopes of the plots in Figures 6.8b and 6.10b of 0.132 ± 0.004 $mA/cm^2rpm^{1/2}$ and 0.133 ± 0.003 $mA/cm^2rpm^{1/2}$ for the G6-OH(Pt_{180}) and G6-OH($Pt_{150}Pd_{30}$) DENs, respectively. The excellent agreement between the calculated and measured B values means that the number of electrons involved in the ORR with these DEN catalysts is four, and thus the predominant product is water. The Koutecky-Levich plots for G6-OH($Pt_{120}Pd_{60}$), G6-OH($Pt_{90}Pd_{90}$), and G6-OH($Pt_{60}Pd_{120}$) have B values of 0.135 ± 0.004 $mA/cm^2rpm^{1/2}$, 0.131 ± 0.005 $mA/cm^2rpm^{1/2}$, and 0.133 ± 0.004 $mA/cm^2rpm^{1/2}$ and are provided in Figure 6.11.

A kinetic analysis for the Pt and PtPd electrocatalysts, determined using the RDVs described previously, was carried out using Tafel plots. Specifically, Figure 6.12 shows plots of potential vs. kinetic current density (j_K), where the j_K values were obtained from the j values of the RDVs (900 rpm) in Figures 6.8a, 6.10a, and Figure 6.11 using Eq. 6.1 and the measured B values.[5,149] Using the region of the Tafel plots between 0.85 V and 0.65 V, Tafel slopes of –0.12, -0.12, -0.11, -0.11, and -0.11 V/decade were calculated for G6-OH(Pt_{180}), G6-OH($Pt_{150}Pd_{30}$), G6-OH($Pt_{120}Pd_{60}$), G6-OH($Pt_{90}Pd_{90}$), and G6-OH($Pt_{60}Pd_{120}$), respectively. These values are comparable to the reported value of 0.128 V/decade for bulk Pt electrodes in 0.5 M H_2SO_4 electrolyte solution at 293 K.[135]

Figure 6.13a shows a comparison of kinetic data for G6-OH(Pt_nPd_{180-n}) obtained from Figure 6.12 at different potentials. As for the CV results (Figure 6.6), the kinetic current density increases in G6-OH($Pt_{150}Pd_{30}$) compared to G6-OH(Pt_{180}) but as the Pd content increases further the current density decreases.

The data in Figure 6.13b were obtained by dividing j_K (Figure 6.13a) by the fraction of Pt used in the DEN synthesis (e.g. 0.5 for G6-OH($Pt_{90}Pd_{90}$)). This makes it possible to compare the relative mass activity of Pt in the PtPd DEN catalysts. For this value to have meaning, it is necessary to assume that Pd does not have measurable activity in the applicable potential range (0.70 – 0.80 V, Figure 6.13). The voltammetry of G6-OH(Pd_{180}) shown in Figure 6.6a confirms this assumption. The key result is that for the data at 0.70 V, there is an enhancement in relative mass activity of 2.5 for the G6-OH($Pt_{150}Pd_{30}$) electrocatalyst compared to G6-OH(Pt_{180}).

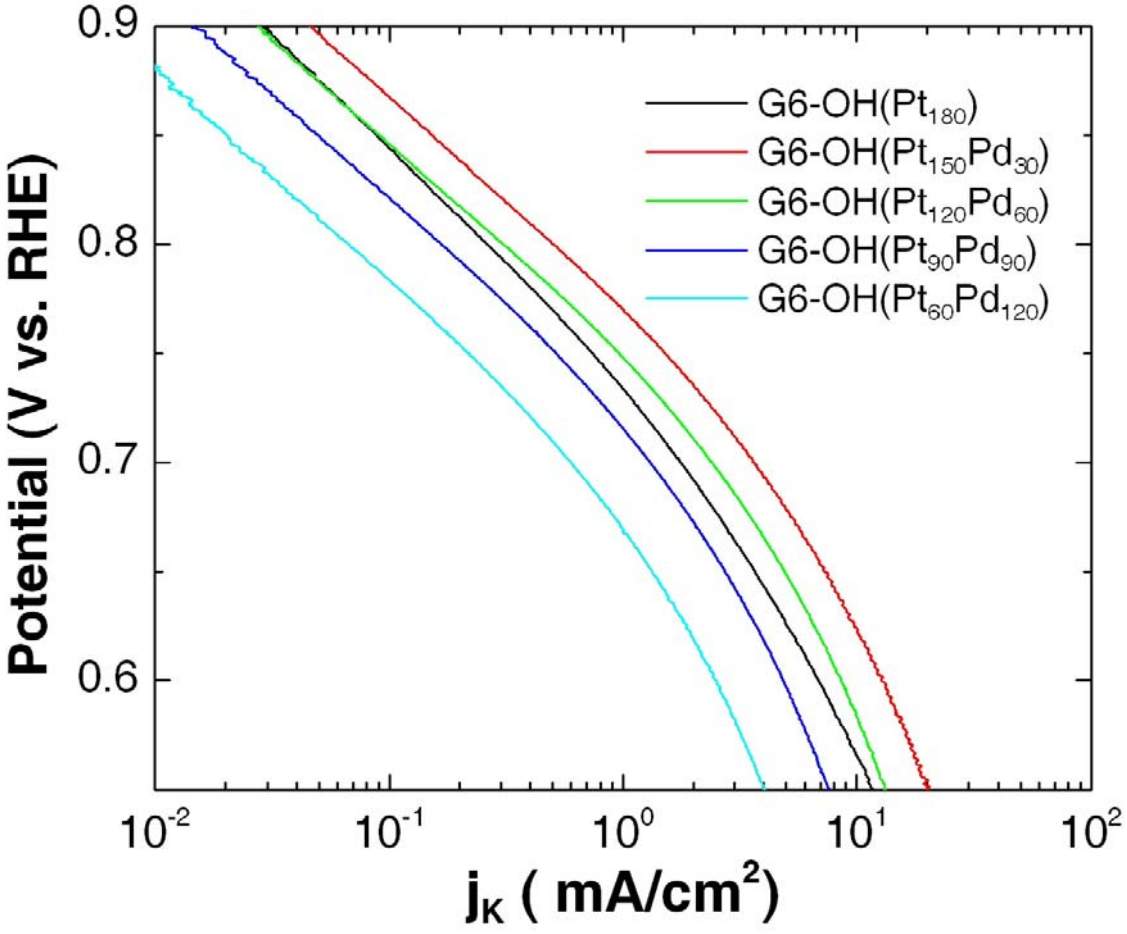

Figure 6.12. Tafel plots for Pt and PtPd catalysts obtained using data from RDVs (900 rpm).

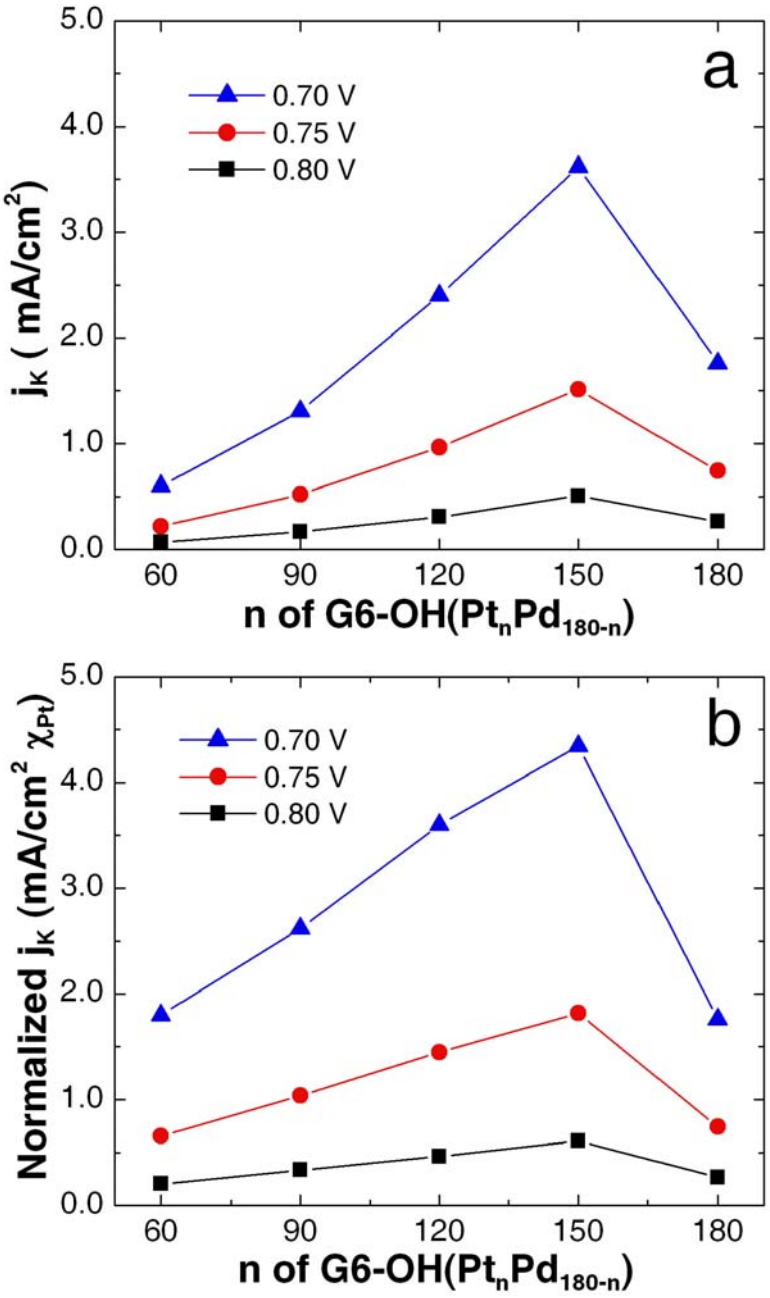

Figure 6.13. Plots of (a) kinetic current density and (b) kinetic current density normalized to the fractional amount of Pt (χ_{Pt}) contained in each nanoparticle composition at different potentials.

Finally, we estimated the specific activity (kinetic current normalized to the total surface area of catalyst) and the mass activity (kinetic current normalized to the total mass of catalyst) for G6-OH(Pt_{180}) at 0.70 V based on the total surface area and mass of Pt discussed earlier. The estimated specific activity for G6-OH(Pt_{180}) ranges from 1.6 - 2.5 mA/cm^2_{Pt}, depending on whether the experimentally measured surface area (0.22 cm^2) or the calculated value (0.14 cm^2) is used. The estimated mass activity for G6-OH(Pt_{180}) is 3.9 $mA/\mu g_{Pt}$ based on the calculated mass of Pt present on the electrode surface (0.088 μg).

6.5 Summary and Conclusions

We have examined the catalytic activity of DENs containing 180 atoms and composed of different Pt:Pd ratios. The most important conclusion of this chapter is that multimetallic nanoparticles having very well-defined compositions can be synthesized, structurally and chemically characterized ex situ, and then their electrocatalytic properties can be studied. This provides a direct route to correlate the structure and function of electrocatalysts.

Cyclic and rotating disk voltammetry results indicate that PtPd bimetallic DENs exhibit relative mass activity enhancements for the ORR of up to a factor of 2.5 compared to monometallic Pt DENs. However, the Pt and PtPd DEN catalysts presented in this chapter require 10 - 50 mV of additional overpotential compared to commercial carbon-supported Pt catalysts in other ORR kinetic studies.[5,31,115] This could be the result of different experimental conditions, such as temperature, electrolyte composition, and

hysteresis in the voltammetry. Alternatively, or in addition, there could be a particle-size effect that suppress catalytic activity: the catalysts used in this study were composed of ~1.7 nm particles, but others have reported that the optimal size for the ORR is in the range of 3 - 4 nm.[5,46] Finally, if our model is correct (Figure 6.1), there could be an overpotential required for electron tunneling between the electrode and the catalytic nanoparticles. It is important to keep in mind, however, that the G6-OH(Pt_{180}) catalyst films reported here consists of single monolayers consisting of only 0.45 μg/cm^2 of Pt. This amount corresponds to 30 to 100 times less metal per unit electrode area than typical RDE studies carried out using Nafion films.[5,31,34,35,115]

At present, we are examining the effect of the size of Pt-only DENs on the activity of the ORR. Subsequent electrocatalytic studies will focus on other types of multimetallic DENs in both alloy and core-shell forms.

CHAPTER VII

SUMMARY AND CONCLUSIONS

In this dissertation, we have shown that 1-2 nm monometallic and bimetallic nanoparticles can be prepared within PAMAM dendrimers and characterized by UV-vis spectroscopy, HRTEM, and EDS. These dendrimer-encapsulated nanoparticles (DENs) were immobilized on electrode surfaces and were utilized as electrocatalysts for the oxygen reduction reaction. Key points from each chapter are summarized next.

First, synthesis, physical and chemical properties, and stability of Pd DENs prepared within poly(amidoamine) dendrimers were intensively studied in aqueous solution. The following four important findings emerged from this part of my research: (1) the maximum Pd ion loading in the dendrimer is correlated, in a 1:1 stoichiometric ratio, to the number of interior amines available for complexation; (2) Pd DENs can be synthesized within amine-terminated Pd DENs by controlling solution pH; (3) the oxidative stability of Pd DENs is significantly improved by removal of solution-phase impurities using dialysis; (4) exposure to hydrogen gas reversibly converts partially oxidized Pd DENs back to the zerovalent DENs.

Second, Pt and Pd nanoparticles were prepared within amine-terminated PAMAM dendrimers by selective protonation of the terminal amine groups and selective metal-ion complexation with interior amine groups. The properties of the metal nanoparticles are about the same as those we have previously prepared within hydroxyl-terminated PAMAM dendrimers, but the presence of the amine groups provides a

reactive handle for linking DENs to surfaces. For this, the free amine groups on the dendrimer surface were used to link Pd DENs to Au surfaces via an intermediate self-assembled monolayer adhesion layer. And this provided robust DEN films on Au surfaces.

Third, Pt DENs were prepared with hydroxyl-terminated PAMAM dendrimer and immobilized on glassy carbon electrode using an electrochemical attachment method. The resulting Pt DEN films were electrochemically active for the oxygen reduction reaction and also robust, surviving up to 50 consecutive electrochemical scans for the oxygen reduction reaction and sonication up to 10 min in 0.5 M H_2SO_4 solution with no significant activity change.

Finally, this strategy was expanded to bimetallic PtPd DENs. Here, PtPd bimetallic nanoparticles containing an average of 180 atoms and composed of seven different Pt:Pd ratios were prepared within sixth-generation, hydroxyl-terminated, PAMAM dendrimers and also linked onto glassy carbon electrodes. The resulting films were used to precisely correlate the effect of catalyst composition to the efficiency of the oxygen reduction reaction via rotating disk voltammetry technique. The maximum rate for the ORR occurs at a Pt:Pd ratio of 5:1, which corresponds to a relative mass activity enhancement of 2.5 compared to otherwise identical monometallic Pt nanoparticles.

Currently, we are optimizing this strategy to obtain better catalytic activity of DENs for the ORR, and we are investigating the effect of the particle size of Pt DENs on the catalytic activity. Following electrocatalytic studies will focus on other types of multimetallic DENs in both alloy and core-shell structures. This will be an important

study not only for developing better catalysts for fuel cells but also for understanding dendrimer-encapsulated nanoparticles.

REFERENCES

(1) Crooks, R. M.; Zhao, M.; Sun, L.; Chechik, V.; Yeung, L. K. *Acc. Chem. Res.* **2001**, *34*, 181-190.

(2) Scott, R. W. J.; Wilson, O. M.; Crooks, R. M. *J. Phys. Chem. B* **2005**, *109*, 692-704, and references therein.

(3) Carrette, L.; Friedrich, K. A.; Stimming, U. *Fuel Cells* **2001**, *1*, 5-39.

(4) Markovic, N. M.; Schmidt, T. J.; Stamenkovic, V.; Ross, P. N. *Fuel Cells* **2001**, *1*, 105-116.

(5) Gasteiger, H. A.; Kocha, S. S.; Sompalli, B.; Wagner, F. T. *Appl. Catal. B: Environ.* **2005**, *56*, 9-35.

(6) Wilson, O. M.; Scott, R. W. J.; Garcia-Martinez, J. C.; Crooks, R. M. *J. Am. Chem. Soc.* **2005**, 1015-1024.

(7) Zhao, M.; Crooks, R. M. *Adv. Mater.* **1999**, *11*, 217-220.

(8) Niu, Y.; Crooks, R. M. *C. R. Chimie* **2003**, *6*, 1049-1059.

(9) Niu, Y.; Yeung, L. K.; Crooks, R. M. *J. Am. Chem. Soc.* **2001**, *123*, 6840-6846.

(10) Wilson, O. M.; Knecht, M. R.; Garcia-Martinez, J. C.; Crooks, R. M. *J. Am. Chem. Soc.* **2006**, *128*, 4510-4511.

(11) Scott, R. W. J.; Datye, A. K.; Crooks, R. M. *J. Am. Chem. Soc.* **2003**, *125*, 3708-3709.

(12) Scott, R. W. J.; Wilson, O. M.; Oh, S.-K.; Kenik, E. A.; Crooks, R. M. *J. Am. Chem. Soc.* **2004**, *126*, 15583-15591.

(13) Yeung, L. K.; Crooks, R. M. *Nano Lett.* **2001**, *1*, 14-17.

(14) Yeung, L. K.; Lee, C. T.; Johnston, K. P.; Crooks, R. M. *Chem. Commun.* **2001**, 2290-2291.

(15) Rahim, E. H.; Kamounah, F. S.; Frederiksen, J.; Christensen, J. B. *Nano Lett.* **2001**, *1*, 499-501.

(16) Li, Y.; El-Sayed, M. A. *J. Phys. Chem. B* **2001**, *105*, 8938-8943.

(17) Garcia-Martinez, J. C.; Lezutekong, R.; Crooks, R. M. *J. Am. Chem. Soc.* **2005**, *127*, 5097-5103.

(18) Lang, H.; Maldonado, S.; Stevenson, K. J.; Chandler, B. D. *J. Am. Chem. Soc.* **2004**, *126*, 12949 -12956.

(19) Lang, H.; May, R. A.; Iversen, B. L.; Chandler, B. D. *J. Am. Chem. Soc.* **2003**, *125*, 14832-14836.

(20) Scott, R. W. J.; Wilson, O. M.; Crooks, R. M. *Chem. Mater.* **2004**, *16*, 5682-5688.

(21) Scott, R. W. J.; Sivadinarayana, C.; Wilson, O. M.; Yan, Z.; Goodman, D. W.; Crooks, R. M. *J. Am. Chem. Soc.* **2005**, *127*, 1380-1381.

(22) Glass, J. T.; Cahen, G. L., Jr.; Stoner, G. E.; Taylor, E. J. *J. Electrochem. Soc.* **1987**, *134*, 58-65.

(23) Paffett, M. T.; Beery, J. G.; Gottesfeld, S. *J. Electrochem. Soc.* **1988**, *135*, 1431-1436.

(24) Toda, T.; Igarashi, H.; Watanabe, M. *J. Electroanal. Chem.* **1999**, *460*, 258-262.

(25) Toda, T. I., Hiroshi; Uchida, Hiroyuki; Watanabe, Masahiro *J. Electrochem. Soc.* **1999**, *146*, 3750-3756.

(26) Hwang, J. T.; Chung, J. S. *Electrochim. Acta* **1993**, *38*, 2715-2723.

(27) Mukerjee, S.; McBreen, J. *J. Electroanal. Chem.* **1998**, *448*, 163-171.

(28) Beard, B. C. R., Philip N., Jr. *J. Electrochem. Soc.* **1990**, *137*, 3368-3374.

(29) Mukerjee, S. S., Supramaniam *J. Electroanal. Chem.* **1993**, *357*, 201-224.

(30) Min, M.-K.; Cho, J.; Cho, K.; Kim, H. *Electrochim. Acta* **2000**, *45*, 4211-4217.

(31) Paulus, U. A.; Wokaun, A.; Scherer, G. G.; Schmidt, T. J.; Stamenkovic, V.; Radmilovic, V.; Markovic, N. M.; Ross, P. N. *J. Phys. Chem. B* **2002**, *106*, 4181-4191.

(32) Murthi, V. S.; Urian, R. C.; Mukerjee, S. *J. Phys. Chem. B* **2004**, *108*, 11011-11023.

(33) Boucher, A.-C. A.-V., N.; Dassenoy, F.; Vogel, W. *Langmuir* **2003**, 10885-10891.

(34) Yang, H.; Alonso-Vante, N.; Leger, J.-M.; Lamy, C. *J. Phys. Chem. B* **2004**, *108*, 1938-1947.

(35) Yang, H.; Vogel, W.; Lamy, C.; Alonso-Vante, N. *J. Phys. Chem. B* **2004**, *108*, 11024-11034.

(36) Jalan, V. T., E. J. *J. Electrochem. Soc.* **1983**, *130*, 2299-2302.

(37) Anderson, A. B.; Roques, J.; Mukerjee, S.; Murthi, V. S.; Markovic, N. M.; Stamenkovic, V. *J. Phys. Chem. B* **2005**, *109*, 1198-1203.

(38) Zhang, J.; Vukmirovic, M. B.; Sasaki, K.; Nilekar, A. U.; Mavrikakis, M.; Adzic, R. R. *J. Am. Chem. Soc.* **2005**, *127*, 12480-12481.

(39) Xu, Y.; Ruban, A. V.; Mavrikakis, M. *J. Am. Chem. Soc.* **2004**, *126*, 4717-4725.

(40) Balbuena, P. B.; Altomare, D.; Vadlamani, N.; Bingi, S.; Agapito, L. A.; Seminario, J. M. *J. Phys. Chem. A* **2004**, *108*, 6378-6384.

(41) Wang, Y.; Balbuena, P. B. *J. Phys. Chem. B* **2005**, *109*, 18902-18906.

(42) Nørskov, J. K.; Rossmeisl, J.; Logadottir, A.; Lindqvist, L.; Kitchin, J. R.; Bligaard, T.; Jónsson, H. *J. Phys. Chem. B* **2004**, *108*, 17886-17892.

(43) Fernández., J. L.; Raghuveer, V.; Manthiram, A.; Bard, A. J. *J. Am. Chem. Soc.* **2005**, *127*, 13100-13101.

(44) Raghuveer, V.; Manthiram, A.; Bard, A. J. *J. Phys. Chem. B* **2005**, *109*, 22909-22912.

(45) Shao, M.-H.; Sasaki, K.; Adzic, R. R. *J. Am. Chem. Soc.* **2006**, *128*, 3526-3527.

(46) Kinoshita, K. *J. Electrochem. Soc.* **1990**, *137*, 845-848.

(47) Peuckert, M.; Yoneda, T.; Dalla Betta, R. A.; Boudart, M. *J. Electrochem. Soc.* **1986**, *133*, 944-947.

(48) Sattler, M. L.; Ross, P. N. *Ultramicroscopy* **1986**, *20*, 21-28.

(49) Takasu, Y.; Ohashi, N.; Zhang, X.-G.; Murakami, Y.; Minagawa, H.; Sato, S.; Yahikozawa, K. *Electrochim. Acta* **1996**, *41*, 2595-2600.

(50) Mayrhofer, K. J. J.; Blizanac, B. B.; Arenz, M.; Stamenkovic, V. R.; Ross, P. N.; Markovic, N. M. *J. Phys. Chem. B* **2005**, *109*, 14433-14440.

(51) Bett, J.; Lundquist, J.; Washington, E.; Stonehart, P. *Electrochim. Acta* **1973**, *18*, 343-348.

(52) Watanabe, M.; Saegusa, S.; Stonehart, P. *Chem. Lett.* **1988**, 1487-1490.

(53) Watanabe, M.; Sei, H.; Stonehart, P. *J. Electroanal. Chem.* **1989**, *261*, 375-387.

(54) *JEOL 2010F Transmission Electron Microscope Manual Part*. JEOL LTD.: Tokyo, Japan, 2003

(55) Crooks, R. M.; Lemon, B. I.; Sun, L.; Yeung, L. K.; Zhao, M. *Topics Curr. Chem.* **2001**, *212*, 81-135.

(56) Zhao, M.; Crooks, R. M. *Angew. Chem. Int. Ed.* **1999**, *38*, 364-366.

(57) Chechik, V.; Zhao, M.; Crooks, R. M. *J. Am. Chem. Soc.* **1999**, *121*, 4910-4911.

(58) Chechik, V.; Crooks, R. M. *J. Am. Chem. Soc.* **2000**, *122*, 1243-1244.

(59) Ooe, M.; Murata, M.; Mizugaki, T.; Ebitani, K.; Kaneda, K. *Nano Lett.* **2002**, *2*, 999-1002.

(60) Zhao, M.; Sun, L.; Crooks, R. M. *J. Am. Chem. Soc.* **1998**, *120*, 4877-4878.

(61) Esumi, K.; Suzuki, A.; Aihara, N.; Usui, K.; Torigoe, K. *Langmuir* **1998**, *14*, 3157-3159.

(62) Gröhn, F.; Bauer, B. J.; Akpalu, Y. A.; Jackson, C. L.; Amis, E. J. *Macromolecules* **2000**, *33*, 6042-6050.

(63) Chung, Y. M.; Rhee, H. K. *Cat. Lett.* **2003**, *85*, 159-164.

(64) Lemon, B. I.; Crooks, R. M. *J. Am. Chem. Soc.* **2000**, *122*, 12886-12887.

(65) Elding, L. I.; Olsson, L. F. *J. Phys. Chem.* **1978**, *82*, 69-74.

(66) Watanabe, S.; Regen, S. L. *J. Am. Chem. Soc.* **1994**, *116*, 8855-8856.

(67) Sun, L.; Crooks, R. M. *J. Phys. Chem. B* **2002**, *106*, 5864-5872.

(68) Niu, Y.; Sun, L.; Crooks, R. M. *Macromolecules* **2003**, *36*, 5725-5731.

(69) Creighton, J. A.; Eadon, D. G. *J. Chem. Soc. Faraday Trans.* **1991**, *87*, 3881-3891.

(70) Ershov, B. G. *Russ. Chem. Bull* **1996**, *45*, 299-302.

(71) Henglein, A. *J. Phys. Chem. B* **2000**, *104*, 6683-6685.

(72) Aiken, J. D.; Finke, R. G. *J. Mol. Catal. A: Chem.* **1999**, *145*, 1-44.

(73) Hornstein, B. J.; Finke, R. G. *Chem. Mater.* **2003**, *15*, 899-909.

(74) Scherrenberg, R.; Coussens, B.; van Vliet, P.; Edouard, G.; Brackman, J.; de Brabander, E.; Mortensen, K. *Macromolecules* **1998**, *31*, 456-461.

(75) Wilson, O. M.; Scott, R. W. J.; Crooks, R. M., Unpublished data, 2003.

(76) Nuzzo, R. G.; Allara, D. L. *J. Am. Chem. Soc.* **1983**, *105*, 4481-4483.

(77) Zheng, J.; Petty, J. T.; Dickson, R. M. *J. Am. Chem. Soc.* **2003**, *125*, 7780-7781.

(78) Esumi, K.; Nakamura, R.; Suzuki, A.; Torigoe, K. *Langmuir* **2000**, *16*, 7842-7846.

(79) Oh, S.-K.; Kim, Y.-G.; Ye, H.; Crooks, R. M. *Langmuir* **2003**, *19*, 10420-10425.

(80) Scott, R. W. J.; Ye, H.; Henriquez, R. R.; Crooks, R. M. *Chem. Mater.* **2003**, *15*, 3873-3878.

(81) Niu, Y.; Crooks, R. M. *Chem. Mater.* **2003**, *15*, 3463-3467.

(82) Kim, Y.-G.; Oh, S.-K.; Crooks, R. M. *Chem. Mater.* **2004**, *16*, 167-172.

(83) Gröhn, F.; Gu, X.; Grüll, H.; Meredith, J. C.; Nisato, G.; Bauer, B. J.; Karim, A.; Amis, E. J. *Macromolecules* **2002**, *35*, 4852-4854.

(84) Esumi, K.; Satoh, K.; Torigoe, K. *Langmuir* **2001**, *17*, 6860-6864.

(85) Zhao, M.; Crooks, R. M. *Chem. Mater.* **1999**, *11*, 3379-3385.

(86) Wells, M.; Crooks, R. M. *J. Am. Chem. Soc.* **1996**, *118*, 3988-3989.

(87) Tokuhisa, H.; Crooks, R. M. *Langmuir* **1997**, *13*, 5608-5612.

(88) Zhou, Y.; Bruening, M. L.; Bergbreiter, D. E.; Crooks, R. M.; Wells, M. *J. Am. Chem. Soc.* **1996**, *118*, 3773-3774.

(89) Bruening, M. L.; Zhou, Y.; Aguilar, G.; Agee, R.; Bergbreiter, D. E.; Crooks, R. M. *Langmuir* **1997**, *13*, 770-778.

(90) Bergbreiter, D. E.; Tao, G. *J. Polym. Sci., Part A: Polym. Chem.* **2000**, *38*, 3944-3953.

(91) Elding, L. I.; Olsson, L. F. *J. Phys. Chem.* **1978**, *82*, 69-74.

(92) Martin, D. S. *Inorg. Chim. Acta Rev.* **1971**, *5*, 107-125.

(93) Zhao, M.; Crooks, R. M. *Adv. Mater.* **1999**, *11*, 217-220.

(94) Rochon, F. D.; Fleurent, L. *Inorg. Chim. Acta* **1988**, *143*, 81-87.

(95) Henglein, A.; Ershov, B. G.; Malow, M. *J. Phys. Chem.* **1995**, *99*, 14129-14136.

(96) Henglein, A.; Giersig, M. *J. Phys. Chem. B* **2000**, *104*, 6767-6772.

(97) Fu, X.; Wang, Y.; Wu, N.; Gui, L.; Tang, Y. *J. Colloid Interface Sci.* **2001**, *243*, 326-330.

(98) Eberhardt, W.; Fayet, P.; Cox, D. M.; Fu, Z.; Kaldor, A.; Sherwood, R.; Sondericker, D. *Phys. Rev. Lett.* **1990**, *64*, 780-783.

(99) You, T.; Niwa, O.; Horiuchi, T.; Tomita, M.; Iwasaki, Y.; Ueno, Y.; Hirono, S. *Chem. Mater.* **2002**, *14*, 4796-4799.

(100) Ershov, B. G. *Russ. J. Phys. Chem.* **1995**, *69*, 1979-1983.

(101) Henglein, A. *J. Phys. Chem. B* **2000**, *104*, 6683-6685.

(102) Chung, Y.-M.; Rhee, H.-K. *Cat. Lett.* **2003**, *85*, 159-164.

(103) Tokuhisa, H.; Zhao, M.; Baker, L. A.; Phan, V. T.; Dermody, D. L.; Garcia, M. E.; Peez, R. F.; Crooks, R. M.; Mayer, T. M. *J. Am. Chem. Soc.* **1998**, *120*, 4492-4501.

(104) Ye, H.; Scott, R. W. J.; Crooks, R. M. *Langmuir* **2004**, *20*, 2915-2920.

(105) Deinhammer, R. S.; Ho, M.; Anderegg, J. W.; Porter, M. D. *Langmuir* **1994**, *10*, 1306-1313.

(106) Andrieux, C. P.; Gonzalez, F.; Savéant, J.-M. *J. Am. Chem. Soc.* **1997**, *119*, 4292-4300.

(107) Maeda, H.; Yamauchi, Y.; Hosoe, M.; Li, T.-X.; Yamaguchi, E.; Kasamatsu, M.; Ohmori, H. *Chem. Pharm. Bull.* **1994**, *42*, 1870-1873.

(108) Delamar, M.; Hitmi, R.; Pinson, J.; Savéant, J.-M. *J. Am. Chem. Soc.* **1992**, *114*, 5883-5884.

(109) Allongue, P.; Delamar, M.; Desbat, B.; Fagebaume, O.; Hitmi, R.; Pinson, J.; Savéant, J.-M. *J. Am. Chem. Soc.* **1997**, *119*, 201-207.

(110) Brooksby, P. A.; Downard, A. J. *Langmuir* **2004**, *20*, 5038-5045.

(111) Maeda, H.; Itami, M.; Yamauchi, Y.; Ohmori, H. *Chem. Pharm. Bull.* **1996**, *44*, 2294-2299.

(112) Maeda, H.; Katayama, K.; Matsui, R.; Yamauchi, Y.; Ohmori, H. *Anal. Sci.* **2000**, *16*, 293-298.

(113) Gloaguen, F.; Andolfatto, F.; Durand, R.; Ozil, P. *J. Appl. Electrochem.* **1994**, *24*, 863-869.

(114) Schmidt, T. J.; Gasteiger, H. A.; Stab, G. D.; Urban, P. M.; Kolb, D. M.; Behm, R. J. *J. Electrochem. Soc.* **1998**, *145*, 2354-2358.

(115) Paulus, U. A.; Schmidt, T. J.; Gasteiger, H. A.; Behm, R. J. *J. Electroanal. Chem.* **2001**, *495*, 134-145.

(116) Park, S.; Xie, Y.; Weaver, M. J. *Langmuir* **2002**, *18*, 5792-5798.

(117) Waszczuk, P.; Barnard, T. M.; Rice, C.; Masel, R. I.; Wieckowski, A. *Electrochem. Commun.* **2002**, *4*, 599-603.

(118) Chen, C. C.; Bose, C. S. C.; Rajeshwar, K. *J. Electroanal. Chem.* **1993**, *350*, 161-176.

(119) Schrebler, R.; del Valle, M. A.; Gómez, H.; Veas, C.; Córdova, R. *J. Electroanal. Chem.* **1995**, *380*, 219-227.

(120) Giacomini, M. T.; Ticianelli, E. A.; McBreen, J.; Balasubramanian, M. *J. Electrochem. Soc.* **2001**, *148*, A323-A329.

(121) Ye, J.-H.; Fedkiw, P. S. *Electrochim. Acta* **1996**, *41*, 221-231.

(122) Kelaidopoulou, A.; Abelidou, E.; Kokkinidis, G. *J. Appl. Electrochem.* **1999**, *29*, 1255-1261.

(123) Yahikozawa, K.; Fujii, Y.; Matsuda, Y.; Nishimura, K.; Takasu, Y. *Electrochim. Acta* **1991**, *36*, 973-978.

(124) Zoval, J. V.; Lee, J.; Gorer, S.; Penner, R. M. *J. Phys. Chem. B* **1998**, *102*, 1166-1175.

(125) Kokkinidis, G.; Papoutsis, A.; Stoychev, D.; Milchev, A. *J. Electroanal. Chem.* **2000**, *486*, 48-55.

(126) Kokkinidis, G.; Stoychev, D.; Lazarov, V.; Papoutsis, A.; Milchev, A. *J. Electroanal. Chem.* **2001**, *511*, 20-30.

(127) Dai, J.; Bruening, M. L. *Nano Lett.* **2002**, *2*, 497-501.

(128) Shen, Y.; Liu, J.; Wu, A.; Jiang, J.; Bi, L.; Liu, B.; Li, Z.; Dong, S. *Langmuir* **2003**, *19*, 5397-5401.

(129) Cherstiouk, O. V.; Simonov, P. A.; Savinova, E. R. *Electrochim. Acta* **2003**, *48*, 3851-3860.

(130) Sun, L.; Crooks, R. M. *Langmuir* **2002**, *18*, 8231-8236.

(131) Deutsch, D. S.; Lafaye, G.; Liu, D.; Chandler, B.; Williams, C. T.; Amiridis, M. D. *Catal. Lett.* **2004**, *97*, 139-143.

(132) Bartholomew, C. H.; Agrawal, P. K.; Katzer, J. R. *Adv. Catal.* **1982**, *31*, 135-242.

(133) Barbier, J.; Lamy-Pitara, E.; Marecot, P.; Boitiaux, J. P.; Cosyns, J.; Verna, F. *Adv. Catal.* **1990**, *37*, 279-318.

(134) Ye, H.; Crooks, R. M. *J. Am. Chem. Soc.* **2005**, *127*, 4930-4934.

(135) Stamenkovic, V.; Schmidt, T. J.; Ross, P. N.; Markovic, N. M. *J. Phys. Chem. B* **2002**, *106*, 11970-11979.

(136) Wakabayashi, N.; Takeichi, M.; Uchida, H.; Watanabe, M. *J. Phys. Chem. B* **2005**, *109*, 5836 -5841.

(137) Salgado, J. R. C.; Antolini, E.; Gonzalez, E. R. *J. Phys. Chem. B* **2004**, *108*, 17767 -17774.

(138) Zhang, J.; Lima, F. H. B.; Shao, M. H.; Sasaki, K.; Wang, J. X.; Hanson, J.; Adzic, R. R. *J. Phys. Chem. B* **2005**, *109*, 22701-22704.

(139) Zhang, J.; Mo, Y.; Vukmirovic, M. B.; Klie, R.; Sasaki, K.; Adzic, R. R. *J. Phys. Chem. B* **2004**, *108*, 10955-10964.

(140) Leff, D. V.; Ohara, P. C.; Heath, J. R.; Gelbart, W. M. *J. Phys. Chem.* **1995**, *99*, 7036-7041.

(141) Biegler, T.; Rand, D. A. J.; Woods, R. *J. Electroanal. Chem.* **1971**, *29*, 269-277.

(142) Pozio, A.; De Francesco, M.; Cemmi, A.; Cardellini, F.; Giorgi, L. *J. Power Sources* **2002**, *105*, 13-19.

(143) Rice, R. J.; McCreery, R. L. *Anal. Chem.* **1988**, *61*, 1637-1641.

(144) Pontikos, N. M.; McCreery, R. L. *J. Electroanal. Chem.* **1992**, *324*, 229-242.

(145) Lee, C.-W.; Bard, A. J. *J. Electroanal. Chem.* **1988**, *239*, 441-446.

(146) Bard, A. J.; Faulkner, L. R. *Electrochemical Methods Fundamentals and Application*, 2nd ed.; John Wiley & Sons: New York, 2001; pp 340-344

(147) Gubbins, K. E.; Robert D. Walker, J. *J. Electrochem. Soc.* **1965**, *112*, 469-471.

(148) Lide, D. R., Ed. *CRC Handbook of Chemistry and Physics, Internet Version 2006, http://www.hbcpnetbase.com*. Taylor and Francis: Boca Raton, FL, 2006.

(149) Maciá, M. D.; Campiña, J. M.; Herrero, E.; Feliu, J. M. *J. Electroanal. Chem.* **2004**, *564*, 141-150.

VITA

Name: Heechang Ye

Address: 9009 Great Hills Trail #2711 Austin, TX 78759

E-mail: hye@mail.utexas.edu

Education: B.S. Chemistry, Yonsei University, Seoul, Korea, 1999

Ph.D. Chemistry, Texas A&M University, College Station, TX, 2006